NATIONAL AERONAUTICS AND SPACE ADMINISTRATION

Technical Report No. 32-919

Design, Development, Testing and Flight Performance of Mariner Mars Planetary Scan System

Robert Y. Wong

JET PROPULSION LABORATORY
CALIFORNIA INSTITUTE OF TECHNOLOGY
PASADENA, CALIFORNIA

July 1, 1966

NATIONAL AERONAUTICS AND SPACE ADMINISTRATION

Technical Report No. 32-919

Design, Development, Testing and Flight Performance of Mariner Mars Planetary Scan System

Robert Y. Wong

Karl W. Linnes

K. W. Linnes, *Manager*
Space Instruments Systems Section

JET PROPULSION LABORATORY
CALIFORNIA INSTITUTE OF TECHNOLOGY
PASADENA, CALIFORNIA

July 1, 1966

Prepared Under Contract No. NAS 7-100
National Aeronautics & Space Administration

CONTENTS

CONTENTS (Cont'd)

TABLES

FIGURES

FIGURES (Cont'd)

ABSTRACT

The planetary scan system was designed and developed to support the planetary encounter activities of the *Mariner* Mars 1964 mission. Its primary functions are to search for, acquire and track the planet Mars in order to orient the television camera properly during the period immediately preceding the TV picture-recording sequence. This Report describes the design, development, fabrication, testing and performance of the system.

The system was designed to scan an instrument platform 180 deg in the process of searching for the planet. The scanning provides motion in one direction while the moving spacecraft on its trajectory provides motion approximately perpendicular to the scanning plane. Limit switch action produces signals to reverse the scan direction at the end of each 180-deg sweep. Planet acquisition and tracking are accomplished by a radiation detector with optics having a 50-deg circular field of view. This detector is used to detect the presence of the planet and to sense the position of the planet relative to the spacecraft. When the planet comes into the detector's field of view, the system switches to planet-tracking operation and proceeds such that the desired portion of the planet is used as the nulling plane for the servo system. A 400-cps motor is used for the searching and tracking. To indicate that the planet has been acquired, a planet-in-view signal is generated and telemetered to Earth in real time. This signal is also used to switch the spacecraft data mode to planet encounter format. Upon receiving a scan inhibit signal from the spacecraft, the scanning and tracking motion of the system ceases.

The *Mariner IV* spacecraft was successfully launched from Launch Complex 12, Air Force Eastern Test Range at Cape Kennedy, Florida, on November 5, 1964. The planetary scan system in this spacecraft was energized three times throughout the flight. It was energized the first time on February 12, 1965, during the early science cover drop sequence, the second time during the 9-hr planet encounter period on July 14, 1965, and the third time during the television dark encounter (calibration) sequence on August 30, 1965. The system operated properly in each of the sequences. The system flight performances in each of these sequences are also included in this Report.

I. INTRODUCTION

One of the primary objectives of the *Mariner* Mars 1964 mission was to obtain close-up television pictures of the surface of Mars. To assist in achieving this objective, a planetary scan system was required. This system operated during the period immediately preceding the TV picture recording sequence. Its primary functions are to search for, acquire and track the planet Mars in order to orient the TV camera properly.

The TV camera is mounted on a scan platform which rotates about the spacecraft roll axis. The scan system drives the platform back and forth through 180 deg of arc searching for the planet. This scanning provides motion in one direction while the motion of the spacecraft on its trajectory provides the motion approximately perpendicular to the scanning plane. Limit switches are used to actuate scan reversals when the platform reaches the end of its travel.

Mounted on the platform and bore-sighted with the TV camera is a wide angle planet detector. This detector is used to detect the presence of the planet and to sense the position of the planet relative to the spacecraft.

When the planet comes into the detector's view, the system proceeds to track the planet such that the TV camera is pointing at the desired portion of the planet. When the spacecraft is in the proper position for picture taking, a scan inhibit signal is initiated by the TV camera, Earth-based ground command or narrow angle Mars gate which is also mounted on the platform. This signal is used to indicate that the planet is in the TV field of view and is used to stop the planet tracking motion prior to the picture recording sequence. The scan trace after the platform has stopped is therefore controlled by the tracking angle at the time of scan inhibit and the motion of the spacecraft as it sweeps across the surface of the planet.

II. SYSTEM REQUIREMENTS

To design and develop a system capable of accomplishing the mission objectives, the major system requirements must be established as design objectives. These are:

1. The system planet tracking range is chosen to be 9000 to 60,000 km from the planet center. This range is selected based on the considerations of the trajectory requirements. With the established aiming point of approximately 25,000 km from planet center and a 3σ rms target error of 15,000 km, the distance at planet encounter can be anywhere in the range of 10,000 to 40,000 km. If it is assumed that the detector has a 50-deg field of view, the detection and acquisition of the planet at 60,000 km provides the system 20 min to 1½ hr of planet tracking prior to the television picture recording sequence.
2. The planet searching and tracking speed is dependent on the speed of the traveling spacecraft relative to the planet and the spacecraft stability with respect to its roll axis during the encounter period. It was anticipated that the spacecraft would be traveling at a speed of about 0.02 deg/sec with respect to the planet and that spacecraft roll rate is not more than 0.03 deg/sec. The searching and tracking speed of 0.5 deg/sec is selected to satisfy these requirements.
3. A planet tracking accuracy of ± 1 deg is specified to meet the television mission requirements.
4. The system is required to have an operating temperature range of -40 to $+75$°C.

The mission restraints and the effects of space environments impose severe requirements on the design of the system. As a guide to the system design, the various requirements were established in the following specifications:

1. Functional Specification, *Mariner C* Spacecraft Flight Equipment, Planetary Scan
2. Design Specification, *Mariner C* Flight Equipment, Planetary Scan Subsystem
3. Design Specification, *Mariner C* Flight Equipment, Planetary Scan System, Power Supply Unit

To obtain a system with a high probability of accomplishing its mission, the following major guidelines are also established in the system design:

1. Simplify the design by the incorporation of devices with minimum number of components consistent with the design requirements.
2. Perform positive logical decisions and identification prior to each critical operational execution.
3. Incorporate systemal redundancies to improve the system reliability.

III. SYSTEM DESIGN

A. Determination of System Configuration

The concept of planetary scan originated on previous *Mariner* programs and a system (Ref. 1) was designed. In this system, the planet-oriented experiment instruments were mounted on a platform which was attached to a boomlike structure. Digital servo systems were used to control the platform position about two scan axes. This system was designed to operate in a spacecraft where weight and power could be amply allocated to the system. Because of the limited weight and power allowed, a new system was designed and developed to be compatible with the *Mariner* Mars 1964 mission requirements.

For the system, a split phase, synchronous, ac motor was selected as a prime mover to rotate the instrument platform. The ac motor was chosen because of its simple construction, light weight and small volume and because it can be operated reliably in space environment as indicated by past experiences. Power required to operate this motor is much less than that for the digital and other

types of motors. An electrooptical system is designed to drive the motor and control the direction of the motor drive during planet searching and tracking operations. Since the motor operates at a fixed constant speed, correction of error in platform positioning is done by discontinuous or "driving or not driving" operation. The use of an on-and-off system is particularly attractive since the full output power is produced at the lowest correctable error after the no-correction dead zone is exceeded. Output power is required at only a few constant levels; therefore only a relatively simple source of power is needed. By eliminating proportional amplifying devices at high power levels, a lighter and simpler control system can be designed. It is seen that an on-and-off system possesses advantages in size and simplicity over a system designed to do the same task on a linear basis.

Figure 1 shows the basic block diagram of the system. The system is divided into the position error measuring device, compensating network, on-and-off element and servomotor and output load as shown. A positioning error signal $\mathcal{E}$ is obtained by comparing the actual controlled position variable θ_o at the output to the reference position input θ_i. The compensating network transforms the error signal $\mathcal{E}$ to a control signal C. The characteristics of the on-and-off element are shown in Fig. 2a. The element initiates either positive or negative correction depending on the algebraic sign of the control signal C. In the

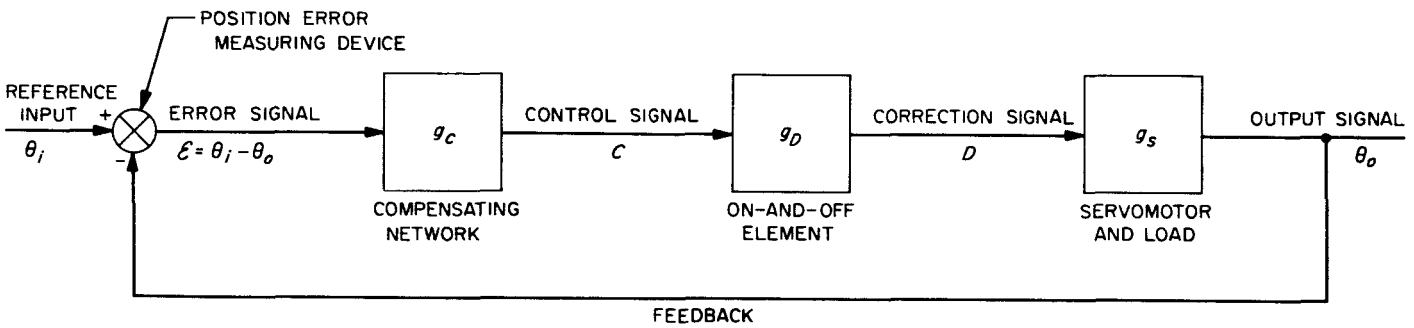

Fig. 1. System basic block diagram

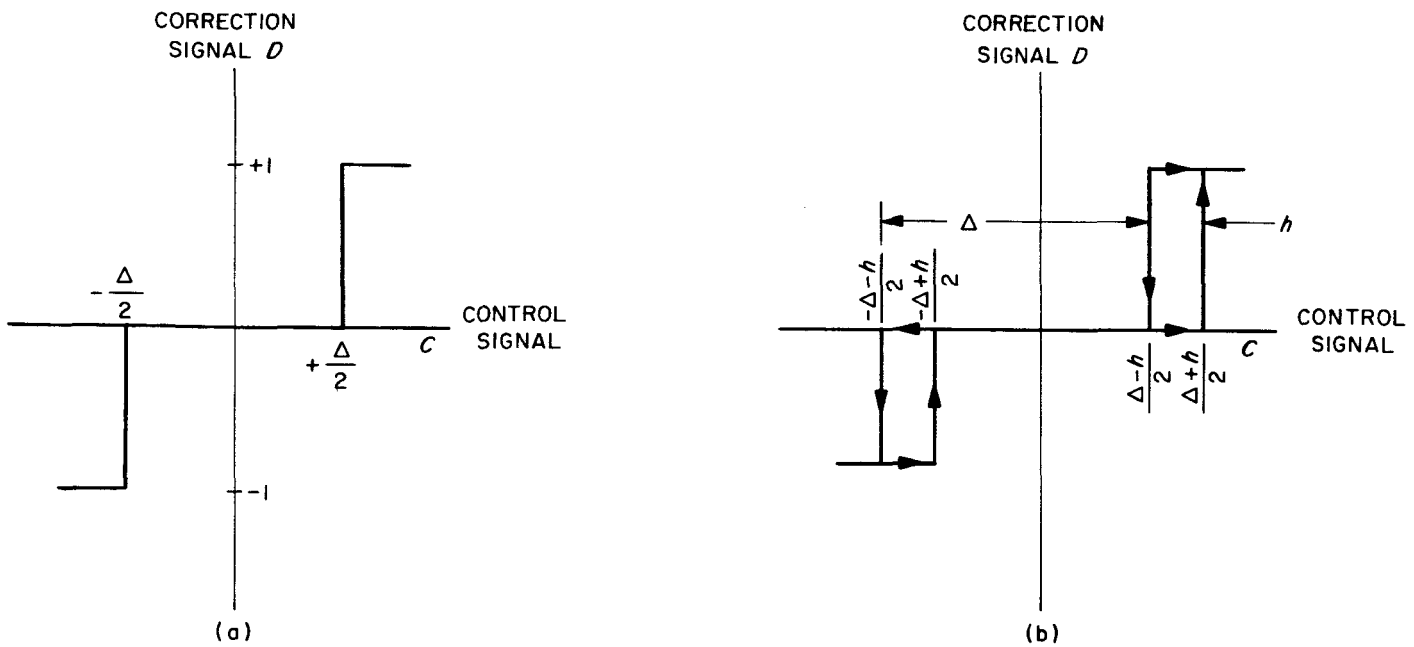

Fig. 2. Characteristics of on-and-off element

inactive or dead zone Δ, no corrective action is taken and the correction signal D is zero. The inactive zone is incorporated to improve the system dynamic stability necessary for the on-and-off operation.

To show that the on-and-off control system is suitable for the application and to determine the various system parameters required to meet the design objectives, the system is analyzed in terms of system stability and the degree of stability.

B. System Design Analysis

1. System Stability

It can be assumed that all the devices except the on-and-off element are linear and a linear transfer function is obtainable for each device. Because of its nonlinear characteristic, the on-and-off element cannot be represented directly by a linear transfer function and the usual linear design technique cannot be used. The frequency response method using a describing function approach in dealing with nonlinear systems has been employed by Johnson and Kochenburger (Refs. 2 and 3). This method approximates the resulting response of the nonlinear element to a sinusoidal input by its fundamental Fourier component. A describing function is used to represent the amplitude and phase angle of the fundamental component.

The transfer function of the servomotor and output load as shown in Fig. 1 is $g_s(S)$:

$$g_s(S) = \frac{\theta_o(S)}{D(S)} = \frac{R}{S(1+\tau S)} \tag{1}$$

where

$\theta_o(S)$ = Laplace transform of the output θ_o

$D(S)$ = Laplace transform of the correction signal D

R = Motor constant output speed

τ = Motor and load time constant

$S = j\omega = j2\pi f$

The characteristics of two of the commonly employed compensating networks are shown in Figs. 3a and 3b and can be expressed in terms of transfer functions $g_c(S)$:

$$g_c(S) = \frac{C(S)}{\mathcal{E}(S)} = \frac{1+j\omega\tau_a}{1+j\omega\dfrac{\tau_a}{\alpha}} \qquad \text{for Fig. 3a} \tag{2}$$

$$g_c(S) = \frac{1+2f_1 j\left(\dfrac{\omega}{\omega_1}\right)-\left(\dfrac{\omega}{\omega_1}\right)^2}{1+2f_2 j\left(\dfrac{\omega}{\omega_2}\right)-\left(\dfrac{\omega}{\omega_2}\right)^2} \qquad \text{for Fig. 3b} \tag{3}$$

where

$C(S)$ = Laplace transform of the control signal C

$\mathcal{E}(S)$ = Laplace transform of the error signal $\mathcal{E}$

$$\tau_a = R_1C_1$$

$$\alpha = 1 + \frac{R_1}{R_0+R_1}$$

$$\omega_1 = \left(\frac{1+R_3/R_2}{\tau_1\tau_2}\right)^{1/2}$$

$$\omega_2 = \frac{1+(R_0+R_1+R_3)/R_2}{\tau_1\tau_2}$$

$$f_1 = \frac{R_2(\tau_1+\tau_2)}{2\omega_1(R_2+R_3)}$$

$$f_2 = \frac{R_2(\tau_1+\tau_2)+R_0\tau_1}{2\omega_2(R_0+R_1+R_2+R_3)}$$

$$\tau_1 = R_3C_3 = R_1C_1$$

$$\tau_2 = \frac{L_2}{R_2}$$

Since $g_c(S)$ and $g_s(S)$ are linear and dependent on the applied frequency ($S = j\omega$), they can be combined to form a frequency variant loop transfer function $g(S)$

$$g(S) = g_s(S) \cdot g_c(S)$$

To simplify the analysis, a dimensionless notation is used as employed by Kochenburger. A convenient base quality such as time base t_b seconds is selected. The variables having the same dimensions are divided by the base quality to form a dimensionless value such as $\phi = t/t_b$. The transfer functions in terms of the dimensionless quality become:

$$g_c(ju) = \frac{1}{ju(1+ju)} \tag{4}$$

$$g_s(ju) = \frac{1+ju\rho_a}{1+ju\dfrac{\rho_a}{\alpha}} \qquad \text{for network in Fig. 3a} \tag{5}$$

$$g(ju) = g_c(ju) \cdot g_s(ju) \tag{6}$$

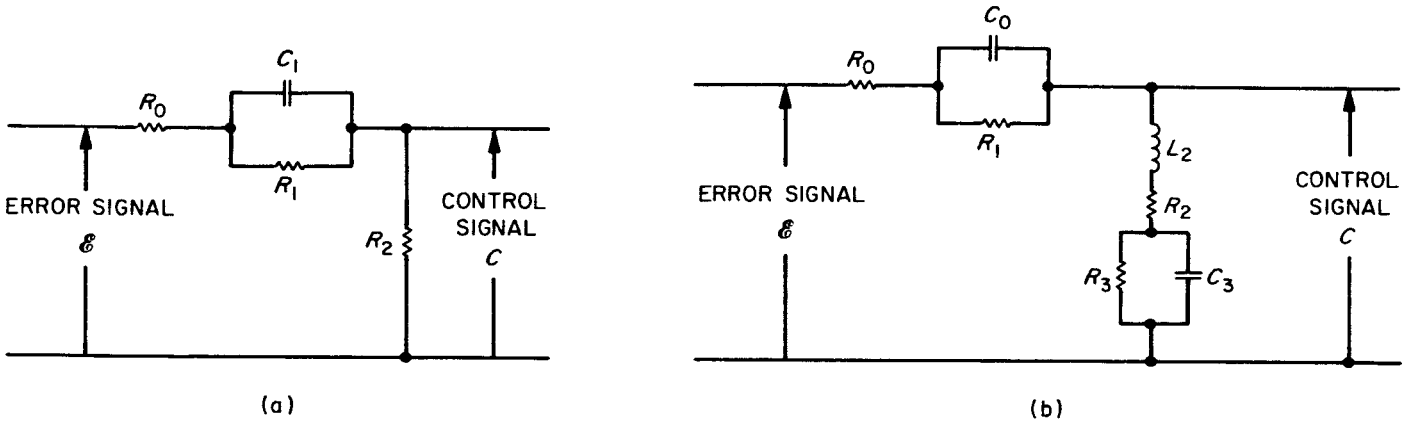

Fig. 3. System compensating network

where

$t_b = \tau$ = Time base

$B = R_\tau$ = Signal base

$u = \omega\tau$

$\rho_a = \tau_a/\tau$

The characteristics of the motor are such that the control signal required to initiate correction is greater than that necessary to cease correction, and a hysteresis effect is produced. Such hysteresis effect affects the dynamic stability of the system and must be included. The characteristic of the on-and-off element as shown in Fig. 2a is revised to include a hysteresis zone h as shown in Fig. 2b. Figure 4a shows the sinusoidal input control signal C with C_0 as the average component and C_1 as the maximum amplitude. Figure 4b shows the resultant correction signal D with $2\beta_1$ as the width of the positive pulse and $2\beta_2$ as the width of the negative pulse; α_1 and α_2 are the phase lags associated with $2\beta_1$ and $2\beta_2$. The on-and-off element will start a positive correction when $C = \Delta/2 + h/2$, stop correction when $C = \Delta/2 - h/2$; start a negative correction when $C = -\Delta/2 - h/2$ and stop correction when $C = -\Delta/2 + h/2$.

The correction signal D can be represented by a dc average term, first harmonic component and higher order harmonic components. Since the contribution of higher order harmonics is small, the correction signal D is represented only by the dc average term D_0 and first harmonic component D_1.

$$D = D_0 + D_1 \cos(u\phi + \angle D_1)$$

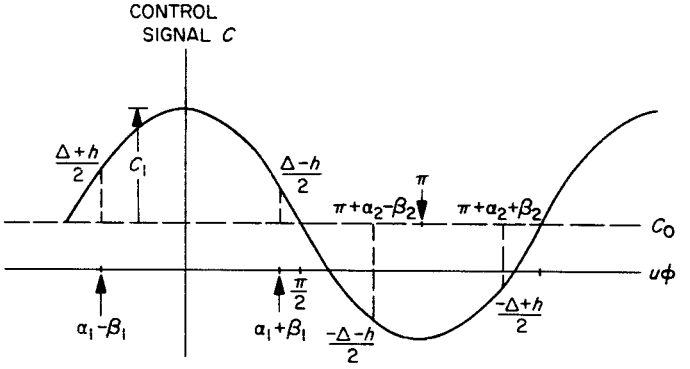

(a) SINUSOIDAL CONTROL SIGNAL AT INPUT OF ON-AND-OFF ELEMENT

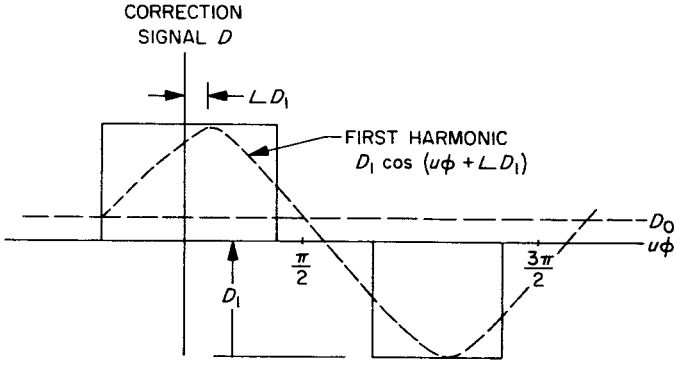

(b) RESULTANT CORRECTION SIGNAL AT THE OUTPUT

Fig. 4. Control and correction signal

where

$$D_1 = \frac{2}{\pi}\left[\sin^2\beta_1 + \sin^2\beta_2 + 2\sin\beta_1\beta_2\cos(\alpha_1 - \alpha_2)\right]^{1/2}$$

$$\angle D_1 = -\tan^{-1}\frac{\sin\alpha_1\sin\beta_1 + \sin\alpha_2\sin\beta_2}{\cos\alpha_1\sin\beta_1 + \cos\alpha_2\sin\beta_2}$$

To determine the relative stability of the system, only the steady-state response needs to be considered here. Under the steady-state condition $D_0 = 0$, $\beta_1 = \beta_2$, $\alpha_1 = \alpha_2$, $D_1 = (4/\pi) \sin \beta_1$ and $\angle D_1 = \angle - \alpha_1$. The describing function of the nonlinear element g_D as indicated in Ref. 4 is

$$g_D = \frac{D}{C} = \frac{4}{\pi} \frac{\sin \beta_1}{C_1} \angle -\alpha_1 \tag{7}$$

where

$$\beta_1 = \frac{1}{2}\left[\cos^{-1}\frac{\Delta - h}{2C_1} + \cos^{-1}\frac{\Delta + h}{2C_1}\right] \tag{8}$$

$$\alpha_1 = \frac{1}{2}\left[\cos^{-1}\frac{\Delta - h}{2C_1} - \cos^{-1}\frac{\Delta + h}{2C_1}\right] \tag{9}$$

The system is now considered containing all linear components and the linear design technique can now be used.

$$\frac{\psi}{\sigma}(ju) = \frac{g^{-1}(ju) + g_D}{g_D} \tag{10}$$

where

$$g^{-1}(ju) = \frac{1}{g(ju)}$$

$\psi = \theta_i/B$ = Input position signal in dimensionless form

$\sigma = \theta_o/B$ = Output position signal in dimensionless form

To determine the system stability, polar plots of $g^{-1}(ju)$ and $-g_D$ are constructed and the intersection of these two plots determines the conditions of stability. To show whether the system is stable without having to use a compensating network, the calculations are made by setting $g_c(ju) = 1$. For the motor under consideration, the output speed is $R = 0.5$ deg/sec. The motor and load time constant is $\tau = 0.8$ sec. Since the inactive zone is the range in which no corrective action is made, it should be selected so that its value is compatible with the ultimate planet tracking accuracy. A value of ⅕ deg is selected for the design. The characteristics of the motor are such that the control signal must decrease to zero volt before corrective action ceases. Therefore, the hysteresis of the system is also $h = \Delta = ⅕$ deg.

With the numerical values of all the variables now selected, $g^{-1}(ju)$ as a function of the frequency u and $-g_D$ as a function of the control signal amplitude C_1 are calculated, plotted on Fig. 5. The loci of the two curves intersect at $C_1 = 0.55$. According to the Nyquist system stability criteria, operation on the amplitudes $C_1 > 0.55$ is stable. Unstable operation with oscillation of increasing amplitude occurs when $C_1 < 0.55$. Operation at $C_1 = 0.55$, a self-sustained oscillation at a frequency of $u = 1.25$, is maintained since operation at the intersection corresponds to the borderline condition of stability. The frequency of oscillation is $f = u/2\pi\tau = 0.25$ cps (for $u = 1.25$ and $\tau = 0.8$ sec) at the intersection.

To improve the system stability, a compensating network as shown in Fig. 3a is now included in the system. The numerical value of the attenuation factor α must now be selected; α must have a relatively high value in order to become effective as a phase-lead network. However, a high value of α transmits high-frequency noise, therefore practical compromise must be made. Plotting loci curves of various trial values indicated that $\alpha = 7.25$ and $\rho_a = 0.59$ provides the system with good stability characteristics. Figure 5 shows the loci with the compensating network included. It is seen that the $g^{-1}(ju)$ and $-g_D$ loci no longer intersect and self-sustained oscillations would not occur.

2. Degree of Stability

With the compensated network incorporated, the system was found to be stable. However, an indication of stability alone is inadequate since any transient oscillation following the correction of the disturbance should involve sufficient damping. The degree of stability is important in determining the system performance. For the degree of stability, the peak value M_p of the output-to-input ratio must now be determined

$$M = \frac{\theta_o}{\theta_i} = \frac{\sigma}{\psi}(ju)$$

$$\frac{\sigma}{\psi}(ju) = \frac{g_D}{g^{-1}(ju) + g_D} \tag{11}$$

In Fig. 6, g_D is represented by the vector **QO**, $g^{-1}(ju)$ by the vector **OP** and $g^{-1}(ju) + g_D$ by **QO** + **OP** = **QP**. For a given value of C_1 the length of **QO** is constant and the maximum value of M or M_p over the frequency range is

$$M_p = \frac{QO}{(\mathbf{QP})_{min}} \tag{12}$$

The minimum length of **QP** is found by drawing an arc of shortest possible radius tangent to the frequency response locus. The values of M_p and u_p as functions of C_1

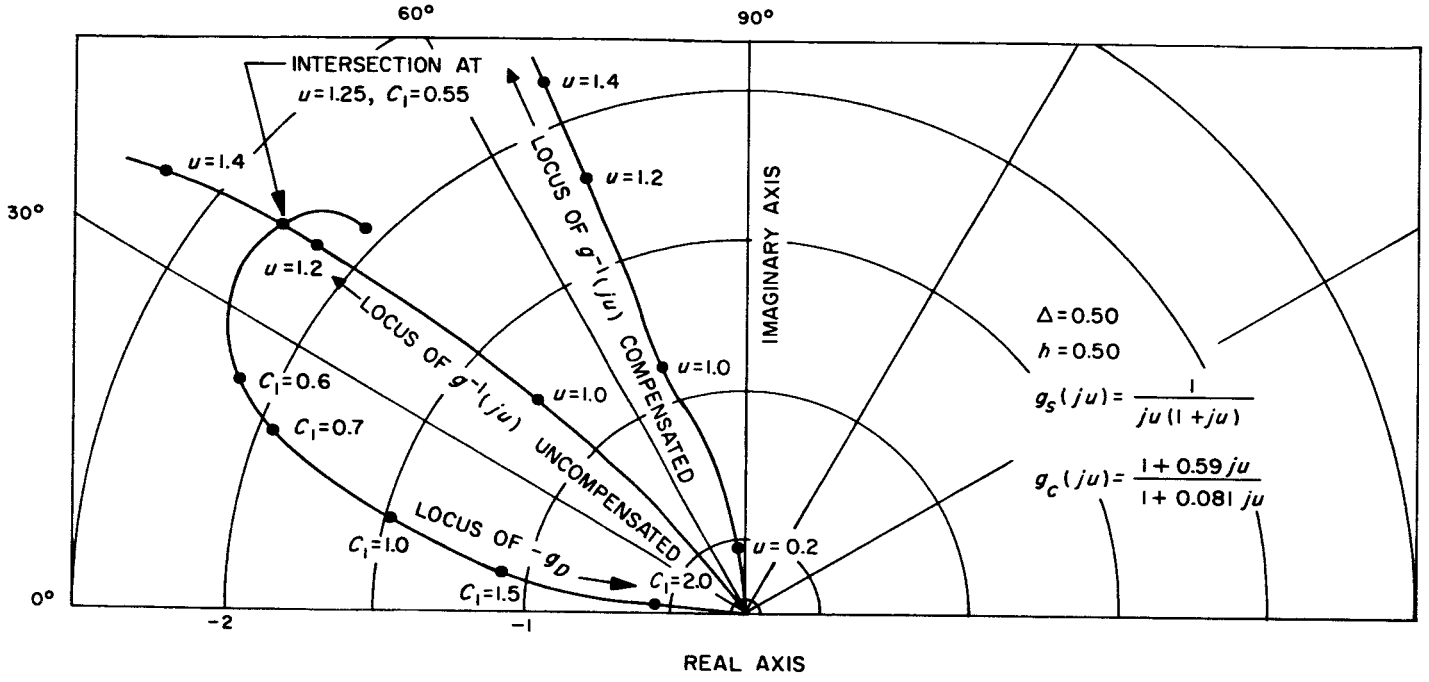

Fig. 5. Frequency and amplitude loci diagram

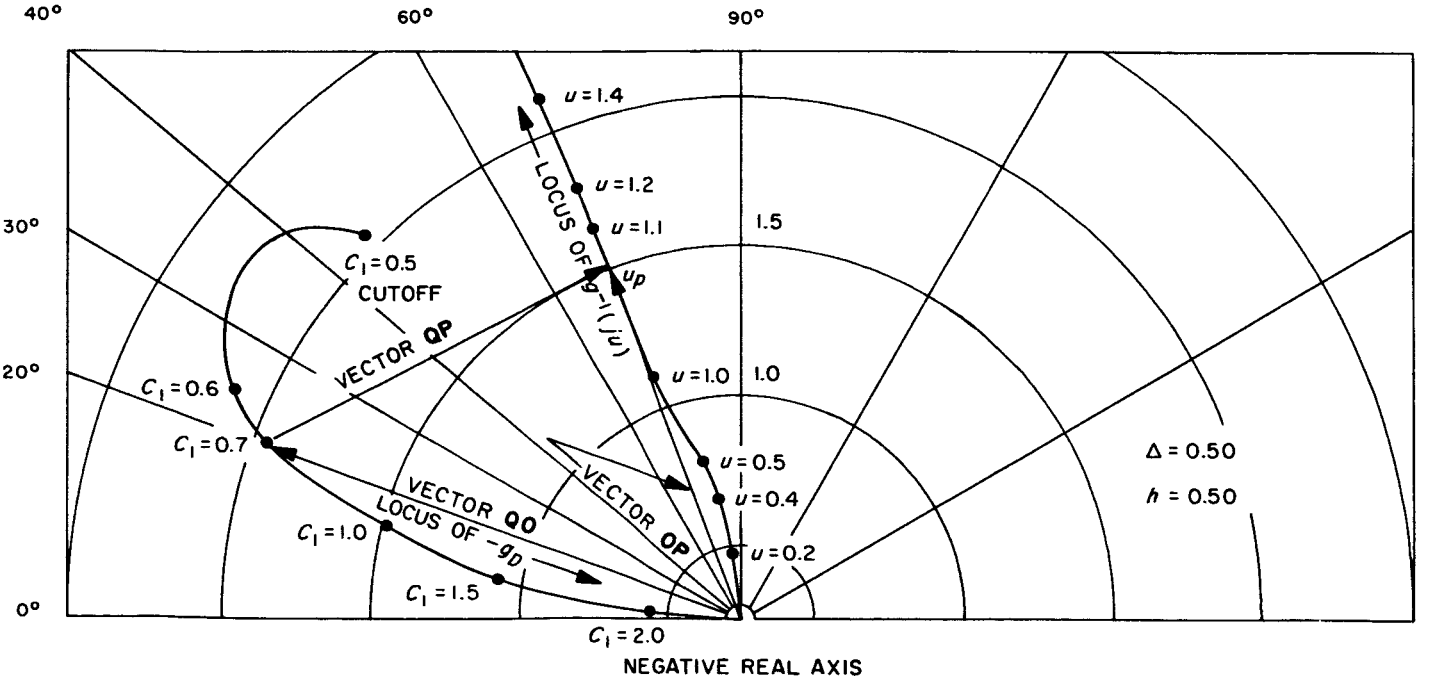

Fig. 6. Diagram for determination of M_p and u_p

provide an indication of the degree of stability. It was found that (for the type of system considered) M_p having a numerical value of 2 to 3 near the cutoff point and 1.3 for higher values of C_1 provides a satisfactory degree of stability.

The values of M_p and u_p as a function of C_1 were calculated and plotted as shown in Fig. 7; M_p was found to be 2.5 at cutoff and 1.20 at $C_1 = 1.0$. Based on criteria discussed, the system with the compensated network incorporated should be adequately stabilized.

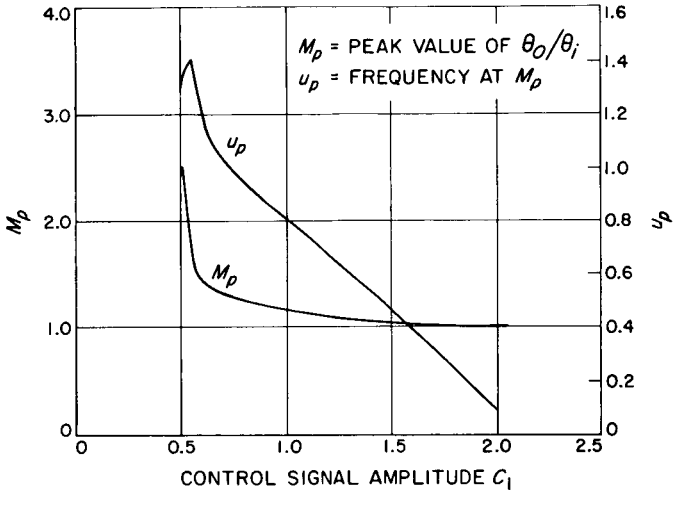

Fig. 7. M_p and u_p vs. C_1 for system relative stability determination

C. System Description

The system in the form of a functional block diagram is shown in Fig. 8. This system is developed based on the concept of using an on-and-off element with a compensating network to provide the mechanism for planet searching and tracking. The system performs four major operations: planet searching, planet detection, planet tracking and scan inhibit.

1. Planet Searching

When the system is energized, a signal from a one-shot multivibrator presets all logic circuits and initiates the planet searching operation. Searching is accomplished by placing a positive dc voltage at the output of the x-axis filter. This voltage, supplied by the searching driver, is phase-detected with a reference signal derived from the 400-cps fixed motor driving signal shifted 90 deg in phase. The phase-detected signal, 90 deg out of phase with the fixed motor driving signal, is amplified and used as the directional driving signal. The system scans 180 deg

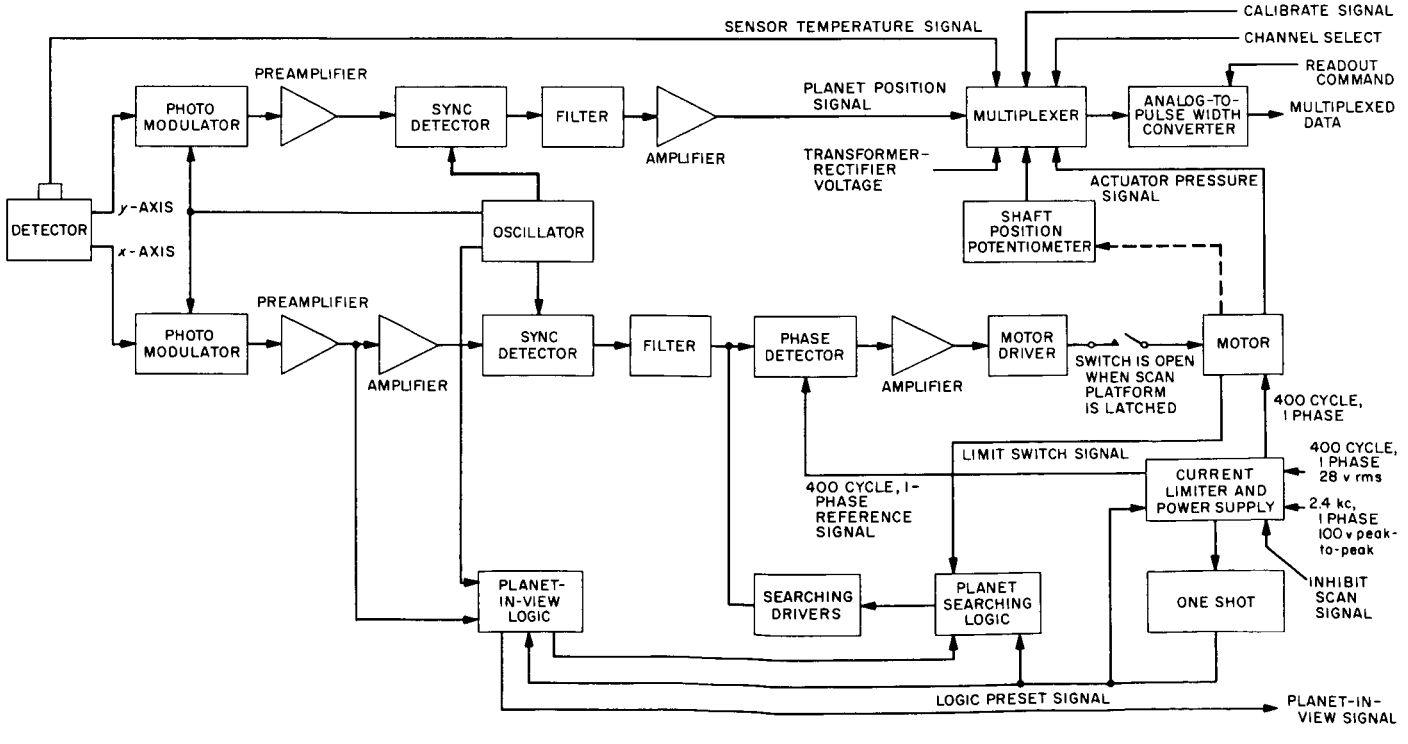

Fig. 8. System functional block diagram

in the process of searching for the planet. Upon completion of each 180-deg search, the motor drive is reversed by the following steps:

a. The planet searching logic is reset by a wave-shaped and noise-filtered signal initiated by limit switch action.

b. A dc voltage of proper polarity is applied to the x-axis filter by the searching driver. A positive dc voltage is used for counterclockwise motor drive and a negative dc voltage is used for clockwise drive.

c. The dc voltage is converted to an ac signal, the phase of which is dependent upon the polarity of the dc voltage. A positive dc voltage is converted to an ac signal which is 90 deg out of phase with the reference signal, and a negative dc voltage is converted to an ac signal which is 270 deg out of phase with the reference signal. The ac signal is then amplified and applied to the motor as the directional drive signal.

2. Planet Detection

A radiation detector is used to detect the presence and location of the planet. When the planet is in view of the detector, a pair of signals is generated to indicate the location of the planet with respect to the spacecraft. The x-axis output is used as the error signal for planet tracking while the y-axis output determines the angular position of the planet with respect to the detector mount. Both signals are modulated by a pair of oscillator-driven modulators prior to entering the preamplifier and amplifier. A pair of synchronous detectors are used to demodulate these signals before filtering. At the output of the preamplifier, the x-axis signal is sampled by the planet-in-view logic where noise filtering and planet signal identification are performed. A planet-in-view signal for the purpose of data mode switching is delivered to the data automation system for processing and at the same time the searching driver is inhibited, thus changing the system from searching to tracking mode.

3. Planet Tracking

The x-axis output after demodulation, filtering and phase-lead compensation is used as a platform positioning error signal to initiate motor driving action. The magnitude and polarity of the positioning error signal are dependent upon the planet position relative to the line-of-sight of the wide angle detector and TV camera optics. When this signal exceeds the inactive zone limits, platform motion is initiated to track the planet and to minimize the positioning error to within the required planet tracking accuracy. The motor driver and associated circuits, being commonly employed in both searching and tracking operations, perform the same functions while tracking.

The filtered y-axis output signal is amplified and converted from a bipolar to a unipolar signal. This signal, together with the platform position output and other signals, is time-multiplexed and analog-to-pulse-width-converted before transmission to the data automation system for processing.

4. Scan Inhibit

A scan inhibit signal is initiated either by ground command, the TV camera or the narrow angle Mars gate which is mounted on the platform. The signal indicating that the planet is in the field of view of the television is used to stop the scanning and tracking motion of the platform prior to television picture data recording. The scan trace across the planet after planet tracking motion has stopped is dependent upon the tracking angle at the time of scan inhibit and upon the relative motion of the spacecraft on its trajectory as it sweeps across the surface of the planet.

To implement the design, a system was developed consisting of three basic types of equipment: (1) the radiation detector and optics, (2) the electronics and (3) the motor assembly and its associated scan platform.

IV. DETAILED DESIGN AND SYSTEM DEVELOPMENT

A. Radiation Detector and Optics

The presence and relative position of the planet is to be detected by a radiation detector. The detector senses radiation from the planet and transforms the radiant energy into an electrical signal indicating the planet position as well as the amount of radiation received. The requirements imposed on the detector are:

1. A definite spectral range of sensitivity corresponding to the assumed spectral radiance characteristics of the planet
2. The achievement of a high radiant-to-electrical energy conversion efficiency through the proper combination of characteristics of the optical system and detector
3. A definite relationship between the detector electrical output and the magnitude and relative position of the radiation source

The planet can be detected through the sensing of either the planet's black-body radiation in the far infrared spectrum range of 10 to 40 μ or the planet's reflected solar energy in the visible and near infrared spectrum range of 0.4 to 2.0 μ. A detector sensitive in the far infrared region can be utilized for this purpose, but predetection modulation of the infrared signal (usually by mechanical chopping) is required for effective detector operation. At present, infrared detectors of practical application also require active cooling to achieve the desired responsivity. Detectors of the photoconductive type can be used to detect radiation in the visible and infrared regions. For precision planet position and intensity indications, such detectors require highly regulated power supplies to provide bias for their operation. Thermocouple detectors with the proper filters can also be used to sense radiation in the visible and infrared regions. Complications arise in the design of the electronic circuitry required to handle an extremely small output signal from the thermocouple.

To overcome some of these difficulties, a p–n junction silicon detector was chosen. Since the reflected solar radiation from the planet contains 95% of its energy at wavelength shorter than 2 μ, silicon with an absorption edge at 1.8 μ is considered suitable for the application. The output of this detector is self-generating and no bias supply is required. Without bias, the output is obtained with zero volt as reference and predetection chopping of the incoming radiation is not needed as compared with a biased detector which requires signal chopping to separate the signal from the bias voltage.

1. Carrier Collection and Spectral Response

It is known that the performance characteristics of a p–n junction detector are dependent upon its fabrication material, physical geometry, and electronic parameters. An analysis of the effects of these parameters (Ref. 5) showed that the carrier collection efficiency and relative spectral response of the detector, $\eta_c(\lambda)$, can be obtained by

$$\eta_c(\lambda) = \eta_n(\lambda) + \eta_p(\lambda) \tag{13}$$

where

$\eta_n(\lambda)$ = p-layer efficiency

$$\eta_n(\lambda) = \frac{1}{h(\lambda)\left\{1 - \left[\frac{1}{L_n h(\lambda)}\right]^2\right\}}\left\{\frac{\beta_n}{L_n}\exp\left(\frac{a}{L_n}\right) - \frac{\gamma_n}{L_n}\exp\left(-\frac{a}{L_n}\right) - h(\lambda)\exp\left[-h(\lambda)a\right]\right\} \tag{14}$$

$\eta_p(\lambda)$ = n-layer efficiency

$$\eta_p(\lambda) = \frac{1}{h(\lambda)\left\{1 - \left[\frac{1}{L_p h(\lambda)}\right]^2\right\}}\left\{\frac{\beta_p}{L_p}\exp\left(\frac{a}{L_p}\right) - \frac{\gamma_p}{L_p}\exp\left(-\frac{a}{L_n}\right) - h(\lambda)\exp\left[-h(\lambda)a\right]\right\} \tag{15}$$

$$\beta_n = \frac{[\delta + h(\lambda)] \exp\left(-\frac{a}{L_n}\right) - \left(\delta + \frac{1}{L_n}\right) \exp[-h(\lambda)a]}{\left[\delta + \frac{1}{L_n}\right] \exp\left(\frac{a}{L_n}\right) - \left(\delta + \frac{1}{L_n}\right) \exp\left(-\frac{a}{L_n}\right)}$$

$$\gamma_n = \frac{\left[\delta - \frac{1}{L_n}\right] \exp[-h(\lambda)a] - [\delta + h(\lambda)] \exp\left(-\frac{a}{L_n}\right)}{\left(\delta + \frac{1}{L_n}\right) \exp\left(\frac{a}{L_n}\right) - \left(\delta - \frac{1}{L_n}\right) \exp\left(-\frac{a}{L_n}\right)}$$

$$\beta_p = \frac{h(\lambda) \exp\left[\frac{a}{L_p} + h(\lambda)l\right] - \frac{1}{L_p} \exp\left[\frac{l}{L_p} + h(\lambda)a\right]}{\frac{2}{L_p} \cosh\left[\frac{l}{L_p} - \frac{a}{L_p}\right]}$$

$$\gamma_p = \frac{-h(\lambda) \exp\left[\frac{a}{L_p} - \frac{h(\lambda)}{l}\right] - \frac{1}{L_p} \exp\left[\frac{l}{L_p} - h(\lambda)a\right]}{\frac{2}{L_p} \cosh\left[\frac{l}{L_p} - \frac{a}{L_p}\right]}$$

$$\delta = \frac{e}{S_r KT} \mu_n$$

L_n = Diffusion length of free electronics, cm

L_p = Diffusion length of free holes, cm

S_r = Surface recombination rate, cm-sec^{-1}

$h(\lambda)$ = Absorption coefficient as a function of incident wavelength λ (Ref. 4)

μ_n = Mobility of electrons, cm^2-v^{-1}-sec^{-1}

μ_p = Mobility of holes, cm^2-v^{-1}-sec^{-1}

l = n-layer thickness, cm

a = p-layer thickness, cm

K = Boltzmann constant

T = Temperature, °K

e = Electronic charge

It is seen from Eqs. (13), (14) and (15) that proper values for the various parameters can be selected reasonably to match the spectral response of the detector to that of the radiation source. Such a detector is considered capable of converting the incident energy to electrical signal efficiency. To select the proper values for the various parameters, Eq. (13) was solved for a number of cases using an IBM 7094 Computer. Figures 9a and 9b show the resultant p-layer collection efficiency $\eta_n(\lambda)$ and n-layer collection efficiency $\eta_p(\lambda)$ for a detector having a thickness of 5×10^{-2} cm with the various junction depths as the parameters. It is seen that $\eta_n(\lambda)$ starts to rise at longer wavelengths for a deep junction than for a shallow junction. Therefore, a detector with a deep junction uses the infrared radiation more efficiently. However, the over-all efficiency decreases as the junction depth increases. For a deep junction, a considerable percentage of electron–hole pairs are generated near the surface and away from the junction. These minority carriers are not capable of contributing to the junction current because of the recombination process taking place at the surface and inside the p-layer. The p-layer should be made as thin as possible for high collection efficiency in the short and medium wavelength regions. However, the series resistance of the p-layer increases as the junction depth decreases, resulting in a reduction in the efficiency improvement.

Figure 9b shows that quite a large number of carriers are generated in the n-layer by radiation penetrated through the p-layer. To see the effects of the diffusion length and lifetime of the carrier on the n-layer collection efficiency, the dotted line curves in Fig. 9b were generated by assuming the diffusion length of the holes to be 10^{-4} cm instead of 10^{-2} cm. It is seen that the collection efficiency is considerably reduced because of the decrease in diffusion length. To obtain high collection efficiency, therefore, the diffusion length of the n-layer must have a relatively high value. Figure 9c shows the detector collection efficiency $\eta_c(\lambda)$.

$$\eta_c(\lambda) = \eta_p(\lambda) + \eta_n(\lambda)$$

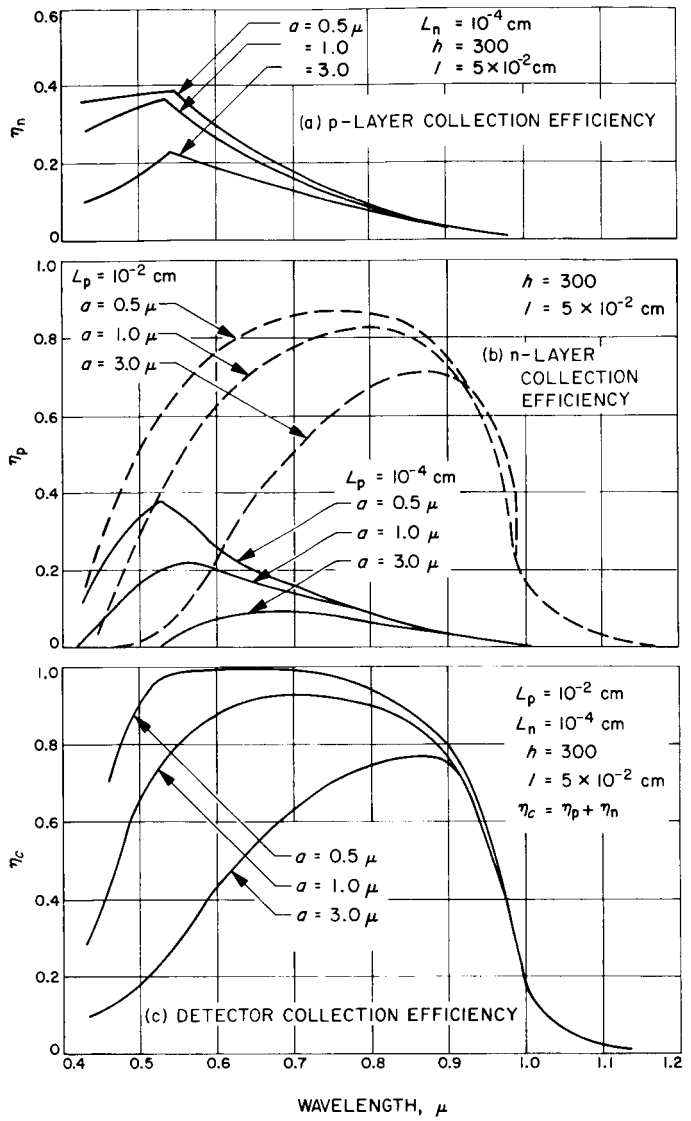

Fig. 9. Detector collection efficiency as a function of wavelength

To establish the over-all radiation collection efficiency for the detector, a number of factors need to be considered. When the radiation is incident upon the detector, some of it is reflected. Also, when the photons absorbed have more energy than is necessary for the generation of electron–hole pairs, the excess energy contributes to lattice vibration and is dissipated as heat. The energy needed for the photon–electron interaction is a function of the energy gap of the material. For every value of the energy gap, an absorption band edge is obtained beyond which the photon energy is not sufficient to create electron–hole pairs and the detector will be transparent to the photons. For a silicon detector, incident photons having a wavelength exceeding 1.0 or 1.1μ will transmit through the detector without interacting with the structure at all. With the various factors taken into consideration, the over-all radiation collection efficiency is

$$\eta(\lambda) = [1 - r(\lambda)]\{1 - \exp[1 - h(\lambda)\, l]\}\, \eta_c(\lambda) \qquad (16)$$

where

$$r(\lambda) = \frac{(n_d - 1)^2 + \left[\frac{\lambda \cdot h(\lambda)}{4\pi}\right]^2}{(n_d + 1)^2 + \left[\frac{\lambda \cdot h(\lambda)}{4\pi}\right]^2} \qquad (17)$$

$r(\lambda)$ = Relative reflectivity as a function of incident wavelength λ

n_d = Refractive index of the detector

$(1 - \exp)[1 - h(\lambda)\, l]$ = Factor accounting for incomplete radiation absorption

$\eta_c(\lambda)$ = Carrier collection efficiency as shown in Eq. (13)

In Eq. (16) $\eta(\lambda)$ was calculated and plotted as Curve 2 on Fig. 10. This curve was generated with $r(\lambda)$ as the reflectivity curve having the value of 4.1% at 0.5μ, zero % at 0.7μ and 6.5% at 1.0μ (Ref. 6). The numerical values chosen for the various detector parameters are:

$$L_n = 1.0 \times 10^{-4} \text{ cm}$$
$$L_p = 2.5 \times 10^{-2} \text{ cm}$$
$$l = 5 \times 10^{-2} \text{ cm}$$
$$a = 0.7\ \mu$$
$$\mu_n = 1200 \text{ cm}^2 \cdot \text{v}^{-1} \cdot \text{sec}^{-1}$$
$$\mu_p = 500 \text{ cm}^2 \cdot \text{v}^{-1} \cdot \text{sec}^{-1}$$
$$S_r = 2 \times 10^4 \text{ cm} \cdot \text{sec}^{-1}$$
$$\delta = 300 \text{ cm}^{-1}$$

2. Physical Description and Detector Output Characteristics

The detector having a calculated spectral response $\eta(\lambda)$, Curve 2 of Fig. 10, was fabricated with a useful area having 1.00-in. diameter. Two straight lines at right angles to each other are chemically etched on the surface of the detector to form four electrically isolated equal area quadrants. The depth of the etches is such that the top layer, including the junction, is physically

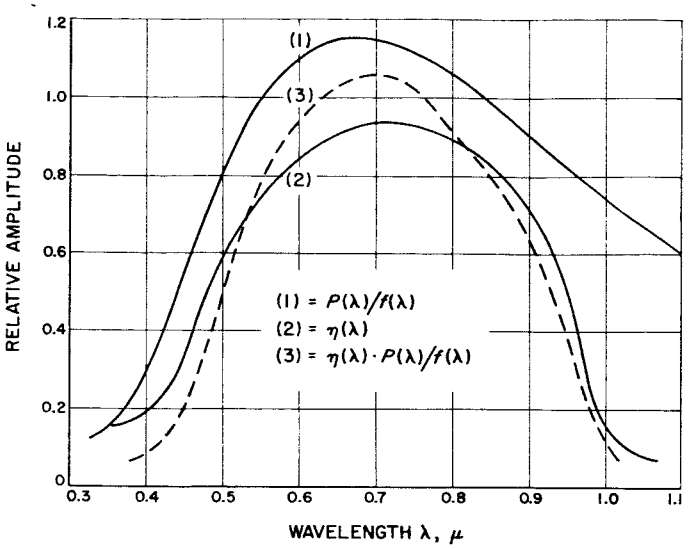

Fig. 10. $P(\lambda)/f(\lambda)$ and $\eta(\lambda)$ as a function of wavelength

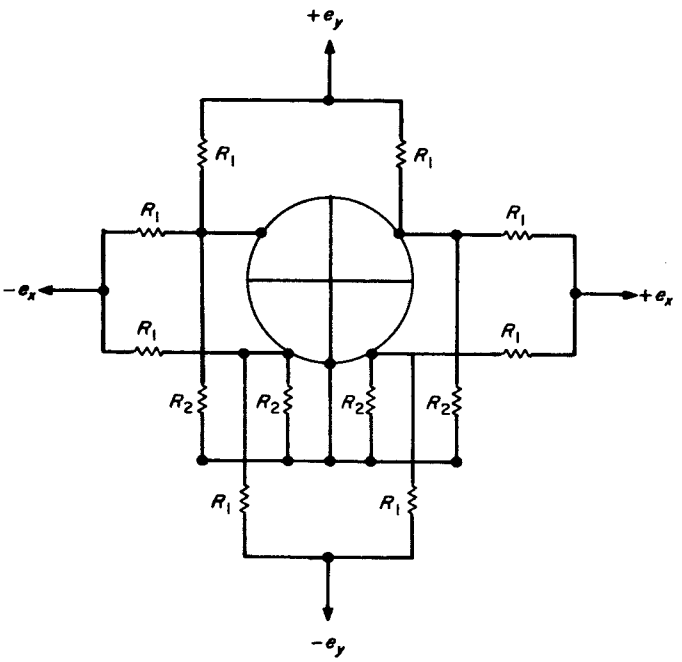

Fig. 11. Detector output resistive matrix

separated from the bottom layer. The two output differential voltage pairs, each formed by taking the outputs of the adjacent quadrants through a resistor matrix, are shown as e_x and e_y in Fig. 11.

The operational concept of the detector is such that the planet image is bisected by the adjacent quadrants and a null point is indicated when each quadrant receives equal energy and the detector outputs are nulled to zero volt. Since the signals of the adjacent pairs are balanced out, the differential signal indicates the angular deviation of the planet position from the null axis.

The detector output voltages e_x and e_y are related to the various parameters as follows:

$$e_x, e_y = [1 - R(\theta)]\,[J(\theta, \beta, \phi)] \cdot \delta(\theta) \cdot E(d, \alpha, \lambda) \cdot H \tag{18}$$

where

$$R(\theta) = \tfrac{1}{2}\left\{\left[\frac{n^2\cos\theta - (n^2 - \sin^2\theta)^{1/2}}{n^2\cos\theta + (n^2 - \sin^2\theta)^{1/2}}\right]^2 + \left[\frac{\cos\theta - (n^2 - \sin^2\theta)^{1/2}}{\cos\theta + (n^2 - \sin^2\theta)^{1/2}}\right]\right\}$$

$R(\theta)$ is the Fresnel coefficient of reflection for unpolarized incident energy as a function of incident angle θ

$$J(\theta, \beta, \phi) = \frac{1}{\pi}\left[k_1^2\cos^{-1}(q/\beta_1) + \cos^{-1}(k - q) - 2\cos^{-1}k_2\right]$$

$$- \frac{1}{\pi}[q\,(k_1^1 - q^2)^{1/2} + (k_2 - q)]\,[1 - (k_2 - q)^2]^{1/2} - 2k_2\,(1 - k^2)^{1/2}$$

$J(\theta, \beta, \phi)$ is the factor relating planet angular semidiameter β, optical angular half field of view ϕ and planet position angle θ

$$q = \frac{k_1^2 + k_2^2 - 1}{2k_2} \qquad k_1 = \frac{\tan\theta}{\tan\beta} \qquad k_2 = \frac{\tan\theta}{\tan\beta}$$

$\delta(\theta) = [1 - \sin 2\theta]$

$\delta(\theta)$ = Factor due to vignetting effect of the optics

H = Detector responsivity

The input energy $E(d, \alpha, \lambda)$ from the planet can be calculated by assuming the planet has the spectral radiance property $P(\lambda)/f(\lambda)$ as shown on Curve 1 of Fig. 10:

$$E(d, \alpha, \lambda) = \frac{E_v \cdot \phi(\alpha) \cdot A \cdot K(\alpha)}{\Delta^2 d^2} \int_{\lambda_1}^{\lambda_2} \frac{P(\lambda)}{f(\lambda)} \eta(\lambda) \tau(\lambda) \, d\lambda \tag{19}$$

where

$E_v = 1.52 \times 10^{-11}$ watt-cm^{-2}-μ^{-1} = monochromatic energy flux at $\lambda = 0.55$ μ corresponding to visual albedos $\alpha = 0$ deg, $\Delta = 1$, $d = 1$

α = Phase angle (Sun–planet–system angle)

$\phi(\alpha)$ = Phase function = 0.406 when $\alpha = 60$ deg

A = Aperture area of the optics = $\pi d/4 = 1.32$ cm^2 for $d = 1.3$ cm

$\tau(\lambda)$ = Transmission efficiency of the optics

$K(\alpha)$ = Illuminated fraction of the planet at phase angle $\alpha = \frac{1}{2}(1 + \cos \alpha)$

d = Distance from planet to the system, A.U.

Δ = Mean distance from planet to Sun, 1.524 A.U.

$P(\lambda)$ = Assumed planet spectral reflectivity

$f(\lambda)$ = Spectral energy function of solar energy

λ_1, λ_2 = Cutoff wavelengths of the system

$\eta(\lambda)$ = Spectral response of the radiation detector as calculated by Eq. (16)

Then e_x, e_y as a function of the planet position θ with the planet angular semidiameter as the parameter was calculated and plotted in Fig. 12. It is seen that the magnitude and polarity of e_x, e_y can be used to determine the position of the planet image with respect to the detector axis, and the magnitude of e_x and e_y can be used to determine the amount of energy received at a distance at which the planet is considered to have an apparent semidiameter of β. Subsequently, e_y was used to indicate the planet position while e_x was used as error signal for planet tracking.

3. Optical System

The planet angular diameter, when viewed at the closest operating distance of 9,000 km, is approximately 41 deg. To accommodate a full field of view of the planet, the optical system must have an optical view of greater than 41 deg. An optical system having an f number of $f/2.3$, a focal length of 30 mm and a circular field of view of 50 deg was chosen. This optical system, when operating at a distance of 9,000 km, formed a planet image of 0.89 in. in diameter. Therefore, the detector, having a sensitive area of 1.000-in. diameter and an overall diameter of 1.125 in., was chosen to accommodate the full field of view of the planet over the entire operating distance range.

The measured transmission efficiency of the lens $\tau(\lambda)$ as a function of the incident wavelength is shown in Fig. 13. The vignetting effect was calculated and is shown in Fig. 14. As a comparison, the measured vignetting curve of the lens is also shown in the same figure.

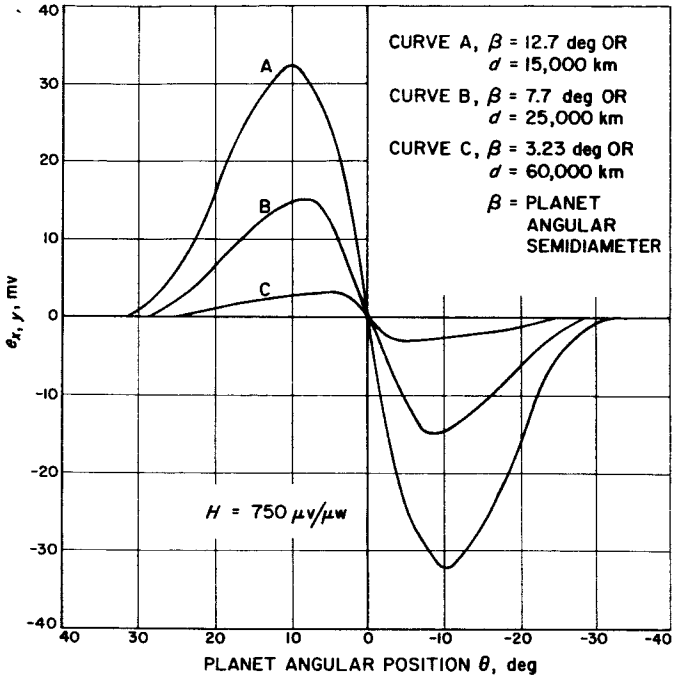

Fig. 12. Calculated detector output as a function of planet angular position

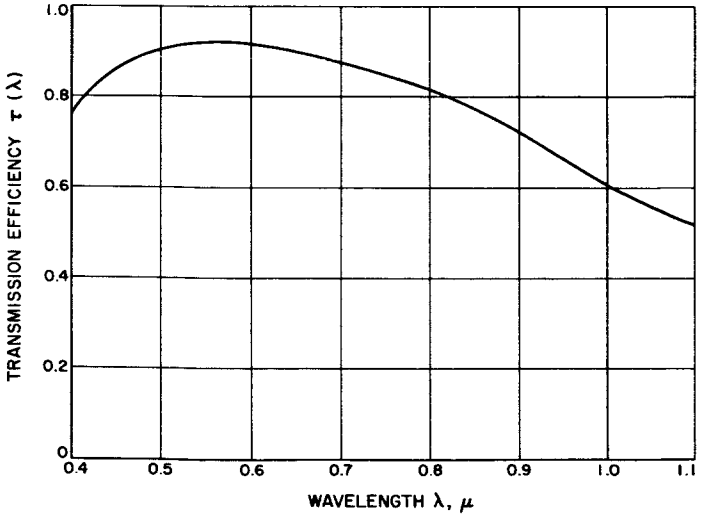

Fig. 13. Optical transmission efficiency as a function of wavelength

B. Electronics

1. Signal Modulation

To simplify the design requirements of the electronic amplification circuitry, the dc outputs of the detector are converted to ac signals by a pair of photomodulators, each consisting of a pair of small neon lamps and a matched pair of cadmium selenide photocells. Then,

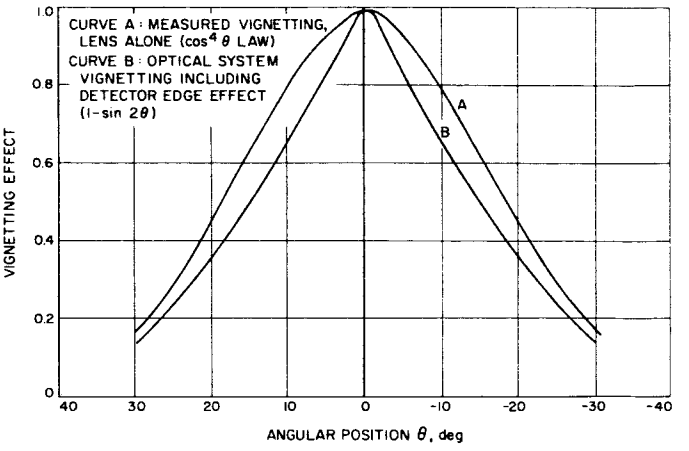

Fig. 14. Optical vignetting effect

amplifying the resultant signal with high-gain, low-noise ac amplifiers can be more readily accomplished. This method of modulation was chosen for its simplicity and reliable operation. It also produces extremely low offset voltages over the required temperature range. Because the photocell's dark-to-light resistance ratio is very high, the photomodulator provides high modulation efficiency. Each pair of lamps is connected in parallel for redundancy and an oscillator is used to provide signals to drive the lamps.

The oscillator frequency was selected to satisfy two conditions: (1) simplicity of amplifier design sets a low-frequency limit, and (2) the photocell time constants impose a high-frequency limit. Based on these considerations, a value of 24 cps was chosen as the oscillator frequency to satisfy both conditions. It is well known that higher than nominal breakdown voltage is required to fire the neon lamp in darkness or after long duration in the nonconducting state in darkness, because the time required for the gas ionization increases when the lamps are pulse fired in the dark. The ionization time can be reduced through the use of a radioactive additive. To further insure proper operation, an applied voltage in excess of the static breakdown voltage was used to fire the lamps.

2. Preamplifiers

The modulated x- and y-axis outputs were amplified by a pair of four-stage ac preamplifiers of identical design. The preamplifier was designed to have a relatively high input impedance to match the operating conditions of the photomodulators. A field-effect transistor was used in the first stage. The input impedance of this transistor is essentially that of a reverse-biased junction and is therefore very high. For the remaining three amplification

stages, 2N930 and 2N1132 transistors were used to take advantage of the transistor's low-noise characteristics. The final design of the preamplifier circuit is shown in Fig. 15a, and its equivalent circuit is shown in Fig. 15b. The preamplifier having an input impedance of 3 megohms is determined primarily by input resistor R_1 since the input impedance to the field-effect transistor is much greater than the resistive value of R_1. The closed loop voltage gain of the preamplifier is

$$A_v = \frac{A_1 A_2}{1 + A_1 A_2 \beta_f} \tag{20}$$

where

$$A_1 = \frac{R_L g_m}{1 + R_L g_m \dfrac{R_s}{R_L}}$$

$$A_2 = \frac{\left(R_3 + Z_2 - \dfrac{Z_2^2}{R_1 + Z_2}\right) A_2'}{\left(R_3 + R_5 + Z_2 - \dfrac{Z_2^2}{R_1 + Z_2}\right) - \left(\dfrac{R_5 Z_2}{R_1 + Z_2}\right) A_2'}$$

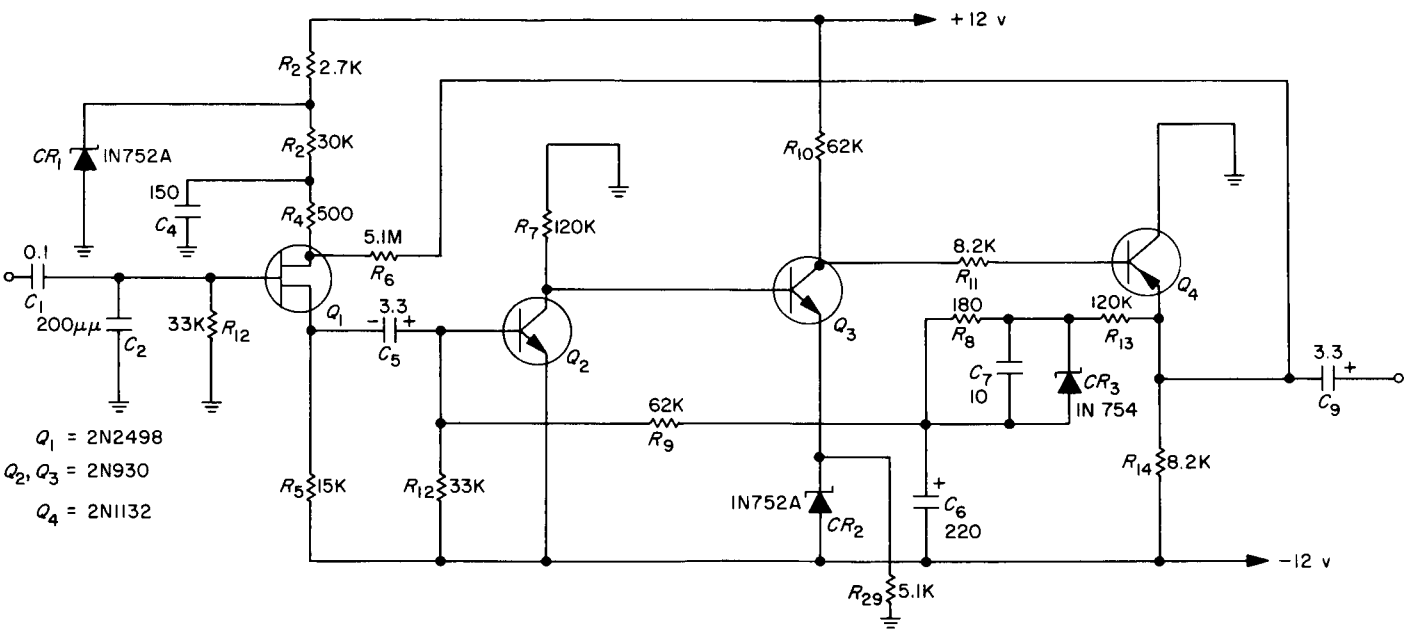

(a) CIRCUIT SCHEMATIC

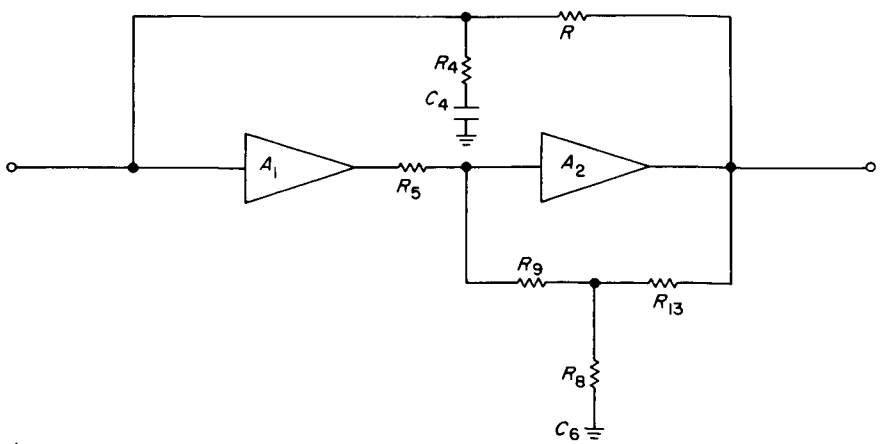

(b) EQUIVALENT CIRCUIT

Fig. 15. Preamplifier

A_v = Closed loop voltage gain of the preamplifier

A_1 = Voltage gain of the first stage

A_2 = Closed loop voltage gain of last three stages

A_2' = Open loop voltage gain of last three stages

β_f = Preamplifier feedback factor $\dfrac{R_4 - j\dfrac{1}{\omega C_4}}{R_6}$

$Z_2 = R_8 - j\dfrac{1}{\omega C_6}$

With the proper values of the various parameters as shown in Fig. 15a substituted into Eq. (20), the gain of the preamplifier was calculated to be

$$A_v = 8300 \angle 5.96°$$

for

$R_L = 15$ kohms

$R_S = 500$ ohms

$g_m = 2750$ μmhos

$A_2' = -6500$

$f = 24$ cps

The actual voltage gain of the preamplifier when measured over the operating temperature of −30 to +70°C is 8000 ±2.5% as compared to the calculated gain of 8300.

3. x-Axis Amplifier

The x-axis output is bandpass-filtered and further amplified by a three-stage, zener-coupled ac amplifier. The incorporation of zener diodes as the coupling elements has the advantages of minimizing the loss of gain, elimination of the need for large coupling or bypass capacitors and providing stable operation over a wide temperature range due to the temperature-compensating effects of the diodes. Figure 16a shows the amplifier circuit and bandpass filter, and Fig. 16b shows the equivalent circuit. The bandpass filter was designed to attenuate noise having frequencies higher and lower than the center frequency of the 24 cps signal. Figure 17 shows the noise discrimination characteristics of the filter. The voltage gain of the amplifier is:

$$A_3 = \frac{A_f\left(R_9 + Z_8 - \dfrac{Z_8^2}{R_7 + Z_8}\right)A_3'}{\left(R_9 + R_{10} + Z_8 - \dfrac{Z_8^2}{R_7 + Z_8}\right) - \left(\dfrac{R_{10}Z_8}{R_7 + Z_8}\right)A_3'} \tag{21}$$

where

A_3 = Closed loop gain of the amplifier including the filter attenuation

A_3' = Open loop gain of the amplifier

A_f = Attenuation factor of the filter as shown in Fig. 17.

$Z_8 = R_{11} - j\dfrac{1}{\omega C_4}$

With the values of the various parameters as shown in Fig. 16a substituted into Eq. (21), the gain of the amplifier was calculated to be

$$A_3 = 1040 \angle 6.2°$$

for

$A_3' = 15{,}000$

$A_f = 0.78$

$f = 24$ cps

4. Signal Demodulation and Phase Compensation

The 24-cps x- and y-axis signals are then separately demodulated, filtered and converted to dc signals by the use of the synchronous detectors and three-stage RC filter networks. A simple synchronous detector using a field-effect transistor as chopping element is as shown in Fig. 18 together with a three-stage RC filter network. A signal derived from the oscillator is utilized as the gate driving voltage so that the demodulated dc output has the same polarity as the detector output signal. The ac-to-dc conversion gain of the demodulator is 0.48 v dc/v rms.

Factors affecting and contributing to the offset of a field-effect transistor have been analyzed in Ref. 7. The offset voltage $V_o(T)$, as a function of the operating temperature and other parameters, can be determined by

$$V_o(T) = \frac{[R_D + R_{ds}(T)]\, I_{GS}(T)}{\eta_D} \tag{22}$$

where R_D is the input resistance to the demodulator as shown in Fig. 18; $R_{ds}(T)$ is the drain-to-source resistance as a function of the operating temperature; $I_{GS}(T)$ is the gate reverse current as a function of temperature and η_D is the chopping efficiency. For transistor 2N2498 operating at a drain current of 100 μa, $R_{ds}(T)$ has a numerical value of 400 ohms at −40°C, 800 ohms at

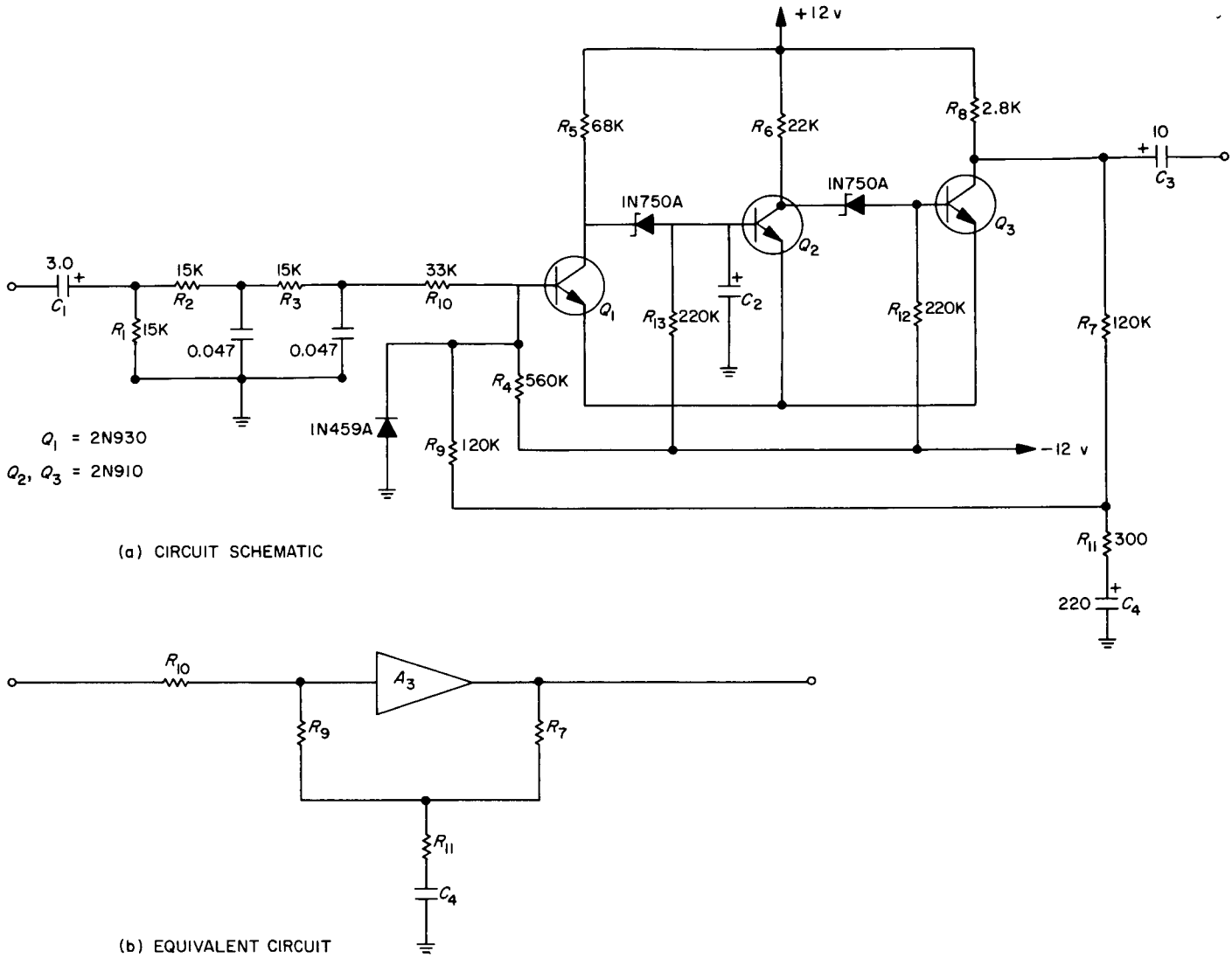

Fig. 16. x-Axis signal amplifier

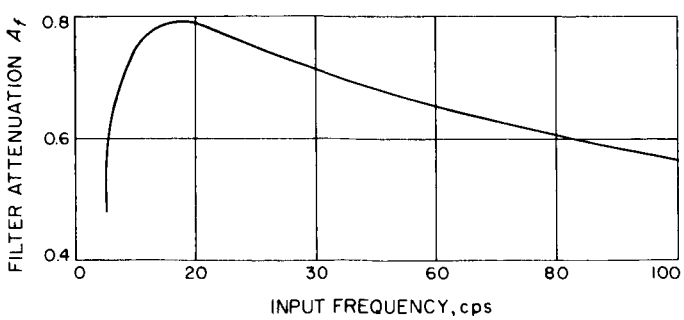

Fig. 17. x-Axis signal amplifier band pass filter characteristics

+25°C and 1.12 kohms at +75°C. The gate cutoff current I_{GS} when the transistor is operating at a gate-to-source voltage of 10 v has a value of 0.0001 μa at −40°C, 0.005 μa at 25°C and 0.05 μa at +75°C. The chopping efficiency is 35% for a sine wave gate drive and better than 90% for a square wave gate drive. Since the demodulator is driven by a square wave, η_D is assumed to be 0.90. With the various numerical values substituted into Eq. (22), the offset voltage was calculated to be

$$V_o(T) = 0.61\ \mu v \qquad \text{at } T = -40°C$$
$$V_o(T) = 3.28\ \mu v \qquad \text{at } T = +25°C$$
$$V_o(T) = 346\ \mu v \qquad \text{at } T = +75°C$$

The effect of the demodulator offset voltage on the planet tracking accuracy is negligibly small since the signal level required for motor actuation at this point is 2.65 v.

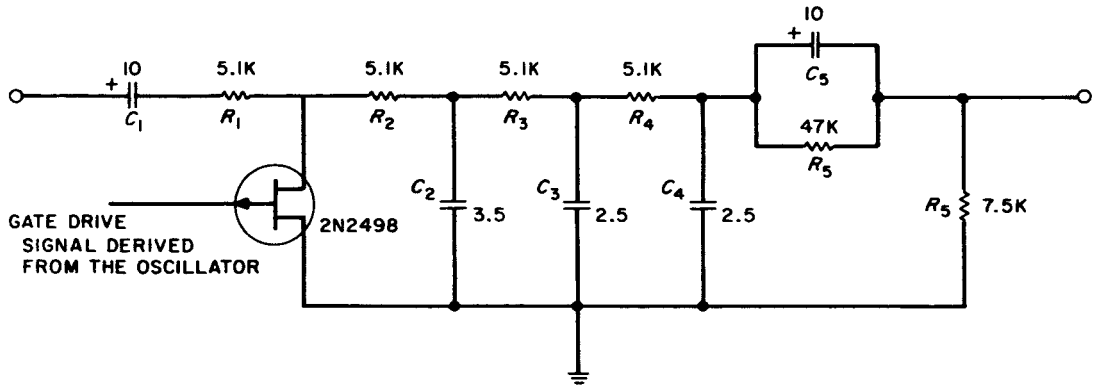

Fig. 18. Synchronous detector, filter and phase-lead compensation network

System design analysis in Section III indicated that without the phase compensation the system is unstable when operating under the condition of $C_1 > 0.55$. With the phase lead compensating network incorporated in the system, the loci of $g^{-1}(ju)$ and g_D no longer intersect and the system is stable. The numerical values of the attenuation factor $\alpha = 7.25$ and $\rho_a = 0.59$ were required for this compensation. To meet these requirements the electrical constants of the network as shown in Fig. 3a are selected as $R_0 = 0$ ohm, $R_1 = 47$ kohms, $R_2 = 7.5$ kohms, $C_1 = 10$ μf. Based on these electrical values and $\tau = 0.8$ sec, ρ_a and α are

$$\rho_a = \frac{\tau_a}{\tau} = \frac{R_1 C_1}{\tau} = 0.587$$

$$\alpha = 1 + \frac{R_1}{R_0 + R_2} = 7.26$$

The signal attenuation in the compensating network is $1/\alpha$ or 0.138.

5. 400-cps Phase Detection

A chopping element is used as the phase detector to convert a positive dc signal to an ac signal. A double emitter transistor (integrated chopper transistor) is selected as the chopping element. This transistor has a low offset voltage V_o. The double emitter transistor consists of a pair of transistors constructed as a single unit. The transistor pair is used in the inverted configuration to obtain low offset voltage. The two transistors in the pair are also closely matched in offset characteristics so that the offset voltages of the pair cancel each other to further reduce the offset.

Figure 19 shows the phase detector. To select the proper operating parameters for the transistor, the offset voltage V_o is analyzed in terms of the base current I_b. The offset voltage V_o is a function of the transistor saturation resistance R_b, and R_b in turn is dependent upon the transistor base driving current I_b. The base current I_b must be sufficiently large to drive the transistor so that

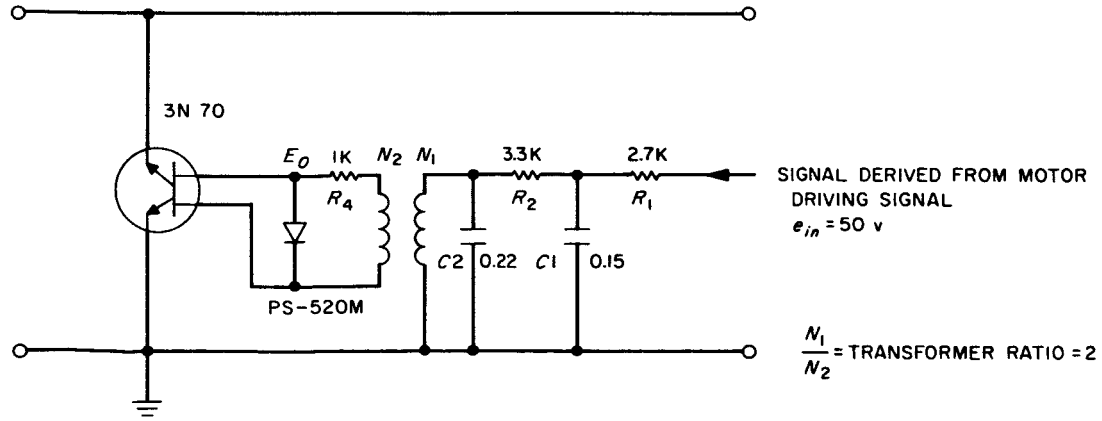

Fig. 19. Phase detector and 90-deg phase shift circuit

R_b is at a low value as shown in Fig. 20. When operating with $I_b = 4$ ma, R_b is 14 ohms and is sufficiently low in value to produce an offset of 250 ± 40 μv over the temperature range of +80 to −25°C. The amount of planet tracking error introduced by the offset voltage when operating with $I_b = 4$ ma is extremely small since the signal amplitude required for motor actuation is 60 mv at this stage.

A phase shift network as shown in Fig. 19 is incorporated. This network is used to supply I_b having the proper phase and amplitude to drive the phase detector. The amount of phase shift can be determined by

$$\frac{e_o}{e_{in}} = \frac{R_3}{(R_1 + R_2 + R_3 - \omega^2 C_1 C_2 R_1 R_2 R_3) + j\left[\omega C_1 R_1\left(R_2 + R_3 + \frac{C_2 R_3}{C_1}\right) + \omega C_2 R_2 R_3\right]} \tag{23}$$

where

$\frac{e_o}{e_{in}}$ = Ratio of the network output to input

$R_3 = (R_4 + R_{in})\left(\frac{N_2}{N_1}\right)^2$

R_{in} = Input impedance of the phase detector = 140 ohms

$\frac{N_2}{N_1}$ = Transformer ratio

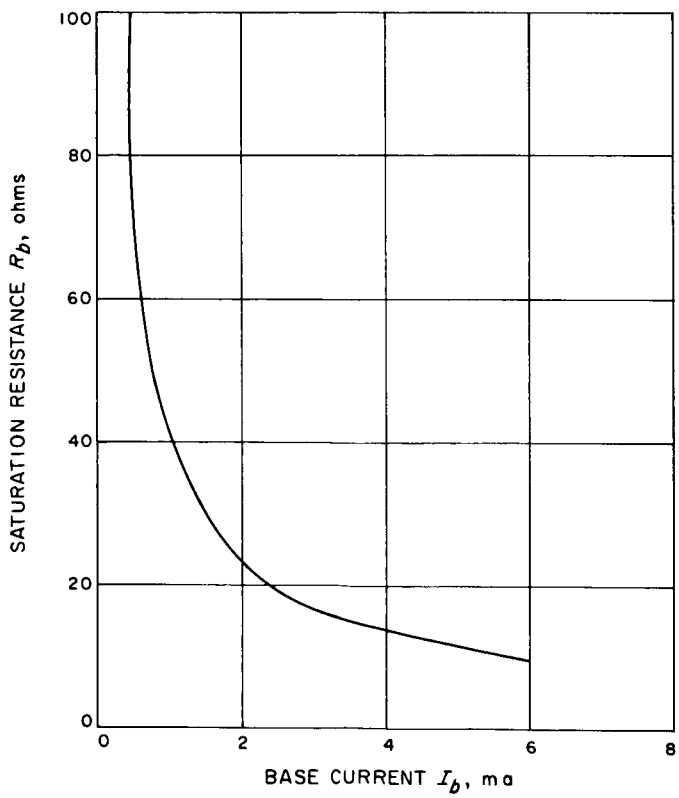

Fig. 20. Double emitter transistor base current as a function of saturation resistance

With the values of the various parameters selected as shown in Fig. 19, the amount of phase shift and network attenuation calculated by Eq. (23) is

$$\frac{e_o}{e_{in}} = 0.194 \angle -85.2°$$

The phase shift of 85.2 deg together with the shift of 5 deg in the motor driving signal amplifiers provides the required 90-deg shift for the phase detector operation. The base current I_b obtained to drive the phase detector is

$$I_b = \frac{0.194 \cdot e_{in}\left(\frac{N_1}{N_2}\right)}{R_3} \tag{24}$$

With the input voltage e_{in} derived from the fixed motor driving signal and having an amplitude of 50 v, the base current I_b calculated by Eq. (24) is $I_b = 4.25$ ma.

6. Motor Driver and Driver Amplifier

The phase detected signal is further amplified by a four-stage driver amplifier with a pair of transistors in a complementary push–pull configuration at its output. The output of this amplifier is then transformer-coupled to a motor drive circuit consisting of a pair of power transistors 2N1050B in a push–pull configuration.

The motor driver and driver amplifier are shown in Fig. 21a. Figure 21b shows the equivalent circuit of the driver amplifier the voltage gain of which can be calculated by Eq. (25):

$$A_4 = \frac{\left(R_{11} + Z_{10} - \frac{Z_{10}^2}{R_9 + Z_{10}}\right) A_4'}{\left(R_{11} + Z_{12} + Z_{10} - \frac{Z_{10}^2}{R_9 + Z_{10}}\right) - \left(\frac{Z_{12} Z_{10}}{R_9 + Z_{10}}\right) A_4'} \tag{25}$$

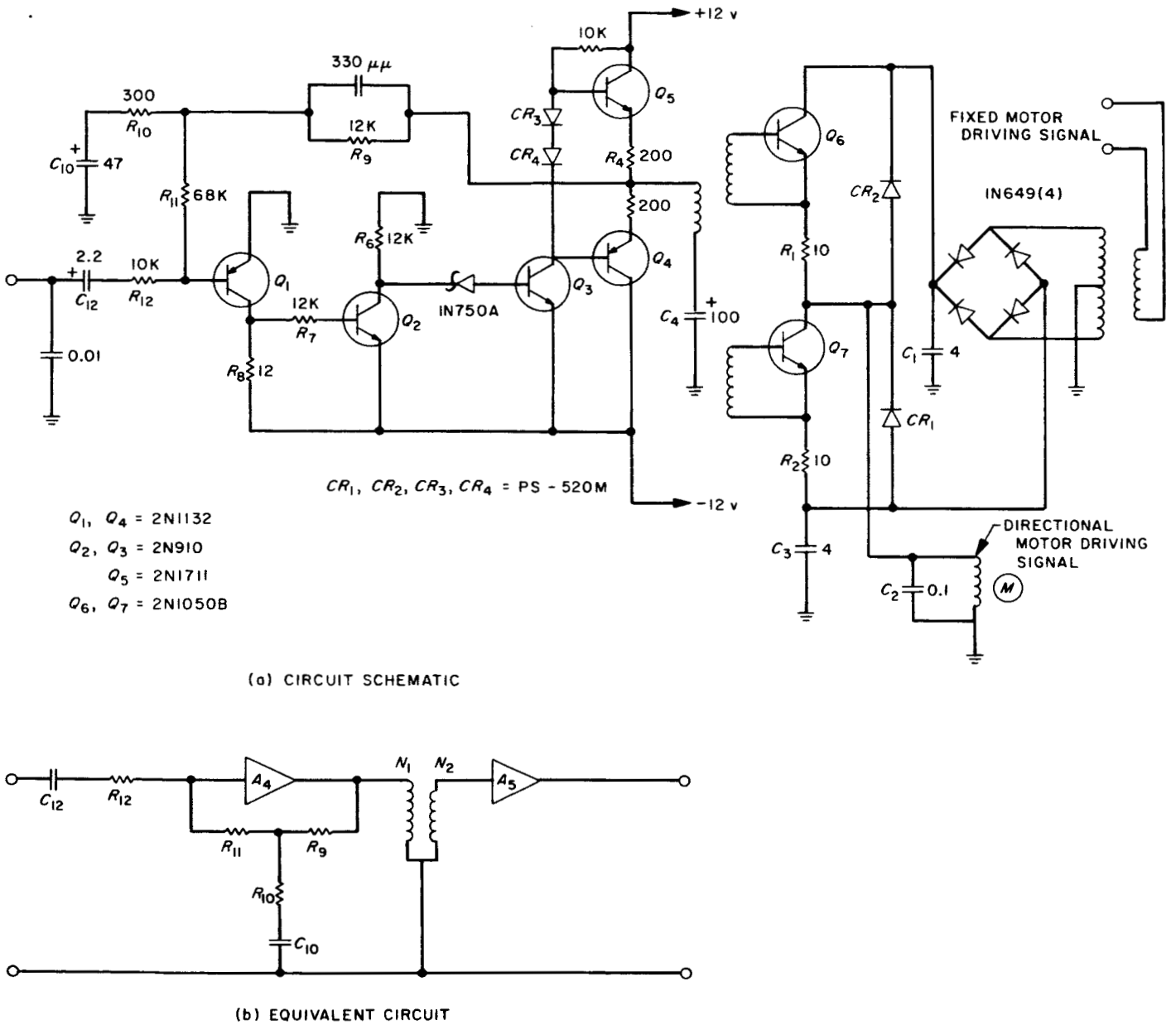

Fig. 21. Motor driver and driver amplifier

where

$$Z_{10} = R_{10} - j\frac{1}{\omega C_{10}}$$

$$Z_{12} = R_{12} - j\frac{1}{\omega C_{12}}$$

A_4' = Open loop voltage gain of the amplifier

A_4 = Closed loop voltage gain of the amplifier

The gain of the driver amplifier when calculated by Eq. (25), with the values of the various parameters as shown in Fig. 21a, is

$$A_4 = 288\angle -2.5° \qquad \text{for } f = 400 \text{ cps}$$

$$A_4' = 25{,}000$$

The measured gain of the actual circuit was 275. The motor driver was also determined to have a gain of 4 with a phase shift of approximately 2.5 deg.

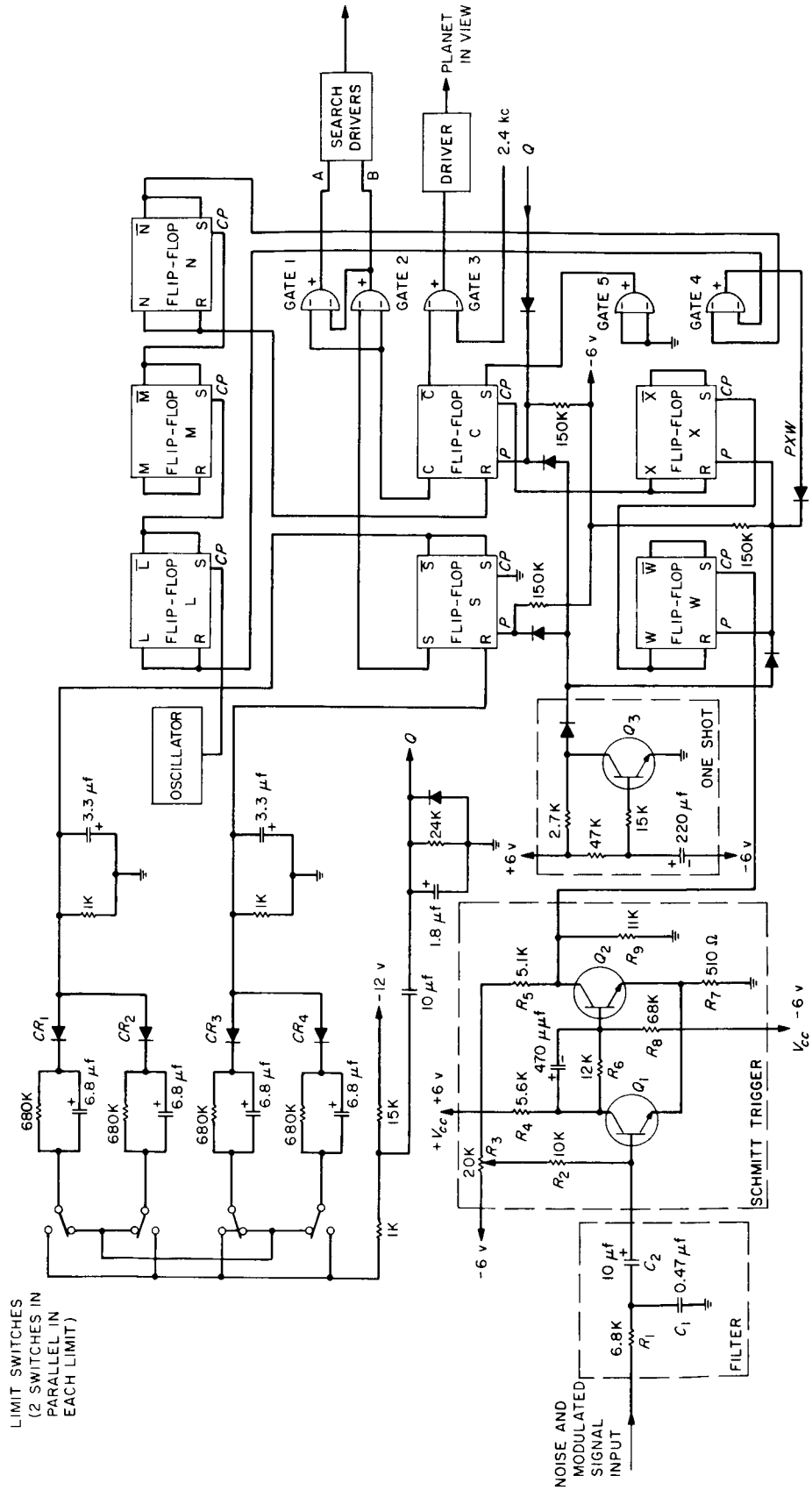

Fig. 22. Threshold and noise discrimination logic circuits

7. Logic and Control Circuits

The planet searching and planet-in-view logic circuits are shown in Fig. 22. Planet searching and tracking operations are controlled by flip-flop C. When the power to the system is applied, a positive going signal from the one-shot circuit presets all the flip-flops to the initiate planet searching operation. This preset signal has a pulse width of 6 sec as determined primarily by the time constant of R_{10} and C_2. The preset pulse with a relatively long pulse width of 6 sec is used to preset the logics and to hold the preset action for the duration of the pulse so that any noise associated with system power turn-on will have no effect on the preset operation. The clockwise and counterclockwise planet searching operations are controlled by flip-flop S. The flip-flop S is in turn being set and reset by the wave-shaped and noise-filtered signals initiated by limit switch action.

When the limit switch is actuated, a negative going pulse having an amplitude of approximately 5.5 v is generated to set or reset flip-flop S. At the same time, a positive going pulse Q as shown in Fig. 22 with an amplitude of about 5.5 v is also generated to set flip-flop C to the planet searching state. Signal Q is used to assure that the system is always operating in the planet searching mode immediately after each scan reversal. To provide redundancy, two limit switches connected in parallel and operated in series are incorporated in each of the two scan reversal limits. Each backup switch is located 2 angular degrees behind the primary switch so that in event the primary switch failed to initiate a scan reversal, the backup switch would be actuated when the scan platform has completed 2 additional angular degrees of travel.

Logic equations for the searching operation are

$$\bar{B} = CS$$

$$B = \bar{S} + \bar{C}$$

$$A = CB = C(\bar{S} + \bar{C})$$

$$A = C\bar{S}$$

$$\bar{A} = S + \bar{C}$$

$$\text{clockwise drive} = AB$$

$$= C\bar{S}(\bar{S} + \bar{C})$$

$$= C\bar{S}$$

$$\text{counterclockwise drive} = \bar{A}\bar{B}$$

$$= (S + \bar{C})(CS)$$

$$= CS$$

Logics A and B as a function of C and S are used to control the search drivers. For a clockwise motor drive, a negative dc voltage having an amplitude of 5 v is generated by the search drivers and applied to the x-axis filter. For a counterclockwise motor drive, a positive dc voltage with an amplitude of 5 v is similarly generated by the search drivers and applied to the x-axis filter.

The planet-in-view logic consists of a signal threshold and noise discrimination logic circuits as shown in Fig. 22. A band pass filter and a Schmitt trigger were used for signal threshold discrimination. The planet signal is bandwidth-limited by the filter and threshold-detected by the Schmitt trigger. A potentiometer R_3 is incorporated to adjust the trigger threshold level. The filter has the characteristics of:

$$\frac{e_o}{e_{in}} = \left[\left(1 + \frac{\tau_1}{\tau_2}\right) + j\left(\omega\tau_1 + \frac{1}{\omega\tau_3} - \frac{1}{\omega\tau_2}\right)\right]^{-1} \tag{26}$$

where

e_o/e_{in} = Ratio of output to input

$$\tau_1 = C_1R_1$$

$$\tau_2 = \frac{C_1Z_{q1}[R_2 + \phi R_3(1-\phi)]}{R_2 + \phi R_3(1-\phi) + Z_{q1}}$$

$$Z_{q1} = \frac{\Delta^h R_{L1} + R_7(1 + \Delta^h + h_{re} + h_{fe}) + R_7R_{L1}h_{oe} + \dfrac{\Delta^h(1 + h_{re}) - h_{re}(h_{fe} - h_{re})}{h_{oe}}}{1 + h_{re} + (R_7 + R_{L1})h_{oe}} \tag{27}$$

$$\Delta^h = h_{ie}h_{oe} - h_{re}h_{fe}$$

$$R_{L1} = \frac{Z_{q2}R_4R_8 + R_4R_8(Z_{q2} + R_8)}{R_4(Z_{q2} + R_8) + Z_{q2}R_8 + R_8(Z_{q2} + R_8)} \tag{28}$$

Z_{q1} is the input impedance of the Schmitt trigger and is related to the circuit components, the input impedance Z_{q2} of transistor Q_2 and the h-parameters of the transistor by Eq. (27). The upper and lower 3-db frequencies, f_1 and f_2, of the network can be determined from Eq. (26) by letting $|e_o/e_{in}|$ equal 0.707 of its value at mid-frequency:

$$\left|\frac{e_o}{e_i}\right| = \frac{0.707\tau_3}{\tau_1 + \tau_3}$$

$$f_1, f_2 = \frac{\left[K^2 + \left(1 - \frac{\tau_1}{\tau_2}\right)^2\right]^{1/2} \pm \left[K^2 - \left(1 - \frac{\tau_1}{\tau_2}\right)^2 - 4\tau_1\left(\frac{1}{\tau_3} - \frac{1}{\tau_2}\right)\right]}{4\pi\tau_1}$$

$$K = \frac{\tau_1 + \tau_3}{0.707\tau_3}$$

$$\Delta f = f_1 - f_2 = \text{Bandwidth of the filter} \tag{29}$$

It is possible to calculate $\Delta f = 120$ cps by Eq. (29) with the numerical values of the various parameters shown in Fig. 23 and $h_{ie} = 1800$ ohms, $h_{oe} = 100$ μmhos, $h_{re} = 2.68 \times 10^{-4}$, $h_{fe} = 15$. The input level V_{in} at which the Schmitt circuit responds can be determined by

$$V_{in} = \frac{V_{cc}(1 + A_i)(R_8 - R_4 - R_6)R_7}{R_8Z_{q2} + (R_4 + R_6)(R_8 + Z_{q2})} + V_{be1} \tag{30}$$

where

$$A_i = \frac{(h_{fe} - h_{re}) - R_7h_{oe}}{1 + h_{re} + (R_7 + R_{L2})h_{oe}}$$

V_{cc} = Power supply voltage to the Schmitt trigger

$$R_{L2} = \frac{R_5R_9}{R_5 + R_9}$$

V_{be1} = Base-to-emitter voltage of transistor Q_1

The input impedance Z_{q2} of transistor Q_2 as a function of the circuit components and h-parameters of transistor Q_2 can be obtained by the use of Eq. (27) with the substitution of R_{L2} in place of R_{L1} on the right hand side of Eq. (27). The proper threshold level is set by adjusting potentiometer R_3 such that the dc biasing level plus noise is less than V_{in}, a condition at which the noise evokes no response from the circuit. The dc biasing level can be determined by the following equation

$$E_{dc} = V_{in} - \gamma(V_n) \tag{31}$$

where E_{dc} is the biasing level, γ is the normalized threshold level as a function of planet detection probability and V_n is the noise level at the filter input. V_{in} with a value of 1.31 v can be calculated by Eq. (30) for $h_{ie} =$ 1800 ohms, $h_{fe} = 15$, $h_{oe} = 100$ μmhos, $h_{re} = 2.68 \times 10^{-4}$ and $V_{be1} = 0.5$ v. This calculated value compared favorably with the measured value of 1.27 v.

The noise discrimination logic consists of a number of flip-flops and gates. A signal from the oscillator having the same frequency as, and either in or 180 deg out of phase with, the modulated x-axis signal is frequency-divided by eight through the use of flip-flops L, M and N. This frequency-divided signal is utilized to control the sampling period with the frequency of 3 cps ($f = 24/8$). Flip-flops X and W are used to count the pulses passing through the Schmitt trigger during each sampling period. If four or more consecutive pulses having the proper spacing are gated per period, flip-flop C changes its state to indicate a planet acquisition. If fewer than four pulses having the proper spacing are gated, flip-flops X and W are reset by the reset pulse

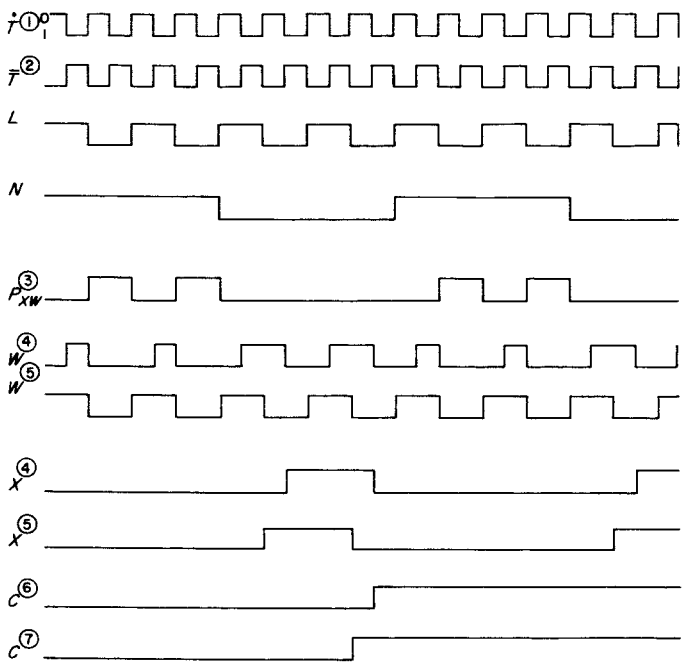

① SIGNAL T FROM SCHMITT TRIGGER WHEN SENSOR SIGNAL IS POSITIVE

② SIGNAL $\bar{T}$ FROM SCHMITT TRIGGER WHEN SENSOR SIGNAL IS NEGATIVE

③ SIGNAL P_{XW} FROM GATE 4 USED TO RESET FLIP-FLOP X AND W

$P_{XW} = N + \bar{L}$; $\bar{P}_{XW} = L\bar{N}$

④ CORRESPOND TO T, CHANGE STATE WHEN P_{XW} IS 1 AND CP CHANGE FROM 0 TO 1

⑤ CORRESPOND TO $\bar{T}$, CHANGE STATE WHEN P_{XW} IS 1 AND CP CHANGE FROM 0 TO 1

⑥ CORRESPOND TO T

⑦ CORRESPOND TO $\bar{T}$

Fig. 23. Planet-in-view logic waveform

from Gate 4 at the end of each period and the gating resumes in the next period. Figure 23 shows the wave form at the outputs of the various flip-flops and gates.

Logic equations for acquisition operation are

$$\begin{aligned}\text{Acquisition mode} &= \bar{A}B \\ &= (S + \bar{C})(\bar{S} + \bar{C}) \\ &= (S\bar{C} + \bar{S}\bar{C} + \bar{C}) \\ &= \bar{C}(S + \bar{S} + 1) \\ &= \bar{C}\end{aligned}$$

The system switches from planet searching to tracking operation when flip-flop C changes its state from C to $\bar{C}$. This is accomplished by removing the search driver's output from the x-axis filter so that the planet signal can now be used to drive the platform. A 2.4-kc planet-in-view signal is also produced by Gate 3 and is delivered to the data automation system for data mode switching.

8. y-Axis Signal Amplifier

The demodulated y-axis output is amplified by a dc-coupled difference amplifier as shown in Fig. 24. The y-axis signal is amplified and inverted from a bipolar signal to a unipolar signal by the difference amplifier. An adjustable negative dc feedback from the amplifier output to the detector y-axis output is employed to convert the wide range of the energy input to a voltage indication over the entire system operating range. The voltage gain of the amplifier as a function of the transistor h-parameters and the various circuit components is

$$A_y = \frac{R_L}{\left(\frac{h_{ie}}{h_{fe}} + R_e\right) + R_L\left(\frac{\Delta^h}{h_{fe}} + h_{oe}R_e\right)} \tag{32}$$

where

$$\Delta^h = h_{ie}h_{oe} - h_{re}h_{fe}$$

With the numerical values of the various parameters as shown in Fig. 24 and with $h_{ie} = 1800$ ohms, $h_{oe} = 100$ mhos, $h_{re} = 2.68 \times 10^{-4}$ and $h_{fe} = 15$, the gain of amplifier determined by Eq. (32) is

$$A_y = 21.8$$

The actual measured voltage gain of the amplifier is 20 and the amplifier was designed such that the voltage amplification is linear within 2% of the measured value over the entire operating range.

9. Scan Inhibit Electronic Circuitry

The scan inhibit signal is initiated by the TV camera, Earth-based ground command or narrow angle Mars gate and is routed to the system through the data automation system. The signal in the form of a 50-msec pulse with an amplitude of 6.0 to 8.0 v is used to operate a relay to disconnect the 400-cps fixed motor driving signal to the motor. To assure that the 400-cps fixed motor driving signal is available to drive the motor when the system is recycled, the 6-sec preset pulse generated by the one-shot circuit is used to drive a relay driver circuit to close the relay connection each time the system is energized. The scan inhibit circuitry is shown in Fig. 25.

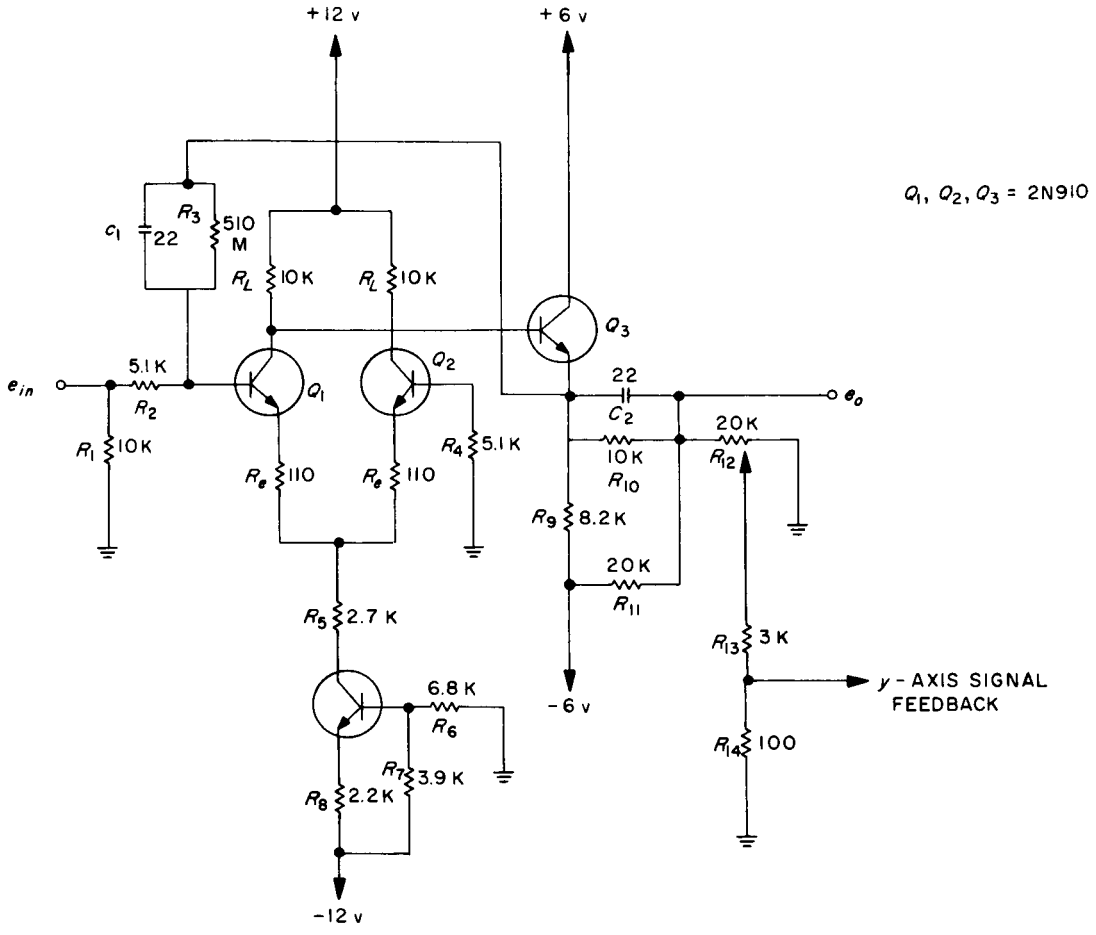

Fig. 24. y-Axis signal amplifier

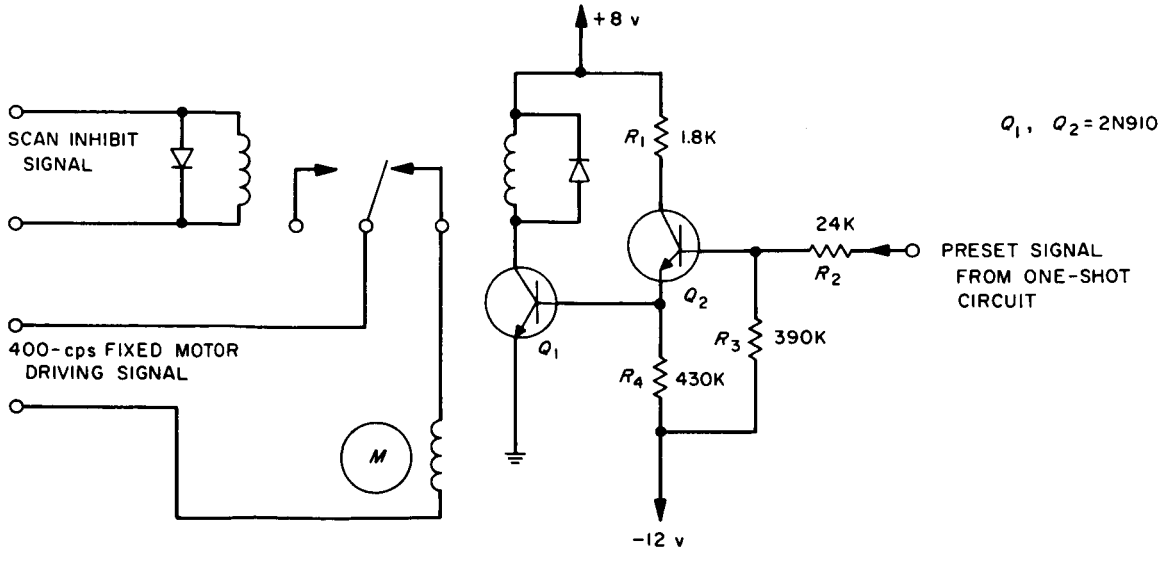

Fig. 25. Scan inhibit circuit

10. Power Supply

Preamplifiers and amplifiers are designed to operate on ±12 v dc and control circuits on ±6 v dc. In addition, a 130-v dc power supply is required to operate the photomodulator, and an 8-v dc supply to operate the motor relay. The various requirements of the power supplies are listed in Table 1.

Table 1. Power supply requirements

Voltage, v	Maximum load current, ma	Regulation (peak to peak), %	Ripple (peak to peak), %	Spikes (peak to peak), %	Load variation, %
+ 12	40	2	1	1	50 to 100
− 12	20	2	1	1	50 to 100
− 12	7	2	1	1	50 to 100
+ 6	60	2	1	1	50 to 100
− 6	20	2	1	1	50 to 100
+ 6	5	0.001/°C	0.1	0.5	90 to 100
+130	5	10	2	1	50 to 100
+ 8	40	20	2	1	50 to 100

To protect the spacecraft power system from overloading, current limiting capability is provided to limit the dc and 400 cps motor drive load currents to a specified limit. The supplies are designed to operate on a single-phase, 2.4-kc spacecraft power having the following characteristics:

a. Input Voltage
100 v peak-to-peak square wave
Voltage regulation ±5%

b. Spikes (Overshoot)
5 v, 2 μsec, normal, 5 μsec maximum

c. Frequency
2.4 kc, stability ±2%
Rise and fall time: 5 μsec ±4 μsec
Source impedance: 2 ohms maximum

The power used to drive the motor is a single-phase square wave, 400 cps with a frequency stability of 1%, 28 v rms with 5% regulation and a rise time of 9 μsec maximum. The power supply is also required to limit the dc current to 150% of the rated current and the 400-cps current to 160 ma rms.

11. Multiplexer and Analog-to-Pulse-Width Converter

Six channels of data are required for system performance evaluation during ground tests and in flight. These channels are: scan platform position, *y*-axis output, calibration voltage, detector temperature, motor assembly pressure and transformer-rectifier (T-R) voltage. Each of the signals has an amplitude range of 0 to 6 v. Before routing to the Data Automation System for processing, the signals are time-multiplexed by a multiplexer. The multiplexer consists of six sets of switching coils and magnetically operated reed switches incorporated as commutating elements. The coil and reed switch assembly is selected for this application because of its low operating power requirement. When open, the assembly has a high open circuit resistance and when closed, it has a low closed circuit resistance. Each coil was designed to have approximately 32,000 turns of wire, requires 17.5 ampere-turns of 9 mw of power at 17.5 v to operate. Open circuit resistance of the switch is in excess of 10^8 ohms and the closed contact resistance including lead resistance is 90 milliohms. Each assembly has a life expectancy of 100 million operations and is tested for 1.3 million successful operations prior to acceptance as a flight unit.

An analog-to-pulse-width converter is used to process the multiplexed data. The converter is capable of converting an analog signal of 0 to +6 v to a pulse width signal with the width range of 3 to 9200 μsec between marking pulses having 5 to 7 v of pulse amplitude and 8 to 12 μsec pulse width. The converter was designed to have an accuracy of 0.5% of full input scale when operating over the temperature range of −10 to +80°C.

12. System Interconnections

For proper system operation, electrical interfaces between the planetary scan system and other systems in the spacecraft are required. Depending on the characteristics of signals, twisted pairs and shielded twisted pair conductors are used to transmit these signals to minimize signal interferences. Each of the signals is ac-coupled and isolated by means of transformers or coils to avoid alternate conducting paths for circuit return currents.

Inputs and outputs required for proper system operation are as follows:

a. Inputs

1. 28 v rms (±5%), 400 cps, single-phase, square wave power from the power system

2. 50 v rms (±5%), 2400 cps, single-phase, square wave power from the power system

3. Inhibit scan signal, 6.0 v minimum, 50 msec, from the DAS
4. Seven data channel select signals for the data multiplexer operation, each 20 v, 50 msec, from the DAS
5. Analog-to-pulse-width converter readout command, 6.0 v, from the DAS

b. Outputs

1. Planet-in-view signal, 3.0 to 6.0 v, peak-to-peak, 2400 cps, single-phase, to the DAS
2. Pulse width data signal with the width range of 3 to 9200 μsec between marking pulses having 5 to 7 v of pulse amplitude and 8 to 12 μsec pulse width to the DAS; the data signal is time-multiplexed and contains the six channels of data required for system performance evaluation during tests and in flight
3. Eight channels of dc signals monitored by the operational support equipment (OSE): +130 v, +12 v, +8 v, +6 v No. 1, +6 v No. 2, −12 v No. 1 and −12 v No. 2
4. Four channels of ac signals monitored by the OSE: 400-cps motor drive signal, 400-cps motor directional drive signal, photomodulator drive and planet-in-view signal

13. System Operational Failure Protection

As mentioned in Section IV-B-7, planet searching and tracking operations are controlled by flip-flop C, and flip-flop C is in turn controlled by the planet-in-view logic. To prevent a system operational failure due to a false switching of flip-flop C to planet tracking operation by abnormal occurrences such as disturbances in the logic power supply, a small dc signal of sufficient magnitude for motor actuation is continuously applied to the output of the x-axis filter. This signal is used to drive the motor in a fixed direction in the absence of a planet signal at the x-axis filter during tracking mode operation. Upon actuation of the limit switch, then, the system automatically switches back to the planet searching mode operation to continue to search for the planet.

C. Motor Assembly

A motor assembly having a maximum torque loading capability of 100 in.-lb is used to drive the platform. This motor assembly consists of a Size 8, 8000-rpm, 400-cps, split phase, synchronous motor, reduction gearing, a shaft position potentiometer and scan limit switches. The 8000-rpm synchronous motor drives an integral gearhead to reduce the output speed to 8.16 rpm. Further reduction gearing is used to reduce the assembly output speed to 0.5 deg/sec. A clutch assembly is provided so that driving slippage occurs when a torque load is equal to or in excess of 40 in.-lb. The clutch assembly is incorporated to protect the motor and the platform from damage in the event the platform is driving against any mechanical obstacles during ground testing. The clutch is adjusted to slip at a torque load of 40 in.-lb, which is twice the actual torque load of the platform.

A shaft position potentiometer geared to the output shaft of the assembly is used to indicate the platform angular position. The potentiometer has a resistance of 5 kohms ±0.5%. The linearity of the potentiometer is 0.15%. Input voltage to the potentiometer is selected to be 6 v to provide an incremental output change of 32 mv per degree of wiper arm travel. With the output properly calibrated for nonlinearity, temperature effects and input voltage changes, the position indication at the output of the analog-to-pulse-width converter is accurate to ⅓ deg.

Two limit switches connected in parallel and operated in a series are incorporated at each of the two scan reversal limits. The two primary switches are installed 180±0.1 deg apart. Each backup switch is located 2 deg behind the primary switch.

The motor assembly is designed to operate in vacuum and space environments. To further increase its operating reliability, the entire assembly is housed in a sealed container and pressurized at 15 psig. A pressure transducer is installed in the container for the motor assembly pressure measurement.

D. Theoretical Planet Tracking Accuracy Evaluation

To determine the planet tracking accuracy of the system, a theoretical planet tracking error analysis was made in which all major sources of error were considered. These were:

1. Error due to variation in responsivity of detector quadrants as a function of temperature, $\Delta\theta_1$
2. Error due to the system dead zone, $\Delta\theta_2$
3. Error due to drift in the photomodulator, $\Delta\theta_3$
4. Error due to offset in the demodulator, phase detector and system operational failure prevention biasing, $\Delta\theta_4$

5. Error due to radiant density gradient of the planet quadrants, $\Delta\theta_5$

1. Error Due to Variation in Responsivity of the Detector Quadrants as a Function of Temperature

The operational concept of the detector is such that the planet image is bisected by the adjacent quadrants. A null point is indicated when each quadrant receives equal energy and the detector output is nulled to zero volt by the action of the servo system. The signals of the adjacent quadrants balanced out only when each quadrant received equal amounts of radiant energy and the energy-to-electrical signal conversion efficiency of each quadrant was equal. Since the properties of the semiconductor material and the behavior of the p–n junction are temperature-dependent, the detector's conversion efficiency or responsivity is a function of the operating temperature. Unless the responsivity of the adjacent quadrants are perfectly matched over the entire operating temperature range, a planet tracking error is introduced and the error magnitude is dependent upon the amount of mismatch in responsivity of the adjacent quadrants.

Figure 26 shows the measured output of each of the four detector quadrants plotted as a function of the operating temperature for a constant energy input. The values of the load resistors in the detector output resistor matrix (as shown in Fig. 11) are selected such that all quadrants have the same output when operating at 20°C. As the operating temperature increases beyond 20°C, the detector output decreases, indicating a decrease in responsivity. On the other hand, when the operating temperature decreases below 20°C, the detector output increases to a maximum at −5°C, below which the detector output begins to reduce as the temperature is further decreased.

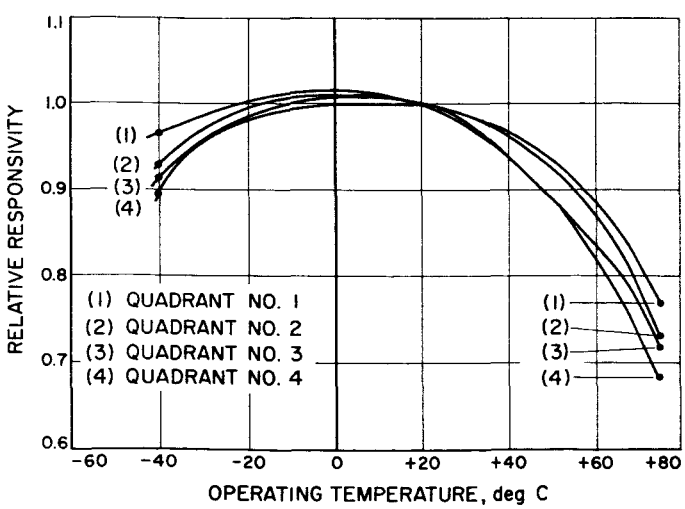

Fig. 26. Detector responsivity as a function of operating temperature

The behavior of the detector at temperature below −5°C is interesting and contrary to the normally anticipated behavior of increasing in output as the operating temperature decreases (Ref. 8). At low temperature, the electron and hole carrier densities are low relative to those at room temperature and recombination rate of the electron–hole pair is reduced, resulting in a higher output. The actual detector behavior is, however, more in line with the analysis made in Ref. 6, indicating that when operating in a particular configuration, the detector's short circuit current actually decreases with temperature, resulting in a decrease in output with temperature.

Figure 26 shows that the outputs of the individual quadrants are not equal when operating over the entire temperature range. At a temperature other than 20°C, a planet tracking error is introduced because a null point is now obtained only when one quadrant receives more energy than the adjacent quadrant, resulting in a shift in the tracking position. The magnitude of this shift is a function of the differential output Δe between the adjacent quadrants, where

$$\Delta e = e_1 - e_2$$

e_1 = Output of one quadrant

e_2 = Output of adjacent quadrant

As shown in Fig. 26, Δe is 9% at 75°C, 0% at 20°C and 6.9% at −40°C. The equivalent tracking error in degrees can be calculated from the planet position and geometry with respect to the detector and determined to be 0.0175θ at 75°C, 0.000θ at 20°C, and 0.014θ at −40°C, where θ is the planet angular diameter. Figure 27 shows the tracking error $\Delta\theta_1$ as a function of the detector-to-planet distance with the detector operating temperature as a parameter.

2. Error Due to the System Dead Zone $\Delta\theta_2$

This is the tracking inactive zone error and is a design characteristic of the servo system. Since the system was designed with a dead zone error of 0.2 deg, $\Delta\theta_2$ is assumed to have a magnitude of 0.2 deg.

3. Error Due to the Drift in the Photomodulator $\Delta\theta_3$

This error is introduced because of the drift in the photomodulator offset voltage when operating over the

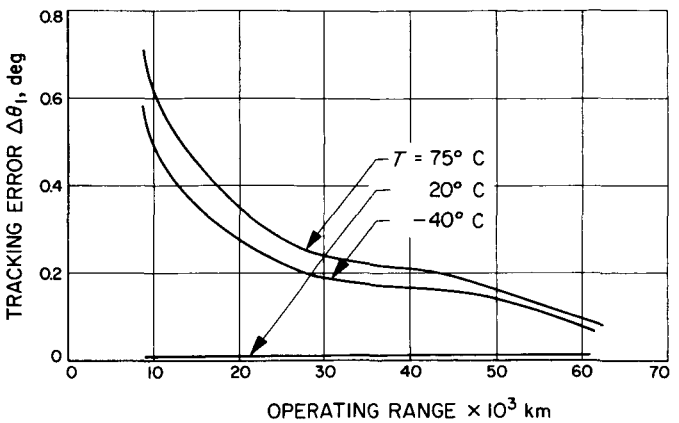

Fig. 27. Planet tracking error due to temperature variation of responsivity of individual detector quadrants

required temperature range. The photomodulation method of signal modulation was selected because of its high reliability, low noise level and low offset voltage. Therefore, it is anticipated that this error would be small. The drift characteristics of the photomodulator were analyzed and tests were performed at the temperatures of +75, +25 and −40°C with a simulated input signal to the photomodulator. The long-term variation in the offset over a period of 24 hr at a given operating temperature was measured to be ±0.5 μv. The amount of drift in offset over the temperature range was ±0.30 μv.

Figure 12 shows the detector output as a function of the planet angular position with the system operating range as parameter. The detector output when operating at the extreme condition of 60,000 km has a value of 1.0 mv per angular degree tilt from the null. The angular equivalent of the drift errors of ±0.5 and ±0.3 μv is indeed very small and its contribution to the over-all system error is negligible.

4. Error Due to Offset in the Demodulator, Phase Detector and System Operating Failure Biasing $\Delta\theta_4$

A field-effect transistor was used as the chopping device in the demodulator and a double-emitter transistor was used in the phase detector circuit. Both transistors were selected for the applications because of their ability to produce low offset voltage when operated over the required temperature range. Calculations in Section IV-B-4 indicated that the offsets produced by the demodulator and phase detector were 346 and 290 μv, respectively. The amount of planet tracking error introduced by these offsets is extremely small, since the signal amplitudes required for motor actuation are 2.65 v and 60 mv at the respective circuits. The amplitude values of 2.65 v and 60 mv represent the dead zone limit of 0.2 deg; therefore, the angular equivalents of the 346 and 290 μv of offsets are indeed small and can be neglected in the planet tracking accuracy evaluation.

To prevent a system operational failure when the system is inadvertently operating in the planet tracking mode in absence of the planet, a small dc signal was continuously applied to the output of the x-axis filter. This signal was used to drive the motor in a fixed direction in the absence of a planet signal. The system automatically switches back to the planet searching when either of the scan limits is reached. During the normal planet tracking operation, however, a tracking error is introduced because of the dc biasing. This biasing signal was selected to have a magnitude just sufficient to actuate the motor and its angular equivalent is equal to the system dead zone limit of 0.2 deg.

5. Error Due to Radiant Density Gradient of the Planet Quadrants $\Delta\theta_5$

This error is due to the fact that all portions of the planet surface do not reflect equal amounts of solar energy. The tracking position is therefore referenced to the integrated radiation bisector rather than the planet's geometrical center line. The geometrical location of the radiation bisector is dependent upon the specific angle from which the planet is viewed, the planet seasons and the type of trajectory used. Since these factors can not be specified precisely in advance, this error has not been taken into consideration and all portions of the planet surface are assumed to have the same radiant density for the purpose of error calculation.

With the various major sources of error taken into consideration, a theoretical planet tracking error of the system $\Delta\theta$ as a function of operating temperature and tracking distance can now be calculated:

$$\Delta\theta = \left[\sum_{0}^{n} (\Delta\theta_n)^2\right]^{1/2} \tag{33}$$

where $\Delta\theta_n$ is an individual source of error when the system is operating at a particular temperature and tracking distance. The system planet tracking error $\Delta\theta$ as a function of tracking distance at the various operating temperatures was calculated by Eq. (33) and the results indicated that the system has a maximum tracking error of 0.776 deg. This error occurs when the system is operating at a tracking distance of 9000 km and a temperature of 75°C.

V. MECHANICAL DESIGN AND SYSTEM FABRICATION

The effects of space environments impose severe requirements on the selection of material, component fabrication techniques and mechanical design of the system. The system must be capable of operating for prolonged periods in a space environment over a wide range of temperature with minimum degradation in performance. In addition, the system must be capable of surviving the mechanical shocks and vibration encountered during spacecraft launching.

A total of 576 electronic components is required for the fabrication of each system. Of the 576 components, 141 are active elements, either transistors or diodes. Wherever possible, components having a high reliability history were chosen, tested and screened to the existing JPL specifications. Components designed and constructed for performing special tasks were also tested and screened to specifications written for that purpose. The system is fabricated and packaged in four units: 31A1—preamplifier, optics and detector assembly; 31A2—power supply and electronics; 31A3—electronics; and 31A4—motor assembly.

A. Preamplifier, Optics and Detector Assembly (31A1)

Unit 31A1 is designed and packaged for mounting on the scan platform which is suspended beneath the spacecraft as shown in Fig. 28. The assembly consists of a lens barrel with optics, detector housing, two preamplifiers and two photomodulators.

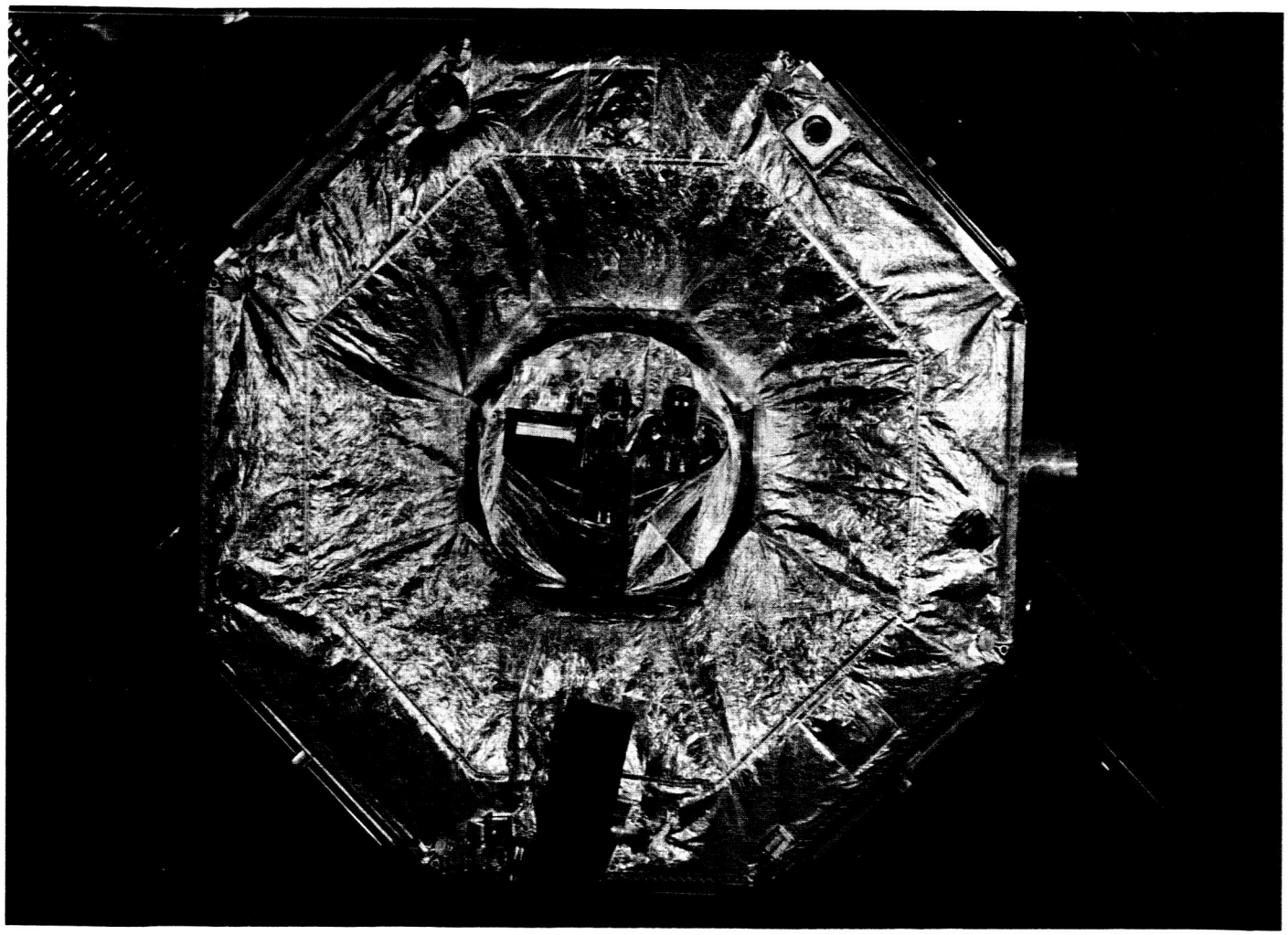

Fig. 28. Scan platform assembly

1. Optical System

The design of the system was such that a standard lens is utilized to serve as the image-forming device. The lens selected is a standard commercial item having a focal length of 30 mm, field of view of 50 deg and *f*-number of 2.3. In addition to meeting all the design requirements, this lens was selected because of its light weight, its small volume and its availability as a standard item. The lens has a resolution of 170 lines/mm on the axis and 80 lines/mm at the extreme field of view.

Being a standard commercial item, this lens is not designed mechanically for space application. Therefore, only the optical elements were acquired and these elements were then mounted in a metal housing. Because of the operating requirements, the material selected for this housing must be capable of meeting the following requirements in addition to those normally required for space applications: (1) thermal coefficient of expansion to be compatible with the optical element; (2) high strength-to-weight ratio; and (3) minimum magnetic field.

A logical choice would be a high-strength aluminum alloy such as alloy 6061T6 because of its low density and nonmagnetic property. An investigation, however, indicated that this alloy has a thermal coefficient of expansion of 24×10^{-6} per degree C, whereas that of the optical element is 9×10^{-6} per degree C. This large difference in thermal coefficients is undesirable in view of the wide operating temperature range. Stainless steel such as AISI 303 is nonmagnetic, with a thermal coefficient of expansion of 14×10^{-6} per degree C. Although the weight of the lens assembly with the stainless steel mount will be higher than that with aluminum alloy, the gain in mechanical strength is worthy of consideration. Since the lens assembly is small in volume, the difference in weight is also small. Figure 29 shows the lens in a stainless steel housing.

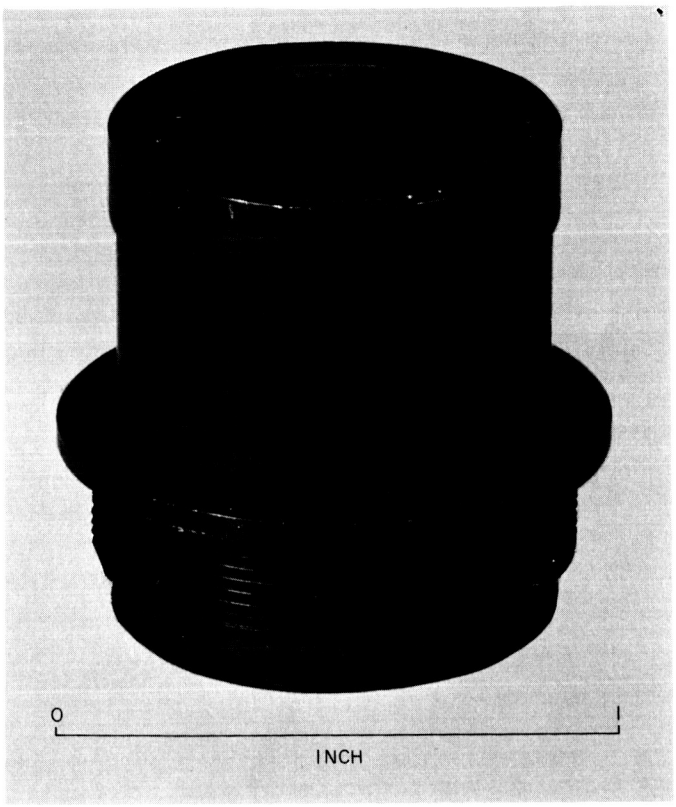

Fig. 29. Optical lens in stainless steel housing

2. Detector Fabrication and Mounting

The p-n junction of the detector was formed by diffusing boron atoms into the top layer of the n-type silicon bulk material to form a p-layer. To obtain the required planet tracking accuracy, the detector's responsivity must be uniform across the surface. Performance evaluations of the early fabricated detectors indicated that the detector's responsivity was not uniform across the surface. This was believed to be due to a nonuniform distribution of the impurity across the surface. The impurity gradient towards the junction was also believed to be nonuniform across the surface, thus producing a nonuniform drift field to speed the minority carriers toward the junction. In addition, the detector had a fragile structure, making mechanical mounting difficult. The fragility was determined to have been caused by cooling the detector too rapidly during the fabrication process. This created excessive thermal stresses because of the difference in mechanical properties between the top and bottom layers.

Various techniques of fabrication were developed to overcome these difficulties. The flight detectors, fabricated by a technique which permitted diffusing of the impurity more uniformly across the surface, were cooled in a closely controlled temperature environment. The local responsivity of these detectors was found to be fairly uniform. To obtain detectors of superior quality, units having superior characteristics were selected from the fabricated lots with a yield of approximately 15%.

To minimize the planet tracking error due to mechanical misalignment, the detector must be carefully positioned on the mount. Therefore, the fragile detector must be carefully mounted to the detector housing so that it can survive the spacecraft launch vibration without causing excess misalignment with respect to the mount. An

adhesive having the proper characteristics for space application is used to mount the detector. It is well known that adhesive compounds tend to lose weight in a vacuum due to sublimation and breakdown of the compound. Extensive studies have been made on the behavior of the various compounds in space environment by JPL (Ref. 9) and the various space agencies (Ref. 10). Since the optical lens is located in the vicinity of the mounted detector, contamination of the optical elements by the sublimated material will have serious effects on the optical properties of the lens. Therefore, the adhesive selected must have a low rate of weight loss.

Because of its wide operating temperature range and low outgassing properties, General Electric RTV-40 compound is used as adhesive for mounting the detector. The detector is mounted on a holder of aluminum alloy 6061T6, black-anodized. An insulation level between the detector negative lead and the holder in excess of 100 megohms was also obtained because of the high insulation property of the compound. In addition to serving as an adhesive, RTV-40 is also used to provide mechanical and thermal shock absorption for the detector. The mounted detector is shown in Fig. 30.

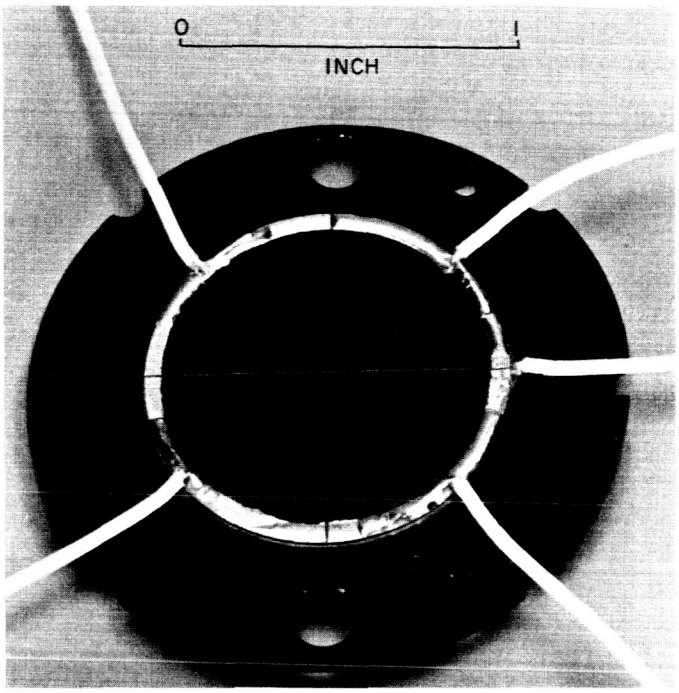

Fig. 30. Detector and mount

3. Photomodulator Housing

The neon lamps and photocells are mounted in a light-tight housing made of aluminum 6061T6. Each pair of photocells and its associated neon lamps are mounted in a separate housing. To increase the amount of light available to the photocells, the interior of the housing is polished to a mirror finish for high reflection of light. Depending on the physical arrangement of the lamps and photocells, a fine mesh metal screen may be needed to shield the photocells from the lamps to minimize the electrostatic coupling between the high-voltage lamp firing signal and the low-level modulated signal. In this application, however, the shielding is not incorporated since the amount of electrostatic coupling is negligibly small. The mesh metal screen shielding, if it were used, would reduce the amount of light received by the photocells, thus decreasing the signal modulation efficiency.

The lamps and photocells are mounted to the aluminum housing with a silicone compound of RTV-102 manufactured by General Electric Company as an adhesive. This compound has a bonding peel strength in excess of 20 lb/in. and a bonding shear strength in excess of 200 lb/in.^{2} In addition to its wide operating temperature range and low outgassing property, the silicone compound has an elongation of 500%, and can also be used as a mechanical absorber for the frail glass envelopes of the lamps and photocells. The photomodulator housing is mounted on and electrically grounded to the preamplifier subchassis.

4. Assembly Packaging

The x- and y-axis preamplifier circuitries are mounted on each of the two sides of the subchassis as shown in Fig. 31a (with the preamplifier cover removed). To conserve weight, the noncritical parts of Unit 31A1, such as the lens barrel and detector housing, were fabricated from aluminum alloy 6061T6. A critical part such as the lens mount was fabricated from stainless steel AISI 303. A further reduction in weight was achieved by the removal of all excess metal which would not in any way weaken the structure strength of the assembly.

The fabricated lens barrel is 2 in. in diameter and 3 in. in length and the detector housing measures $2.7 \times 2.2 \times 1.0$ in. The electronic housing is $2 \times 2 \times 3\frac{1}{4}$ in. The total assembly weighs 1.00 lb. The completed assembly is shown in Fig. 31b. All internal surfaces of the optical subassembly and the external surfaces of the preamplifier cover are black-anodized. All other external surfaces of the assembly are aluminum-polished so that proper operating temperature can be maintained on the Mars trajectory by passive thermal control methods.

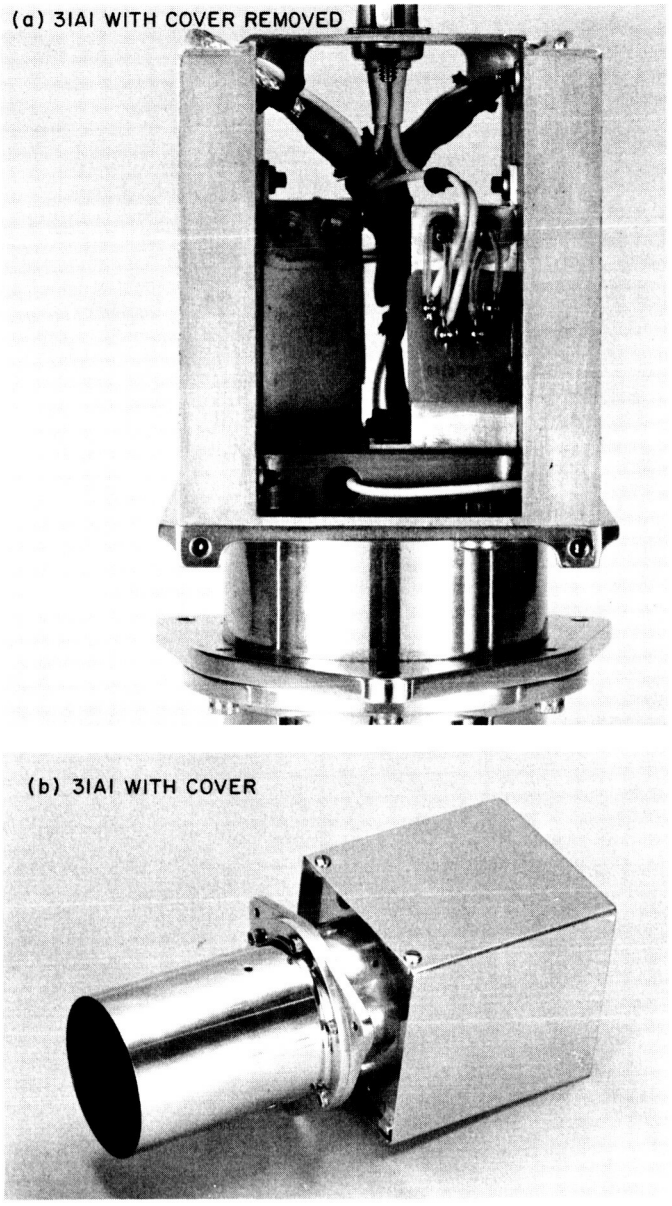

Fig. 31. Detector, optic and preamplifier assembly 31A1

B. Electronic Assemblies (31A2 and 31A3)

The remaining electronic components of the system are mounted on two *Mariner* Mars basic subchassis to form Units 31A2 and 31A3. These two units are to be located in Electronic Assembly III for scientific equipment in the octagonal instrument compartment.

The subchassis made of magnesium alloy has an overall dimension of $6 \times 6 \times 1\frac{1}{2}$ in. Each subchassis is divided into two compartments by a center web so that two circuit boards can be mounted on each side of the subchassis. Electronic components are mounted on the copper-clad laminated printed circuit boards, $\frac{1}{32}$ in. thick. Each circuit board, together with an epoxy fiberglass insulating board 8 mils thick, is mounted to the subchassis using Eccobond 55 compound as adhesive. All large components and cable bundles are spot-bonded to the printed circuit boards and subchassis by a casting resin, Stycast 1090. The mounted circuitry is then conformal-coated with the Solithane 113 compound 5 to 10 mils thick. The conformal coating is applied to provide electrical insulation, preventing possible short-circuit conditions resulting from conductive foreign material. It also provides moisture protection and secures the small components to the circuit boards.

The stud-mounted transistors, 2N1050B, are used in the motor driver and power regulating circuits. To realize the full power handling capabilities, these transistors are mounted on the center web, thus using the subchassis as a heat sink to remove the heat dissipated. The transistor mounting thermal resistance is minimized by using thin layers of silicon grease on each side of the mounting mica washers.

To conserve weight, volume and power consumption without sacrificing reliability, the SN510 and SN515 microelectronic integrated circuits manufactured by Texas Instruments, Inc., were used as flip-flops and gates in the searching, tracking and planet-in-view logic circuits. These integrated circuits along with the other logic electronic components are packaged in welded modules in order to take advantage of their small, flat pack dimensions. Figure 32 shows the two modules containing these logic circuits. Module No. 1, having dimensions of $1.20 \times 0.57 \times 0.40$ in., contains 5 flip-flops, 2 nor gates, 2 resistors and 2 capacitors, Module No. 2, with dimensions of $1.50 \times 0.47 \times 0.43$ in., consists of 4 flip-flops, 4 nor gates, 5 diodes and 3 resistors.

To conserve power, switching coils and magnetically operated reed switches were used as the commutating elements for the data multiplexing. The coil was constructed such that an electrically insulated metal spool was used to contain the wire-wound coil with the spool as a part of the shield. Signal leads were found to be shorted to the grounding shield when operating at high temperatures because of the differences in the thermal coefficient of expansion of the various parts. The fabrication method was modified by the use of a removable spool, thus enabling sufficient insulation to be placed between the coil and the grounding shield.

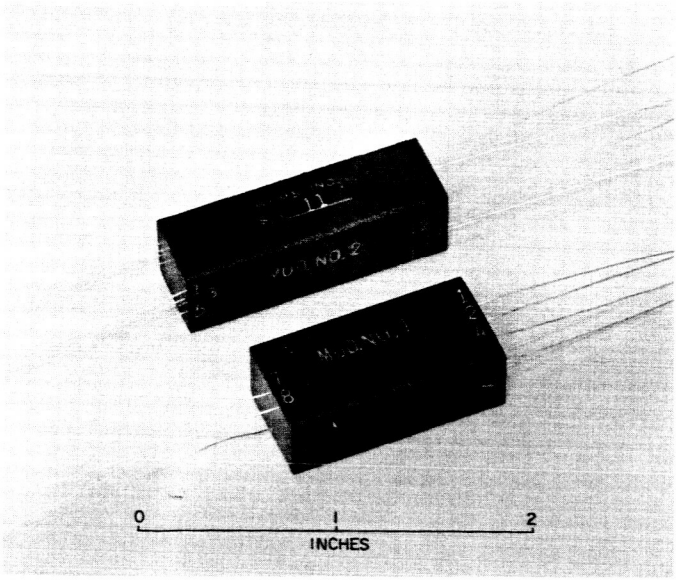

Fig. 32. Logic modules

Unit 31A2, the power supply and electronic assembly, weighs 1.95 lb and is shown in Fig. 33. The electronic assembly, Unit 31A3, weighs 1.45 lb and is shown in Fig. 34.

C. Motor Assembly (31A4)

The motor assembly is encased in a cylindrical housing 3 in. in diameter and 5.75 in. in length. The assembly is mounted on top of a central torque tube which rotates the spacecraft's platform. This torque tube assembly is supported by the spacecraft's basic octagonal structure and is mounted on the center line of the spacecraft.

All shafts and gearings in the assembly are constructed of stainless steel AISI 303. Output and potentiometer gears are made of aluminum alloy 2024-T4, phenolic-bonded with MoS_2. Magnesium alloy AZ-3 is used to construct the gear train support and other supporting numbers.

The four micro-limit switches are stack-mounted on an adjustment plate with a switching cam incorporated to operate the switches. The cam and plate are mounted such that the two primary switches are properly located with respect to the position of the potentiometer shaft. To avoid brinelling damages that can occur in ball bearings subjected to vibration, a teflon compound bushing is used on the output shaft. All aluminum oxide ball bearings with phenolic separators are vacuum-impregnated with silicone oil.

The entire motor assembly is housed in a hermetically sealed cylindrical container of magnesium alloy AZ-3 and pressurized to 15 psig with nitrogen gas. The assembly weighs 2.1 lb and is as shown in Fig. 35. The external surface of the housing is black-anodized to maintain the proper operating temperature by passive thermal control methods.

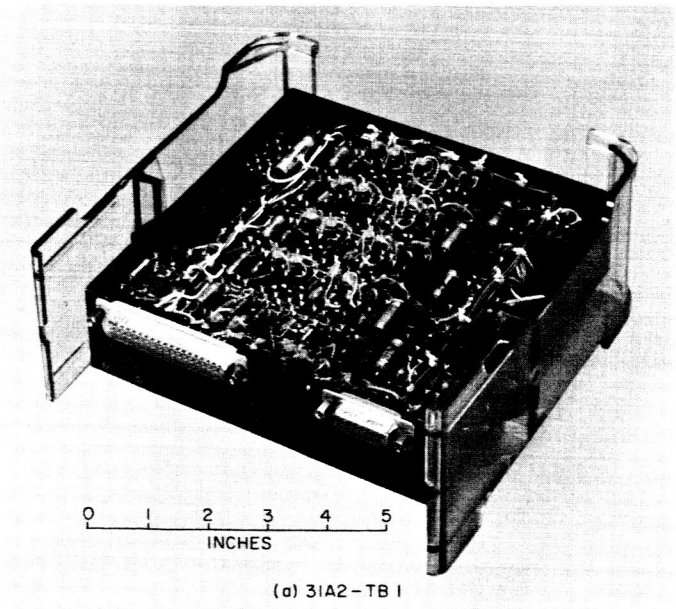

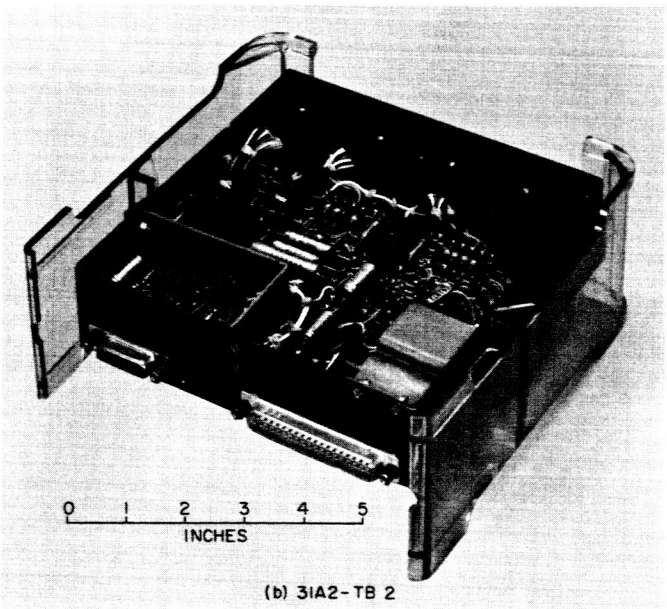

Fig. 33. Electronic and power supply assembly 31A2

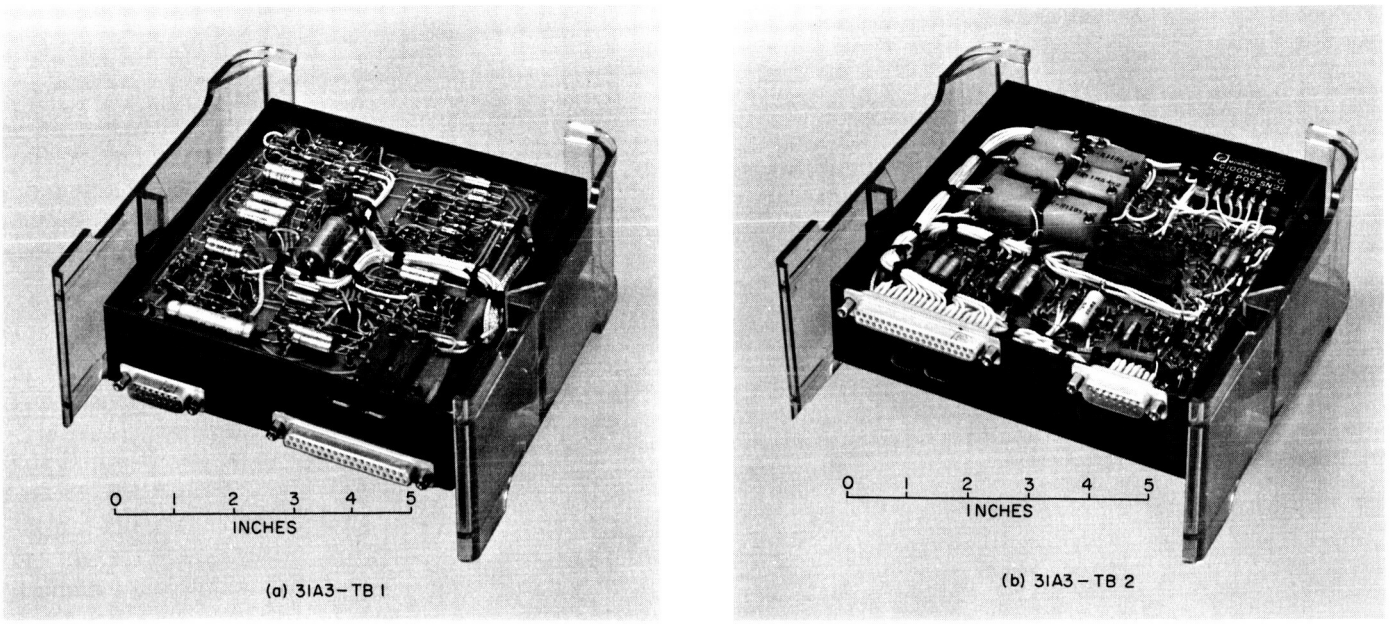

Fig. 34. Electronic assembly 31A3

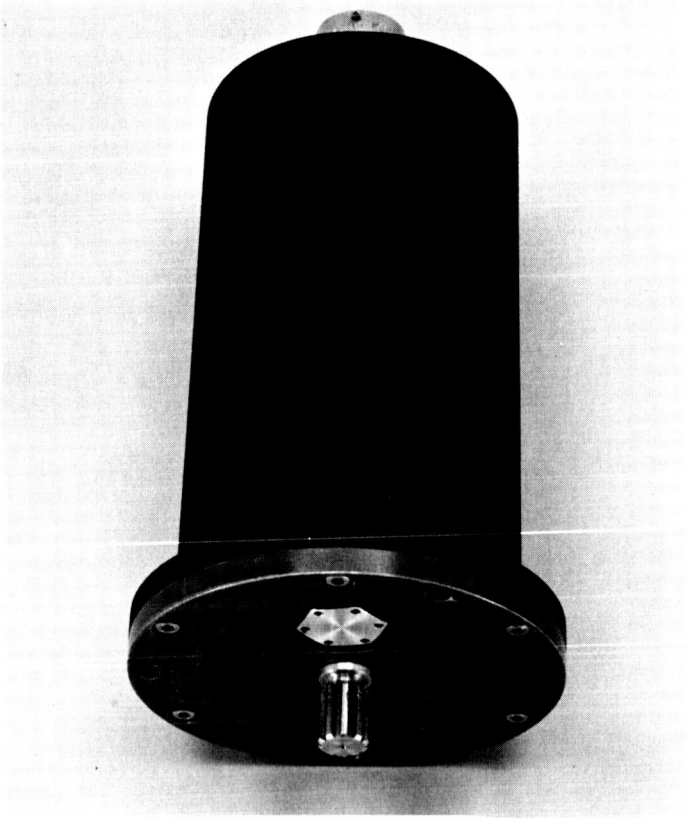

Fig. 35. Motor assembly 31A4

VI. SYSTEM PERFORMANCE

A. Optical System Performance Evaluation

The optical elements of standard design were mounted in a stainless steel housing. Prior to integrating the lens into the system, tests were performed to determine the optical performance and mechanical integrity under a simulated space environment.

To determine the effects of the spacecraft launch vibration and operating temperature cycling on the optical performance, the resolution of the lens was tested prior to and after the thermal and mechanical vibration tests. An NBS high contrast, 1952 target was placed at a distance of 149 in. from the lens. The image was formed on a Geatner microscope with an objective lens of 10 power magnification and an eyepiece of 6.7 power magnification. The horizontal and vertical resolutions were measured and calculated for on-axis and off-axis positions. It was determined that the on-axis resolution was about 170 lines/mm and that of the off-axis was about 80 lines/mm. An energy source with a known spectral distribution was utilized to determine the transmission characteristics of the lens. Spectral distribution of the source energy after it passed through the lens was measured. The results of the transmission efficiency as a function of wavelength including losses due to lens surface reflections are shown in Fig. 13.

Mechanical shock and vibration tests in three planes, in accordance with JPL type approval test requirements, were performed on the lens. Upon completion of these tests, the lens was tested under thermal and vacuum conditions in accordance with the type approval temperature cycling and thermal shock test requirements. This lens was then carefully inspected for possible mechanical damages and resolution and transmission efficiency tests were repeated for possible degradation in optical performances. Inspection and tests indicated that the lens elements were not contaminated by gas sublimated from the lens and mounting material under prolonged exposure to vacuum. No apparent degradation was detected in the over-all optical performances.

B. Planet Acquisition Range and Acquisition Probability

A criterion for the effectiveness with which the system accomplishes its mission is the range at which the system has a high probability of detecting the planet. The maximum range at which the planet can be detected and acquired primarily depends upon whether the planet can be distinguished from the noise appearing with the planet signal. If the noise amplitudes are high, the chance of mistaking a noise pulse for a signal in the absence of the planet is appreciable.

An analysis employing statistical methods (Ref. 11) was used to relate planet distance to the acquisition probability with the design parameters of the planet-in-view circuits taken into consideration. The planet is considered to be detected when the signal-plus-noise voltage to the Schmitt trigger circuit plus the circuit dc bias voltage exceed the triggering level of V_{in} in Eq. (30). Planet acquisition is said to have occurred when a planet-in-view signal is generated by the change of logic state of F/F C as shown in Fig. 22. The probability P_0 that the threshold of the Schmitt trigger is not exceeded in a time t_f, with t_f as the false alarm time, can be determined by

$$p_0 = (1 - p_n)^n \tag{34}$$

where

$$p_n = \int_\gamma^\infty w \exp\left(\frac{-w^2}{2}\right) \exp(-z)\, I_0\left[(2z)^{1/2} \cdot w\right] dw$$

$$p_n \approx (2\pi)^{-1/2} \int_\gamma^\infty \exp\left(\frac{-w^2}{2}\right) dw \tag{35}$$

p_n = The probability that a noise pulse exceeds the threshold

γ = Normalized threshold = $\dfrac{\text{peak threshold voltage}}{\text{rms noise voltage}}$

$= \dfrac{V_b}{V_n}$

n = Number of noise pulses per false alarm time t_f

The probability (p) that at least one signal-plus-noise pulse exceeds the threshold in a planet detection time t_d is

$$p = 1 - (1 - p_s)^m \tag{36}$$

where

$$p_s = (2\pi)^{-1/2} \int_{\gamma-\zeta}^\infty \exp\left(\frac{-w^2}{2}\right) dw$$

ζ = Normalized signal level

$$= \frac{\text{peak signal voltage}}{\text{rms noise voltage}} = \frac{V_p}{V_n}$$

m = Number of signal pulses per detection t_d

p_s = The probability that signal-plus-noise pulse exceeds the threshold

The peak planet signal V_p at a particular planet acquisition distance d is determined by the detector output signal and the voltage gain of the preamplifier

$$V_p = A_v \cdot e_x$$

where

A_v = Voltage gain of the preamplifier

e_x = Detector x-axis output as shown in Eq. (18).

Equations (18) and (19) indicated that the detector output voltage is an inverse square function of the planet acquisition distance. If acquisition distance is normalized by defining d_0 as the acquisition distance at which the signal-to-noise ratio is 1, $S/N = V_p/V_n = 1$, the acquisition distance d as related to d_0 is

$$\left(\frac{d_0}{d}\right)^2 = \frac{V_p}{V_n}$$

The relation of the acquisition distance to the probability that the signal-plus-noise voltage exceeds the threshold according to Eq. (36) is given by

$$p_s = (2\pi)^{-1/2} \int_{(V_b/V_n) - (d_0/d)^2}^{\infty} \exp\left(\frac{-w^2}{2}\right) dw \qquad (37)$$

As described in Section IV-B-7, the planet-in-view logic circuit is used to detect the presence of the planet signal against noise. The planet signal is sampled by the circuit with a sampling signal having a frequency of 3 cps. The detection time t_d and false alarm time t_f are therefore equal to the sampling period, $t_d = t_f = 1/f = 0.333$ sec. The detector must receive incident energy throughout a complete sampling period to obtain a planet-in-view signal; therefore, the number of signal pulses per t_d is $m = 1$. Because of the filtering action prior to threshold discrimination, the noise bandwidth has reduced to 120 cps as calculated by Eq. (29) and the number of noise pulses per t_f is $n = \Delta f \cdot t_f = 40$.

The probability of acquiring the planet as a function of the normalized planet acquisition distance d/d_0 was calculated using Eq. (36) and (37) with $m = 1$ and $n = 40$. Figure 36 shows the results of the calculations; p_0 is assumed to be 0.8 prior to noise discrimination. Assuming $p_0 = 0.8$ implies that, statistically, 80% of the noise pulses do not exceed the threshold. The value of p_0 is, however, increased to near unity through the use of the noise discrimination logic circuitry. The system, when operating under these conditions, requires a threshold level of $\gamma = 2.68$. The required value for γ was calculated by the use of Eq. (34) and (35). The proper threshold setting can be accomplished by adjustment of the Schmitt trigger level according to Eq. (38).

$$E_{dc} = 1.31 - 2.68\,(V_n) \qquad (38)$$

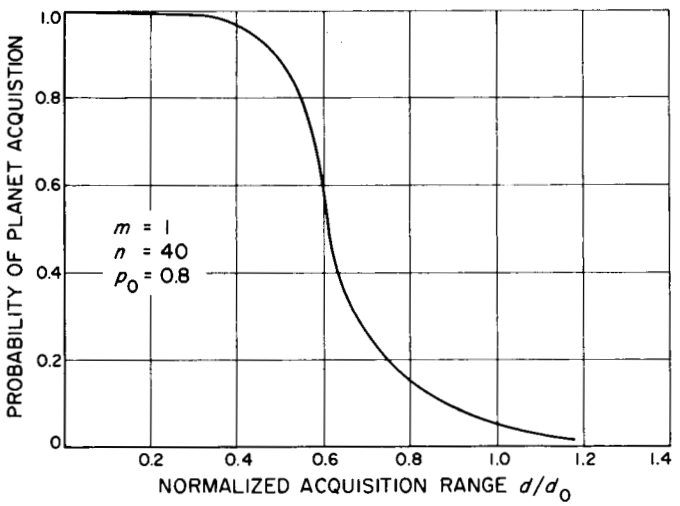

Fig. 36. Planet acquisition probability as a function of normalized acquisition range

where 1.31 v is the trigger level of the Schmitt circuit, 2.68 is the normalized threshold level and V_n is the long-term rms noise level at the filter input. The responsivity of the detector (Fig. 26) and the circuit noise are functions of the operating temperature. The Schmitt trigger level, therefore, must be adjusted at the upper operating temperature limit when the system is operating at its worst-case conditions of low responsivity and high noise. The adjustment of the trigger level according to Eq. (38) at the worst-case conditions assures that the system is operating at a normalized threshold level of $\gamma \geqq 2.68$ over the entire temperature range.

The numerical value of the planet acquisition range at which the normalized distance equals 1 (Fig. 36) can be determined from the operating conditions of the system (i.e., the planet-to-system distance at which S/N at the

input of the threshold stage equals 1 at an operating temperature of 75°C). Figure 37 shows the probability of planet acquisition as a function of acquisition distance. The acquisition probability when the system is operating at the various temperatures is also shown in Fig. 37.

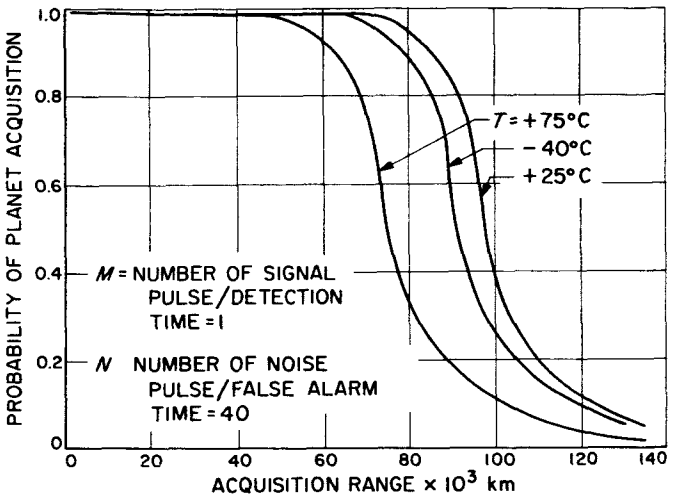

Fig. 37. Planet acquisition probability as a function of acquisition distance

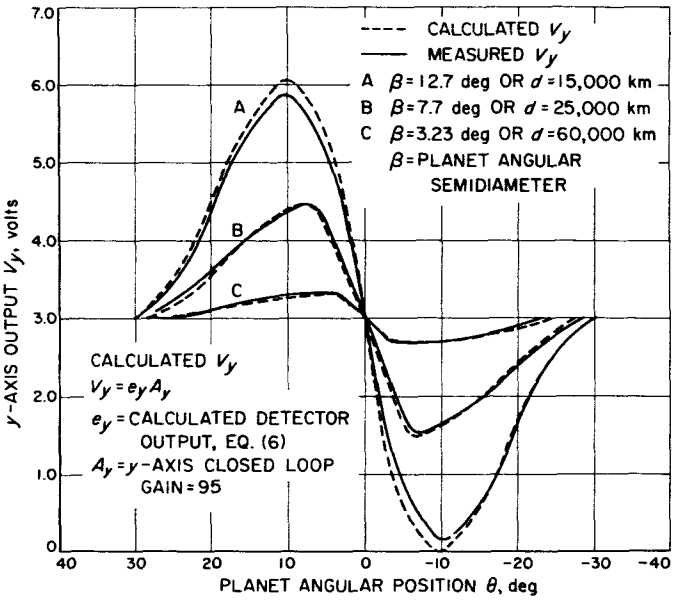

Fig. 38. y-Axis output as a function of planet angular position

C. y-Axis Output and Radiant Energy Experiment

As design data, the amount of solar energy reflected from the planet and incident at the detector was calculated by Eq. (19). To verify the validity of the calculated values, experiments will be performed during the planet encounter to determine the magnitude of the integrated energy in the spectral range of 0.5 to 1.1 μ. Since the output of the detector as a function of the planet position is shown in Fig. 12, the y-axis output can be used to determine both the angular position of the planet, with respect to the detector mount, and the amount of radiation energy received. Figure 38 shows the y-axis output as a function of the various variables. These curves were generated by multiplying y-axis detector output e_y in Eq. (18) by the loop amplification factor of the y-axis circuitries. It should be noted that this signal has been converted from bipolar to unipolar by the dc-coupled difference amplifier.

For comparison, tests were performed on the system using a planetary simulator (Ref. 12). This simulator consists of an illuminated disk having a radius of 6.0 cm, an incandescent lamp source, filters, and an iris diaphragm mounted in a metal housing. The transmission characteristics of the filters are such that only energy having a spectrum and distribution approximately that of the assumed spectral reflectivity curve of the planet as shown in Fig. 10 is allowed to reach the disk. An iris diaphragm is used to adjust the output energy without altering its spectrum. The output energy is measured by means of a thermopile. Figure 38 shows the measured V_y as a solid line when the system was operating at the various conditions. It is seen from these curves that by holding the flyby distance fixed, the y-axis output can be used to determine the relative position of the planet and the amount of radiant energy received. A number of sets of these calibration curves are required to interpret the flight data since the y-axis output is a function of the planet-to-detector distance as well as of the planet angular position in an actual flight trajectory.

Figure 26 shows that the detector output voltage is a function of the operating temperature. This temperature-dependence factor can be taken into consideration by either calculating the y-axis output with Eq. (18) using the proper value for responsivity at the respective operating temperature or by generating additional sets of measured calibration curves at various temperatures.

Additional information can be derived from these curves. As the planet image approaches along the x-axis and becomes centered on the origin, the y-axis output decreases to a value equal to output value with zero energy input and then decreases further as the image passes beyond the origin along the $-x$-axis. The slope

of the curves at the point $\theta = 0$ is a function of the planet angular diameter. Since the planet angular diameter is related to the planet-to-detector distance by the known geometry of the optical system, the approximate flyby distance can be calculated from the observed numerical value of the slope at $\theta = 0$ or

$$\left.\frac{dV_y}{d\theta}\right|_{\theta=0}$$

D. Offsetting of Planet Tracking Angle

One of the objectives of the *Mariner* Mars mission is to take approximately twenty photographs of the Martian surface from the limb to the terminator. The surface photographed must contain both the lighted and dark areas to secure contrasting details of the Martian surface. In order for the television camera to be properly oriented, the output of the detector must be baised such that the TV will be looking at the desired region of the planet surface which is located a few degrees below the radiant energy bisector. Since planet tracking motion ceases prior to initiation of the picture-recording sequence, the television picture scan trace is dependent upon the motion of the spacecraft relative to the planet as the spacecraft sweeps across the planet on its trajectory.

To show the effects of the offset on the tracking angle, Fig. 39 depicts the scan trace without the offset. On the same figure are the various scan traces with different offsets in tracking angle. Figure 40 shows the planet surface covered by the various scan traces for a particular predetermined trajectory. Physically, the offset is accomplished by selecting the proper resistive values for the resistors R_1 and R_2 in the detector output resistive matrix as shown in Fig. 11. The resistive values are selected such that the voltage outputs of the adjacent detector quadrants are at a proper ratio when each quadrant receives equal amounts of energy from the planet image. To obtain the proper TV coverage, Trace B as shown in Fig. 39 is selected and the tracking angle is biased at the voltage output ratio of 3.3. Based on this biased arrangement, the planet tracking error due to the temperature-dependence of the detector responsivity is determined to be 0.006θ at 75°C, 0.000θ at 20°C and 0.003θ with θ as the angular diameter of the planet.

Since the detector output is electrically biased, the magnitude of the angular offset is a function of the planet angular diameter, thus the planet-to-spacecraft distance. Figures 39 and 40 are generated by assuming this distance to be 12,000 km at closest approach.

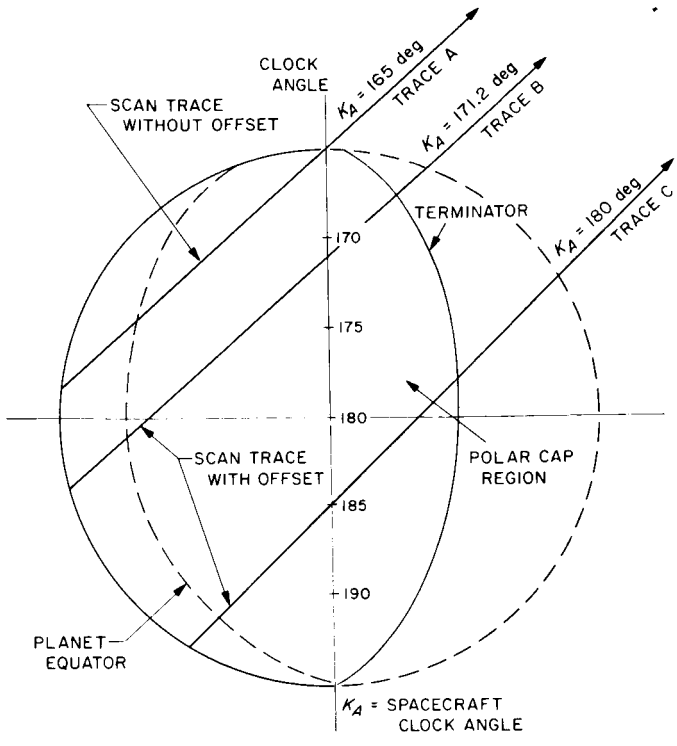

Fig. 39. Scan traces with and without offsetting of planet tracking angle

E. Test Experiences

Six systems were fabricated in accordance with the mission requirements. The systems were designated as the type approval system (TA), proof test model system (PTM), three flight systems (MC-2, MC-3 and MC-4) and a spare parts system (MC-5). Prior to testing, each assembly of the systems was mechanically inspected through the aid of a 60× magnification microscope for proper workmanship (mechanical defects, etc). When required, rework was performed on the assembly to correct minor defects. The assemblies were individually examined and tested for correctness in electrical connections and electrical continuity prior to assembly into the systems for further testing.

A test program was established so that each system was subjected to an orderly and appropriate test program. The various test requirements were established and intended to verify the system design, capability and performances at various environmental levels under simulated flight environments. Test procedures were written for the various types of testing.

1. Bench tests and calibration
2. TA tests

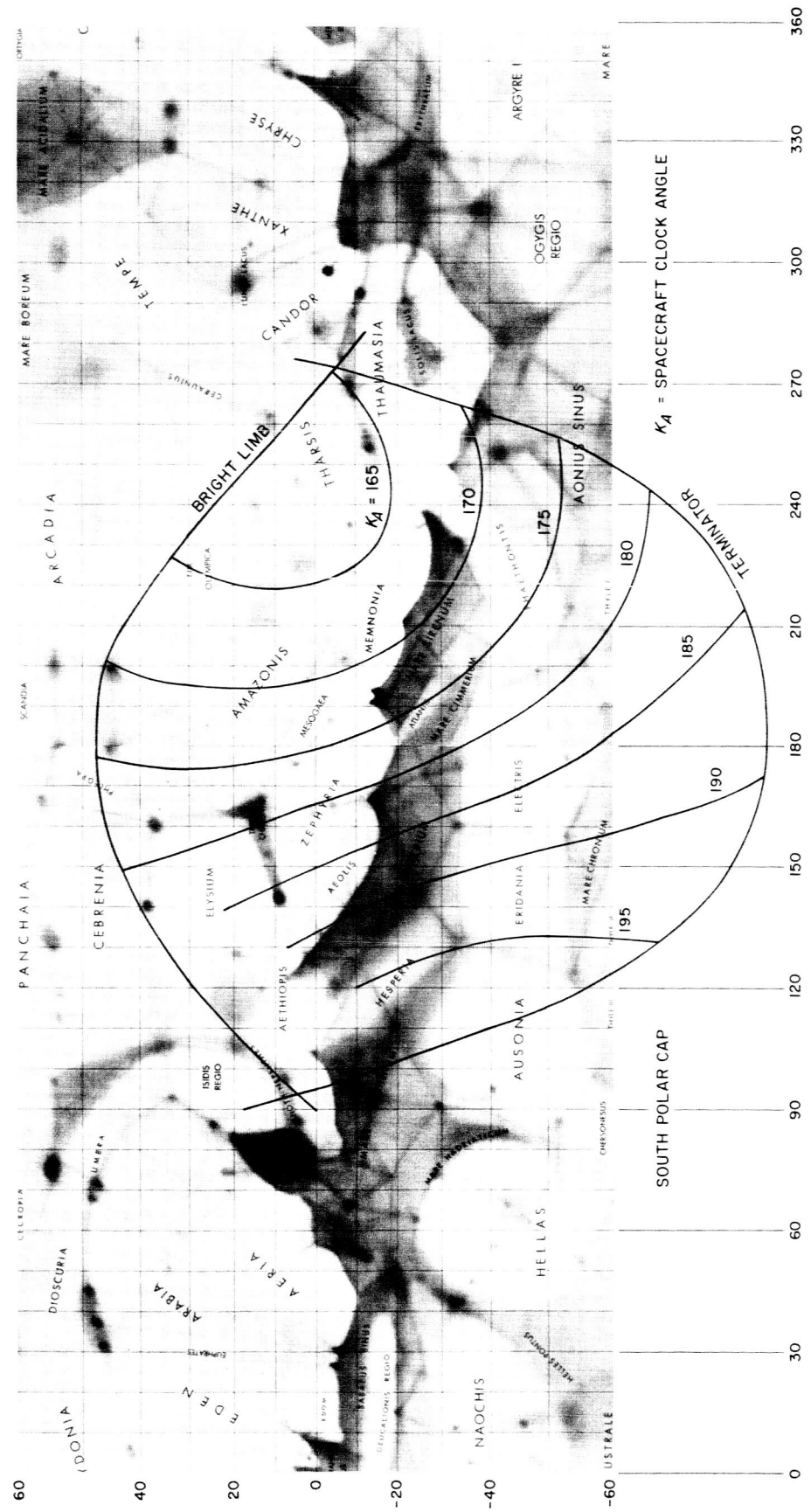

Fig. 40. Martian area covered by the various scan traces

3. Flight acceptance (FA) tests
4. Integrated spacecraft tests
5. Life tests
6. Radiation tests

Each system was required to pass the various required tests with the performance within the limits specified by the design requirements. Each system must be without any indication of degradation in performance as results of the tests.

1. Bench Tests and Calibration

Prior to assembly as a system, each assembly was checked for electrical continuity, and the power supply was energized and tested using simulated dummy loads over the operating temperature limits. Each of the detectors was tested for uniformity in local responsivity. Each system was then assembled and tested for compliance with the design requirements over the operating temperature limits. A complete system operation was performed at each of the four operating temperatures of +80, +25, 0 and −40°C. Figure 41 shows the system test console designed and fabricated for the system testing.

For each system, a set calibration curve was generated. These curves included the y-axis output V_y as a function of the planet angular position with planet-to-spacecraft distance and operating temperature as parameters. The detector temperature and actuator pressure voltage outputs from the analog-to-pulse-width converter were calibrated as functions of operating temperature. To obtain an accurate indication of the scan platform position, the shaft position potentiometer output of each system as a function of platform position angle was also measured and calibrated with the nonlinearity of the potentiometer taken into consideration.

Each system upon completion of the TA or FA tests was bench-tested for possible performance degradation as the result of the system tests.

2. Type Approval Tests

The TA tests were performed to verify the system's capability to operate satisfactorily in an environment which is in excess of that normally expected at launch and in flight. The margin of excess was used to provide a safety factor in the design adequacy. The tests were to be performed on the TA system and consist of the mechanical shocks and vibration, magnetic field measurements, explosive, humidity, radio frequency interference measurements, thermal vacuum and thermal shock tests. Upon completion of the mechanical testing, all assemblies were carefully inspected for possible mechanical damages. The thermal vacuum tests were divided into test cycles at +75 and −40°C.

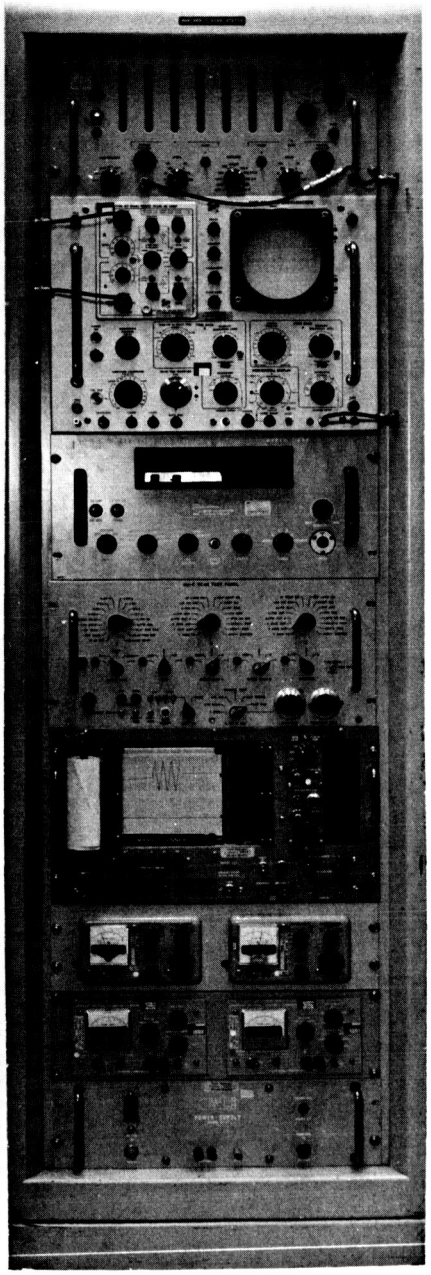

Fig. 41. System test console

The system successfully passed all tests and the performance was within the limit specified. The bench tests

after the TA testing indicated the system suffered no performance degradation. The following minor problems were encountered in TA tests.

During the first cycle of the high-temperature vacuum test, two scan reversals without actuating the limit switches were observed. These occurrences were determined to have been caused by transient noise introduced by monitor switching of the test equipment. The switching functions were then minimized and no subsequent occurrences were observed during the second cycle of the high-temperature vacuum test. Noise isolation arrangements were later incorporated in the test equipment to keep these external interferences to a minimum.

3. Flight Acceptance Tests

The FA tests were performed to confirm the system capability and performances as a flight system meeting the mission requirements. These tests were performed at a level more consistent with normal flight conditions. The PTM and all flight systems were subjected to these tests which consisted of mechanical shock and vibration, magnetic field measurements and thermal vacuum tests. The thermal vacuum tests were divided into test cycles at +55 and 0°C.

The test results indicated that all systems had successfully passed the tests with the performances meeting the specified limits. Bench evaluations of a system performance upon completion of the flight acceptance tests indicated, however, that the responsivity of the detector incorporated in the MC-4 unit had decreased and was unstable. Since these tests were used to verify the ultimate detector stability, the detector was replaced and applicable portions of the tests were repeated.

4. Integrated Spacecraft System Tests

The system tests were performed on the PTM system integrated into a complete spacecraft in a flight configuration. This PTM spacecraft was constructed and subjected to an extensive series of testing consisting of full-scale vibration, shock, acoustic, space simulated and thermal vacuum tests. These tests were performed to verify the system functional integrity and operational compatibility with the other spacecraft systems. A number of minor design changes had been incorporated in the system as a result of these tests. Similarly, each of the three FA tested flight systems was integrated into the flight spacecraft. These spacecraft were subjected to tests at a reduced level compatible with the normal flight conditions. For the system tests, the spacecraft were operating through an entire simulated mission from on-pad tests to planetary encounter under thermal vacuum conditions.

All systems operated successfully without failure in the system tests with the following single exception. A 140 msec interruption of the planet-in-view signal was experienced during a spacecraft system test using the flight system MC-3. Extensive analysis and tests were made on this unit to determine the cause of this behavior, but no conclusive test evidence was secured to indicate any system operational abnormality. Investigations were subsequently initiated in an attempt to locate a cause external to the system and results were equally inconclusive. Consequently, the MC-3 unit was designated as a flight spare rather than a prime flight unit.

5. Life Tests

The purpose of the life test was to determine the system's operational capability under prolonged exposure to a vacuum environment. The TA system was used in the system life testing. A total of 531 operating hours had been accumulated by this system before life testing. This consisted of 272 hr of TA testing, 171 hr of spacecraft system testing, 62 hr of bench testing and calibration and 26 hr of new test equipment checkout.

A simulated scan platform was used to mount the preamplifier detector-and-optic assembly and the motor assembly. The platform assembly, together with the other assembly of the system, was mounted in a thermal-vacuum chamber as shown in Fig. 42. The life test was performed in a vacuum equal to or less than 10^{-3} mm Hg and at a temperature of 25 ±5°C. The scanning area was free of obstacles so that the system had a clear field of view with an instantaneous scan circular field of view of 50 deg when scanned through 180 deg of arc during planet searching operation. The planetary simulator was used in the planet tracking test. Its position with respect to the detector simulated a flyby distance of 25,000 km.

Life testing consisted of the following operational sequences repeated throughout the test:

a. Planet searching mode, operating for 24 hr

b. Planet tracking mode, operating for 24 hr

c. False planet acquisition "failure" mode

d. Scan platform inhibit

e. Between sequences power off for 24 hr

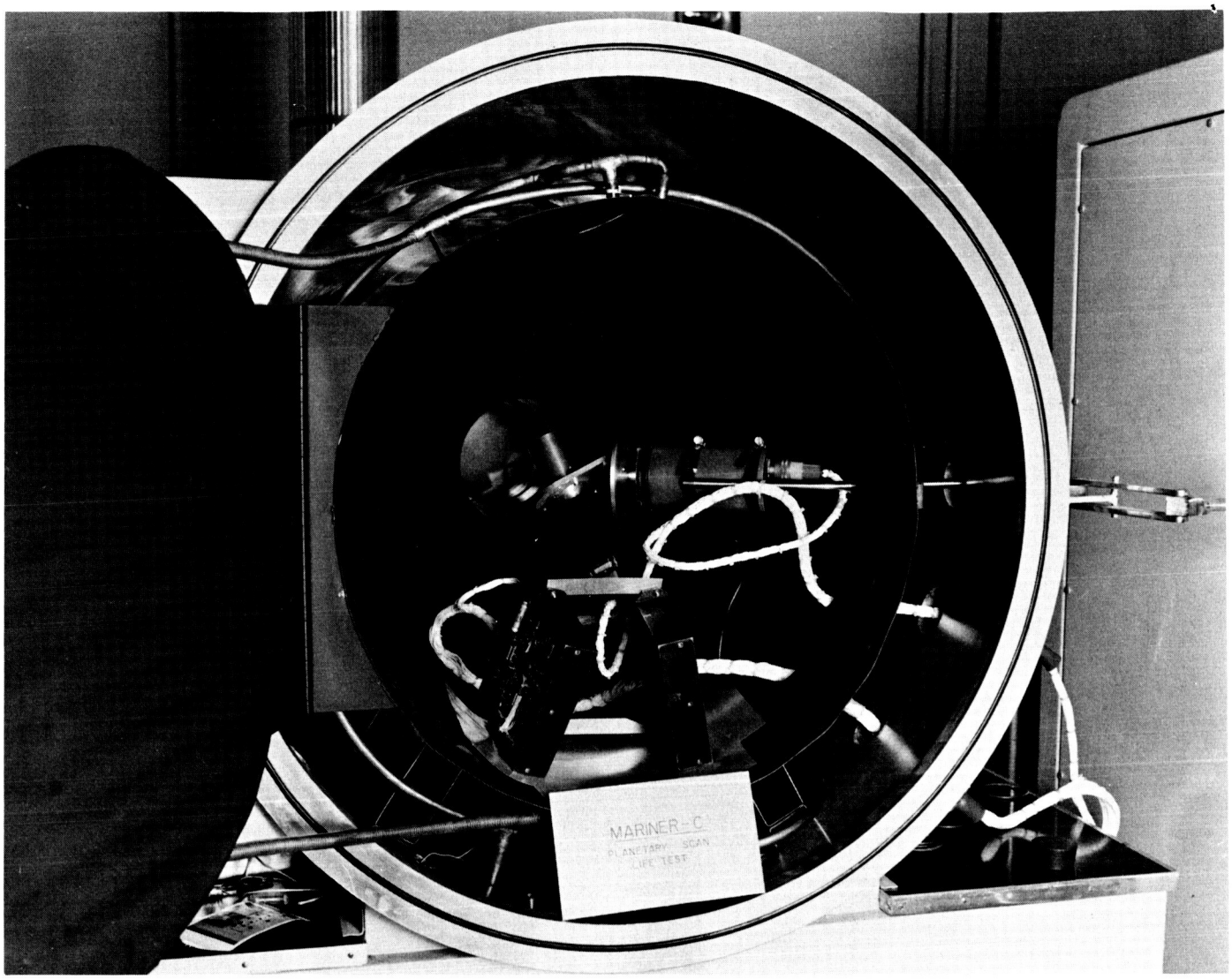

Fig. 42. System life testing

a. Planet searching operation. The following operational characteristics were checked during each planet searching period:

(1) Internal logic: initial direction of scan motion must be correct after power-on

(2) Motor operation: scan reversals must occur at primary limit switches

(3) System must remain in Mode 2 operation (search mode)

(4) Planet-in-view signal must not be indicated on continuously recorded data

(5) Scan position output curves, as continuously recorded, must be within specified linearity limits

(6) Scan y-axis output must have the proper value, indicating the detector has no input

(7) Scan calibration and transformer–rectifier voltages, temperature signal and pressure output must be within the specified limits

In addition, a total of eight dc and two ac voltage signals were monitored and recorded during each operation.

b. Planet tracking mode. When power to the planetary simulator was on and the simulator was within the field-

of-view of the detector, the system was required to track the simulator. The following conditions had to be met:

(1) Planet-in-view must be indicated

(2) System must be switching to Mode 3 (Tracking Operation)

(3) System must have the required tracking accuracy as indicated by the tracking position recording

(4) All other signals must be within the specified limits

c. False Planet Acquisition "Failure" Mode Operation. Upon completion of the planet tracking test, the power to the simulator was turned off to simulate either a loss of the planet or a false planet acquisition. The system was required to scan in a clockwise direction and revert to planet search operation when the limit switch was actuated.

d. Scan platform inhibit. This operation was performed to verify ground command capability of stopping the scan motion.

System life testing was initiated on August 25, 1964, and concluded on July 4, 1965. A total of 3194 operating hours, including 531 hr of operation prior to life testing, was accumulated. A failure was experienced on October 2, 1964, after 1061 hr of operation. The system failed to track properly. Failure analysis indicated that the 180-deg neon lamps of the photomodulator operated intermittently and that higher than nominal voltage was required for positive firing. Since this system had been used to check out a new system checkout console, excessive current was believed to have been drawn through these lamps accidentally during the equipment checkout. To verify the cause of this failure, further testing was performed by drawing excessive currents of various amounts and durations through a number of new neon lamps. Test results indicated that the firing voltage of these lamps increased after exposure to the over currents. The magnitude of the firing voltage was found to be proportional to the amount and duration of the excessive current drawn. The damaged lamps, which had accumulated 1061 operating hours, were subsequently replaced and life testing was resumed.

A second life test interruption was experienced on February 12, 1965, after 2400 operating hours. The neon lamps were known to have limited life and for reliable operation, replacement was required after 500 hr of operation for flight units and 2000 hr for other units as specified. The 0-deg lamps were replaced and life testing resumed on February 16, 1965.

The test results indicate that a total of 9450 search cycles had been performed during the life tests with each of the search cycles operating properly. Except for the events listed above, the system operated normally and within the specified limits at all times. The planet tracking accuracy was within ± 1 deg throughout the tests. The range over which the monitored parameters varied during the life test is summarized in Table 2.

Table 2. System performance summary, life tests

Signal	Magnitude and tolerance		Measurement during testing		Maximum measured deviation
			High	Low	
+130 v	131.0	± 13.0 v dc	131.3	122.5 v dc	−8.5 v dc
+ 12 v	12.0	± 0.25 v dc	12.00	11.98 v dc	−0.02 v dc
+ 8 v	9.69	± 0.8 v dc	9.70	8.98 v dc	−0.71 v dc
+ 6 v (1)	5.80	± 0.12 v dc	5.89	5.78 v dc	+0.09 v dc
+ 6 v (2)	6.03	± 0.12 v dc	6.03	6.02 v dc	−0.01 v dc
− 6 v	6.01	± 0.12 v dc	6.02	6.01 v dc	+0.01 v dc
− 12 v (1)	11.92	± 0.25 v dc	11.95	11.90 v dc	+0.03 v dc
− 12 v (2)	12.13	± 0.25 v dc	12.15	12.12 v dc	+0.02 v dc
400-cps supply	28.00	± 2.8 v rms	28.50	26.40 v rms	−1.60 v rms
400-cps motor drive	28.00	± 2.8 v rms	28.80	26.00 v rms	−2.00 v rms
y-axis output with no input	2.91	± 0.30 v dc	2.96	2.89 v dc	+0.05 v dc
Calibrate signal	0.965	± 0.030 v dc	0.990	0.964 v dc	+0.025 v dc
T/R voltage	4.780	± 0.050 v dc	4.860	4.777 v dc	+0.080 v dc

6. Radiation Tests

To determine the effects of radiation on the performances of the system, the TA system was subjected to a series of electron radiation tests. The system was bombarded by electron radiation having an energy range of 0.5 to 1.5 mev and flux levels of 10^7 to10^{10} electrons/cm^2-sec. The system operated properly at flux levels up to and including 10^9 electrons/cm^2-sec throughout the electron energy test range. Improper operation was observed at various flux levels above 2×10^9 electrons/cm^2-sec. It was observed that the system noise level increased with the electron flux level and an erroneous signal was produced at the detector output. This signal, when superimposed on a planet signal, caused the system to track erroneously. As the flux level increased to 4×10^9 electrons/cm^2-sec, the radiation-induced signal from the detector had a sufficiently large amplitude to cause the system to switch falsely to planet tracking operation

in the absence of a planet simulation. The system recovered and operated properly each time the radiation beam was removed.

F. System Flight Performance

1. Operational Sequence

The operational sequence of the system is as follows. Approximately 9½ hr before television picture recording, the power to the system and other planet encounter instruments is turned on by either the on-board central computer and sequencer function MT-7 or the Earth command DC-25. The planetary scan system enters into a planet-searching operation by driving the platform back and forth through 180 deg of arc searching for the planet at a rate of 0.5 deg/sec. When the planet comes into the detector's 50-deg field of view, the system generates a planet-in-view (PIV) signal and orients the TV toward the desired portion of the planet. The PIV signal is also routed to the data automation system (DAS) to switch the data format from Data Mode 2 to Data Mode 3. When the spacecraft reaches the proper position for picture taking, a scan inhibit signal is initiated by either the narrow angle Mars gate, which was also mounted on the platform, or by the television system itself. This signal indicates that the planet is in the TV field of view, stops the platform motion, and initiates the picture-recording sequence.

2. Telemetry Channels

Six channels of data were available for system performance evaluation in flight. These data were time-multiplexed and telemetered back to Earth in near real time. The various data channels together with their functions and DAS channel allocation are shown on Table 3. The planetary scan system operates under two data modes: Data Mode 2 and Data Mode 3. During Data Mode 2 (planet searching operation) only the Scan Position No. 1 data (DAS Channel No. 21) is available. In Data Mode 3 (planet tracking operation) all six channels of data are received.

3. Prelaunch Calibration

Two launches were provided in the *Mariner* Mars 1964 program. The planetary scan system MC-2 was incorporated in the *Mariner III* spacecraft and System MC-4 was installed in the *Mariner IV* spacecraft. Just prior to launch, a final calibration verification was performed on each system. Tests were performed to verify the proper alignment of the system optics to the television and narrow angle Mars gate. The prelaunch scan platform stowed position of each spacecraft in terms of the spacecraft clock angle was also accurately measured and was later used as data for system flight performance analysis.

Table 3. System telemetry data channel

Channel	DAS channel No.	Functions
Scan position No. 1	21	Indicates pointing direction of platform
y-axis output	29	Indicates brightness and relative position of planet
Calibration signal	36	For calibration of scan position data and for indicating proper operation of electronic power supply
Detector temperature and scan actuator pressure	37	Indicate temperature and pressure in alternate data frames
T/R voltage	40	For calibration of scan position data and for indicating proper operation of electronic power supply
Scan position No. 2	42	Indicates pointing direction of platform

G. Flight System Performance

1. Performance of System MC-2

The *Mariner III* spacecraft was launched from Launch Complex 13, Eastern Test Range (ETR) at Cape Kennedy, Florida, at 19:22:05 GMT, November 5, 1964. The nose cone failed to eject from the spacecraft and prevented the solar panel from deploying. A ground command, DC-25, was initiated at 23:21:30 GMT to turn on power to the planetary scan system and other planet encounter instruments. Upon receiving the command, the system initiated a planet searching operation and a platform scan motion of 2 deg was observed. Because of a narrow angle acquisition received soon after DC-25, the platform was inhibited and no further scan motion was observed. The data format remained in Mode 2 and the information from the other five channels was not received. Command DC-26 was initiated at 23:29:05 GMT to turn off power to the system and other encounter instruments.

2. Performance of System MC-4

The *Mariner IV* spacecraft was successfully launched from Launch Complex 12, ETR, on November 28, 1964. This system was energized three times throughout the flight. It was energized the first time on February 12, 1965,

during the early science cover drop sequence, the second time during the 9-hr planet encounter period on July 14, 1965, and the third time during the television dark encounter sequence on August 30, 1965.

The first block of system flight performance data was obtained during the early science cover drop sequence on February 12, 1965, 76 days after launch. The scan system responded properly to the Encounter Science Power On Command (DC-25) by immediately entering the search mode. The correct initial search direction was obtained and the system made a total of ten search cycles. Analysis of the received data indicated the system was operating under the following conditions:

a. All scan reversals were actuated by the primary switches since each of the reversals occurred at the proper limiting positions. The redundant or backup switches were not used.

b. All searching logic, including the microelectronic integrated circuits, operated properly and there were no premature scan reversals due to improper logic state changes.

c. The average searching time had decreased by 4 sec per search cycle from the prelaunch scan period of 717 sec per cycle.

d. The pressure readout indicated that the motor was operating under full pressure with an insignificant amount of change over the prelaunch value of 30 psia.

e. The detector and optics operated at a temperature of $-3°C$ as compared to the operating temperature of 0°C for the neighboring instrument, the TV optics assembly.

The y-axis output indicated that no objects having radiation energy of 1.0 μw or greater in the integrated spectral range of 0.5 to 1.1 microns were observed by the detector. The numerical value of this output remained constant at a value corresponding to no significant input.

At that time, it was decided to time the Scan Inhibit Command (DC-24) to stop the scan motion. This operation was performed for two reasons: (1) to determine whether the platform could be stopped accurately at a predetermined position, and (2) to stop the platform at a position which would ensure the attainment of at least some television pictures of Mars in the event of any later spacecraft failure which would prevent platform motion at encounter. Accordingly, the time for the initiation of DC-24 was calculated, based on the desired TV pointing direction, in terms of spacecraft clock angle, and the scan speed calculated from the data received for the first six scan cycles. The command time was projected for four scan cycles ahead to allow for calculation time, the various transmission delays and time for command processing. Upon receiving DC-24, the platform stopped 0.72 deg away from the desired position.

The success of this platform positioning operation via ground command led to the consideration of using this method as another means of positioning the TV camera. Subsequent tests with the PTM spacecraft indicated that it was possible to preposition the scan platform over a simulated communication range of 135 million miles with a positioning accuracy of 1 deg. The performance of the scan system during the early science cover drop sequence is summarized in Table 4.

Table 4. Summary of system performance during early science cover drop sequence, February 12, 1965

Function	Prelaunch or predicted value		Actual data readout in flight	
	(DN)[a]	Engineering quantity	(DN)[a]	Engineering quantity
Average scan search time per cycle, sec		717.0		712.9
Desired platform inhibit position, deg		—		177.19
Actual platform inhibit position, deg		—		177.94
Calibrate signal, v	(85)	0.998	(85)	0.998
T/R voltage, v	(417)	4.896	(417)	4.896
Detector temperature, °C			(318)	−3.0
Motor pressure, psia	(143)	30	(146)	30
y-axis output with no input, v	(261)	3.064	(261)	3.064

[a](DN) is Data Number representing an engineering measurement in number of 00 = 0.000 v and 511 = 6.000 v.

On July 14, 1965, 228 days after launch, the scan system responded to the Encounter Science Power On Command DC-25 by initiating a planet searching operation at 14:40:33 GMT at the spacecraft. The system began its search in the correct direction. To evaluate the planet searching performance, a graph of the platform position as a function of search time was generated based on the received real time flight data. Analysis of the graph

indicated that the system was operating properly under the following conditions:

a. The scan reversals occurred at the predicted position as indicated by the magnitude of the position output voltage. Each of the reversals was actuated by a primary switch.

b. The linearity of scan platform position as a function of search time and the position output voltages at the reversal points were within the specified limits. Therefore, no corrections were required on the established conversion table of scan position voltage to scan position in terms of spacecraft clock angle.

c. All searching logic, including the microelectronic integrated circuits, operated properly and there were no premature scan reversals due to improper logic state changes.

d. The average searching time per cycle was within ½ sec of the rate calculated during the early science cover drop sequence.

e. The pressure readout indicated that the actuator was operating at a pressure of about 26 psia or a decrease of 4 psi after some 7.6 months of space travel.

f. The system detector and optics operated at a temperature of −8.5°C.

Because of the occultation experiment, the final prelaunch trajectory change was such that the scientific value of TV pictures with automatic planet tracking was not optimum. The original encounter operating plan was revised such that with the operational and scan system conditions permitting, the Scan Inhibit Command DC-24 would be used to preposition the platform. The command

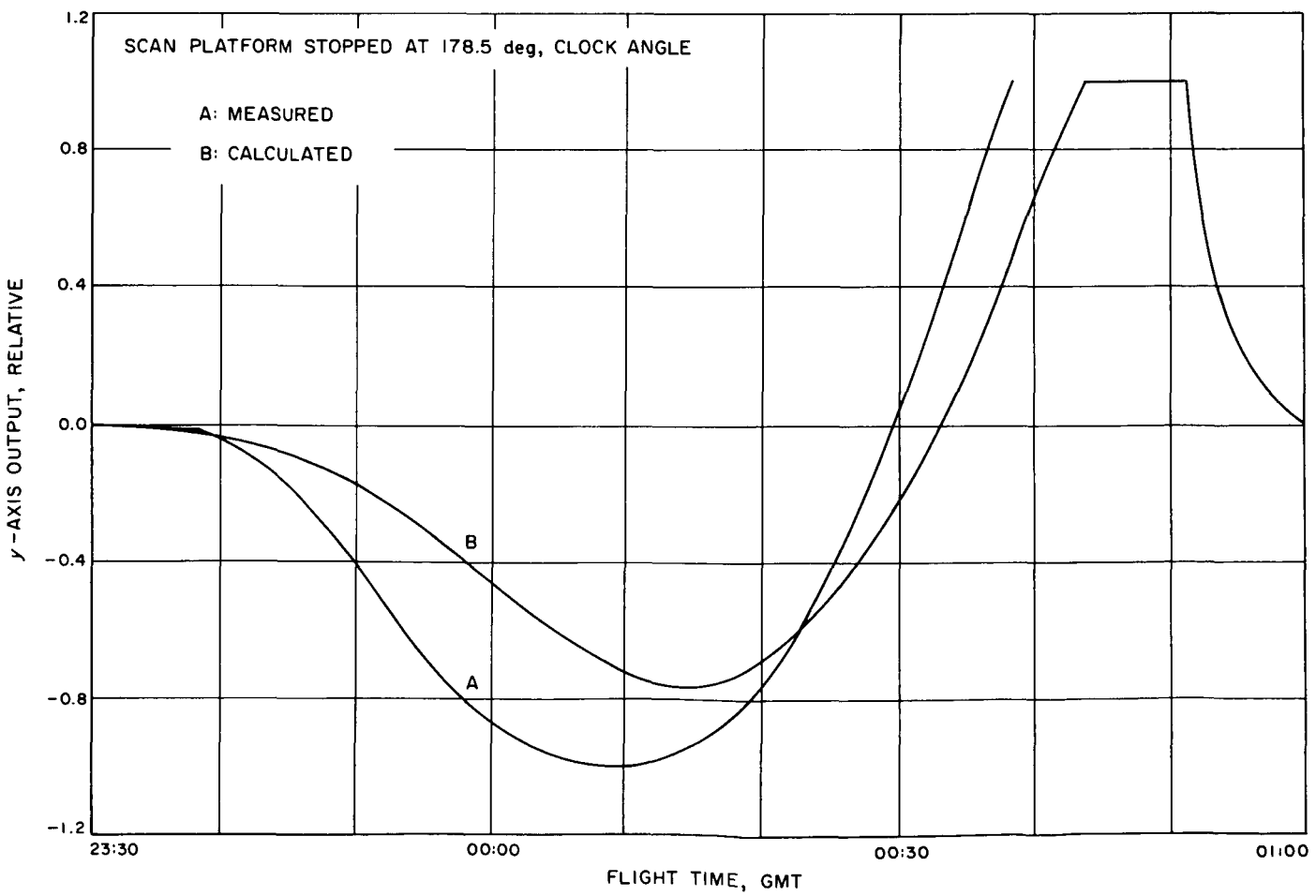

Fig. 43. y-Axis output vs. flight time, GMT, July 15, 1965

initiation time was calculated to stop the platform at a position for optimum pictures.

The automatic planet tracking sequence was to be used as the backup operation in the event the prepositioning could not be exercised or failed to produce the intended results.

Accordingly, a command initiation time was calculated based on the desired TV pointing direction, the calculated scan search speed averaged over the first seven search cycles, the communication transmission delay and the command processing time. The initiation time of DC-24, projected seven scan cycles ahead, was calculated to be 17:10:18 GMT for a desired inhibit position of 179.19 deg in clock angle. The calculation was based on the following selected parameters:

a. Average scan search time per cycle, 713.4 sec

b. Communication transmission delay time for the last frame of scan data used in the command time calculation, 11 min, 59.8 sec

c. Communication transmission delay time at time of command initiation, 12 min, 00.0 sec

d. Command processing time, 37.3 sec

e. Motor coastdown time, 0.2 sec

Upon receipt of DC-24, the scan platform motion was inhibited at a clock angle of 178.45 deg, or 0.72 deg away from the desired position. This positioning was considered acceptable since the TV pictures at the actual inhibited position would have essentially the same value as pictures taken at the desired pointing position.

At 23:42:00 GMT at the spacecraft, the detector detected the edge of the planet and generated a wide angle PIV signal. Twenty-three minutes later, the planet came into the television camera field of view. The y-axis output, as the planet entered and swept across the detector's field of view, varied in accordance with the relative planet/spacecraft position and the amount of radiant energy received. Figure 43 shows the actual y-axis output as a function of GMT (Curve A) along with the calculated y-axis output based on the pre-encounter trajectory data (Curve B). Because of the y-axis amplifier feedback adjustment, the y-axis output was saturated part of the time; the y-axis output curve has been expanded through extrapolations and calculations. It is seen in Fig. 43 that Curve B is located to the left of Curve A, indicating that the planet entered the detector field of view about 5 min earlier than expected. This deviation is partially due to an error in the prediction of the spacecraft arrival time and partially due to error in the y-axis output calculation based on the predicted trajectory. Comparison of Curves A and B indicated that the detector received 20 to 30% more energy than expected. Therefore, the calculated energy level and the data used in the energy calculations must be modified for use in designing future systems.

The performances of the scan system during the planet encounter period are summarized in Table 5.

Table 5. *Mariner IV* planetary scan system flight performance summary

Function	Prelaunch or predicted value	Data read-out during early science cover drop	Data read-out during planet encounter	Data read-out during dark encounter
Average scan time per cycle, sec	717.0	712.9	713.4	713.5
Desired platform inhibit position, deg	—	177.19	179.19	148.80
Actual platform inhibit position, deg	—	177.94	178.45	148.43
Calibration signal, v	0.998 (85)[a]	0.998 (85)	0.998 (85)	0.998 (85)
T/R voltage, v	4.896 (417)	4.896 (417)	4.896 (417)	4.896 (417)
Detector temperature, °C	−10°C for encounter operation	−3.0 (318)	−8.5 (351)	−11.0 (371)
Motor pressure, psia	30 (143)	30 (146)	26 (187)	26 (192)
y-axis output with no input, v	3.064 (261)	3.064 (261)	3.076 (262)	3.076 (262)
Number of search cycle performed		10	14	11

[a]Number enclosed by parentheses indicates the data number.

To provide the calibration data for the 21 television pictures of the planet Mars, a TV dark encounter sequence was performed on August 8, 1965. In this sequence, pictures of the dark space were taken and the data was telemetered back to Earth.

The system operated properly throughout the sequence. Upon the receipt of encounter science power resulting from DC-25, the system responded by initiating a planet searching operation in the correct search direction. Eleven search cycles were performed; each reversal was actuated by the primary limit switches. During this time, the system sensor and optics assembly was operating at a temperature of −11.0°C as compared to −8.5°C at

planet encounter. The y-axis output remained constant at a numerical value corresponding to no significant input, i.e., the y-axis output indicated that no objects having radiation energy of 1.0 μw or greater in the integrated spectral range of 0.5 to 1.1 μ were observed by the wide angle detector. All other signals were well within the specified and predicted limits.

The initiation time for the scan inhibit command DC-24 was based on the flight data received for the first four scan cycles and a one-way communication delay time of 15 min, 18.3 sec. The average searching time per cycle was 713.5 sec, or 0.1 sec longer than that calculated during the planet encounter sequence on July 14, 1965. The calculated initiation time for DC-24, projected seven scan cycles ahead, was 22:48:33 GMT for a desired inhibit clock angle of 148.80 deg. Upon receipt of DC-24, the scan platform motion was inhibited at a clock angle of 148.43 deg, 0.37 deg from the desired position.

The performance of the system during the dark encounter sequence is summarized in Table 5.

NOMENCLATURE

a	p-layer thickness, cm
A	Aperture area of optics
A_f	Attenuation factor of filter
A_v	Closed loop voltage gain of preamplifier
A_y	Voltage gain of y-axis signal amplifier
A_1	Voltage gain of first stage of preamplifier
A_2	Closed loop voltage gain of first three stages of preamplifier
A_2'	Open loop voltage gain of last three stages of preamplifier
A_3	Closed loop voltage gain of amplifier including filter attenuation
A_3'	Open loop voltage gain of amplifier
A_4	Closed loop voltage gain of equivalent circuit of driver amplifier
A_4'	Open loop voltage gain of equivalent circuit of driver amplifier
B	Signal base R_T
C	Sinusoidal input control signal
C_0	Average component of C
C_1	Maximum amplitude of C
$C(S)$	Laplace transform of C
d	Distance from planet to system in A.U.
d_0	Planet acquisition distance at which signal-to-noise ratio is 1
d/d_0	Normalized planet acquisition distance
D	Correction signal
D_0	Average dc component of D
D_1	First harmonic component of D
$D(S)$	Laplace transform of D
e	Electronic charge
e_{dc}	dc biasing level
e_{in}	Network input
e_o	Network output
e_x	Detector output differential voltage along x-axis
e_y	Detector output differential voltage along y-axis
e_1	Output of one quadrant
e_2	Output of adjacent quadrant
E_r	Monochromatic energy flux at $\lambda = 0.55$ μ corresponding to visual albedos $\alpha = 0$ deg, $\Delta = 1$, $d = 1$
$E(d, \alpha, \lambda)$	Input energy from planet
$\mathcal{E}$	Positioning error signal
$\mathcal{E}(S)$	Laplace transform of $\mathcal{E}$

NOMENCLATURE (Cont'd)

f Frequency of oscillation $u/2\pi\tau$

$f/$ Ratio of diameter of effective diaphragm aperture to focal length of optics

$f(\lambda)$ Spectral energy function of solar energy

g_D Describing function of nonlinear element

$g(S)$ Frequency variant loop transfer function

$g_c(S)$ Transfer function of compensating networks

$g_s(S)$ Transfer function of servomotor and output load

h Hysteresis zone

h_{fe} Forward current transfer ratio

h_{ie} Input impedance

h_{oe} Output admittance

h_{re} Reverse voltage transfer ratio

$h(\lambda)$ Absorption coefficient as a function of incident wavelength λ

H Detector responsivity

I_b Transistor base driving current

$I_{GS}(T)$ Gate reverse current as a function of temperature

K Boltzmann constant

$K(\alpha)$ Illuminated fraction of planet at phase angle α

l n-layer thickness, cm

L_n Diffusion length of free electrons, cm

L_p Diffusion length of free holes, cm

m Number of signal pulses per detection time t_d

M Ratio θ_o/θ_i

M_p Peak value of output-to-input ratio

n Number of noise pulses per false alarm time t_f

n_d Refractive index of detector

N_2/N_1 Transformer ratio

p_n Probability that a noise pulse exceeds threshold

p_s Probability that signal-plus-noise pulse exceeds threshold

p_n Probability that threshold of Schmitt trigger is not exceeded in time t_f

$P(\lambda)$ Assumed planet spectral reflectivity

Q Signal which assures that system is always operating in planet searching mode immediately after each scan reversal

$r(\lambda)$ Relative reflectivity as a function of incident wavelength λ

R Motor constant output speed

R_b Transistor saturation resistance

R_{ds} Drain-to-source resistance as a function of operating temperature

R_D Input resistance to demodulator

R_{in} Input impedance of phase detector

$R(\theta)$ Fresnel coefficient of reflection for unpolarized incident energy as a function of incident angle θ

S $j\omega = 2\pi f$

S_r Surface recombination rate, cm-sec^{-1}

S/N Signal-to-noise ratio

t_b Time base

t_d Planet detection time

t_f False alarm time

T Temperature, °K

u $\omega\tau$

V_b Peak threshold voltage

V_{be1} Base to emitter voltage of transistor Q_1

V_{in} Input level at which Schmitt circuit responds

V_n Noise level at filter input

$V_o(T)$ Offset voltages as a function of operating temperature

V_p Peak planet signal voltage at a particular planet acquisition distance d

V_y y-axis output

NOMENCLATURE (Cont'd)

x Axis of error signal for planet tracking

y Axis of angular position of planet with respect to detector mount

α Phase angle (Sun–planet–system angle)

β Planet semidiameter

β_f Preamplifier feedback factor

β_1 Half-width of positive pulse D

β_2 Half-width of negative pulse of D

γ Normalized threshold V_b/V_n

$\delta(\theta)$ Factor due to vignetting effect of optics

Δ Inactive or dead zone; also, mean distance from planet to Sun, 1.524 A.U.

Δe Differential output between adjacent quadrants

Δf Bandwidth of filter $f_1 - f_2$

$\Delta\theta$ Theoretical planet tracking error of system as a function of operating temperature and tracking distance

$\Delta\theta_n$ Individual source of error when system is operating at a particular temperature and tracking distance

$\Delta\theta_1$ Error due to variation in responsivity of detector quadrants as a function of temperature

$\Delta\theta_2$ Error due to system dead zone

$\Delta\theta_3$ Error due to drift in photomodulator

$\Delta\theta_4$ Error due to offset in demodulator, phase detector and system operational failure prevention biasing

$\Delta\theta_5$ Error due to radiant density gradient of planet quadrants

ζ Normalized signal level V_p/V_n

η_D Demodulator chopping efficiency

$\eta(\lambda)$ Spectral response of radiation detector

$\eta_c(\lambda)$ Carrier collection efficiency

$\eta_n(\lambda)$ p-layer efficiency

$\eta_p(\lambda)$ n-layer efficiency

θ Planet position angle or angular diameter of planet

θ_i Reference position input

θ_o Actual controlled position variable at output

$\theta_o(S)$ Laplace transform of output

λ_1, λ_2 Cutoff wavelength of system

μ_n Mobility of electrons, $cm^2\text{-}v^{-1}\text{-}sec^{-1}$

μ_p Mobility of holes, $cm^2\text{-}v^{-1}\text{-}sec^{-1}$

ρ_a τ_a/τ

σ Output position signal in dimensionless form, θ_o/B

τ Motor and load time constant

$\tau(\lambda)$ Transmission efficiency of lens

ϕ Optical angular half field-of-view; also phase function

ψ Input position signal in dimensionless form, θ_i/B

REFERENCES

1. Nicklas, J. C., *Analysis, Design and Testing of a Position Servo Utilizing a Stepper Motor*, Technical Report No. 32-206, Jet Propulsion Laboratory, Pasadena, California, January 25, 1962.
2. Johnson, E. C., "Sinusoidal Analysis of Feedback-Control System Containing Nonlinear Elements," *AIEE Transactions*, Vol. 72, 1952, pp. 169–181.
3. Kochenburger, R. J., "A Frequency Response Method for Analyzing and Synthesizing Contractor Servomechanisms," *AIEE Transactions*, Vol. 69, 1950, pp. 1079–1088.
4. Sridhar, R., "A General Method for Deriving the Describing Functions for a Certain Class of Nonlinearities," *IRE Transactions*, Vol. AC-5, June 1960, pp. 135–141.
5. Wong, R. Y., "Carrier Collection and Spectral Response of Radiation Detector," *Space Programs Summary No. 32-27*, Vol. IV, Jet Propulsion Laboratory, Pasadena, California, June 30, 1964, pp. 92–97.
6. Prince, M. B. and M. Wolf, "New Developments in Silicon Photovoltaic Devices," *Journal of British IRE*, October 1958, pp. 583–596.
7. Shipley, M., "FET Low-Level Choppers," *Electronic Equipment Engineering*, February 1964, pp. 63–65.
8. Wysocki, J. J. and P. Rappaport, "Effect of Temperature on Photovoltaic Solar Conversion," *Journal of Applied Physics*, Vol. 13, No. 3, March 1960, pp. 571–578.
9. Jaffe, L. O. and J. B. Rittenhouse, *Behavior of Materials in Space Environment*, Technical Report No. 32-150, Jet Propulsion Laboratory, Pasadena, California, November 1961.
10. Material, Research and Development Technical Handbook, *Space/Aeronautics*, July 1963.
11. Wong, R. Y., "Planet-Acquisition-Range Prediction of a Planetary Scan System," *Space Programs Summary No. 37-28*, Vol. IV, Jet Propulsion Laboratory, Pasadena, California, August 1964, pp. 101–108.
12. "Planetary Simulation for *Mariner* C Planetary Scan Subsystem," *Space Programs Summary No. 37-25*, Vol. VI, Jet Propulsion Laboratory, Pasadena, California, January 1964, pp. 56–58.

ACKNOWLEDGMENTS

The planetary scan system was designed and developed at JPL. The author wishes to express appreciation to the many at JPL who have contributed to the work presented in this Report. J. Collier, R. Denning, W. Hodges and G. Osborn participated in the design and development of the system. The motor subassembly was designed and developed under the cognizance of E. L. Floyd. System component screening and testing were handled by W. Powell. J. Jodele furnished leadership in the electronic packaging. J. Collier, R. Denning, W. L. Momsen and G. Osborn participated in the system performance evaluation and testing.

Thanks are due the manufacturers who made contributions toward the completion of the system. Dynamics Instrumentation Company, Monterey Park, California, fabricated the electronics. Fairchild Space and Defense System, Los Angeles, California, mounted the lens and fabricated the optics and detector housings. Design, development and fabrication of the power supply was done by Glentronics, Inc., Glendora, California. Hoffman Semiconductor Division, El Monte, California, developed and fabricated the detectors, and Wems, Inc., Hawthorne, California, performed the packaging design and fabrication of the logic modules.

Thanks are also due W. G. Fawcett and F. L. Schutz of JPL who were responsible for integration of the scan system into the scientific subsystem of the *Mariner* spacecraft.